Western Graduate&PostdoctoralStudies

Western University
Scholarship@Western

Electronic Thesis and Dissertation Repository

12-12-2012 12:00 AM

Photocalytic Degradation of Malic Acid Under Thin Coated TiO2

Vanessa Silveira Rodgher
The University of Western Ontario

Supervisor
Hugo I. de Lasa
The University of Western Ontario

Graduate Program in Chemical and Biochemical Engineering
A thesis submitted in partial fulfillment of the requirements for the degree in Master of Engineering Science
© Vanessa Silveira Rodgher 2012

Follow this and additional works at: https://ir.lib.uwo.ca/etd

Part of the Catalysis and Reaction Engineering Commons, and the Food Processing Commons

Recommended Citation

Rodgher, Vanessa Silveira, "Photocalytic Degradation of Malic Acid Under Thin Coated TiO2" (2012). *Electronic Thesis and Dissertation Repository*. 1015.
https://ir.lib.uwo.ca/etd/1015

This Dissertation/Thesis is brought to you for free and open access by Scholarship@Western. It has been accepted for inclusion in Electronic Thesis and Dissertation Repository by an authorized administrator of Scholarship@Western. For more information, please contact wlswadmin@uwo.ca.

PHOTOCALYTIC DEDRADATION OF MALIC ACID UNDER THIN COATED TiO_2

(Spine title: Photocatalytic degradation of malic acid under thin coated TiO_2)

(Thesis format: Monograph)

by

Vanessa Rodgher

Graduate Program in Engineering Science
Department of Chemical and Biochemical Engineering

A thesis submitted in partial fulfillment
of the requirements for the degree of
Master in Science

The School of Graduate and Postdoctoral Studies
The University of Western Ontario
London, Ontario, Canada

© Vanessa Rodgher 2012

THE UNIVERSITY OF WESTERN ONTARIO
School of Graduate and Postdoctoral Studies

CERTIFICATE OF EXAMINATION

Supervisor

_____
Dr. Hugo de Lasa

Co-Advisor

_____
Dr. Domenico Santoro

Examiners

_____
Dr. Ajay K. Ray

_____
Dr. Shahzad Barghi

_____
Dr. Ron R. Martin

The thesis by

Vanessa Silveira Rodgher

entitled:

PHOTOCALYTIC DEDRADATION OF MALIC ACID UNDER THIN COATED TiO_2

is accepted in partial fulfillment of the
requirements for the degree of
Master in Science

_____
Date:

_____
Chair of the Thesis Examination Board

Abstract

Opaque fluids have a limited irradiation transmission. Thus, their decontamination employing near UV irradiation poses significant technical challenges. In the present study, a thin UV-transparent/waterproof glue layer coated with a 1.5 wt% of TiO_2 and a new PhotoReactor Cell were implemented. TiO_2 irradiation in the PhotoReactor Cell was effected on the TiO_2 particle side, not directly in contact with the fluid, allowing the postulation of an "h^+" site mobility mechanism on photocatalysis.

Photocatalytic degradation experiments with malic and malonic acid in water at 10, 20, 30 and 40 ppm showed the complete degradation of malic acid after 5 to 8 hours. Its minimum concentration was reached with the maximum concentration of malonic acid formed. Mass transfer effects and photolysis were found to be negligible in this setup. Macroscopic balance measurements showed that 92% of the irradiation was absorbed by the TiO_2-film and quantum yields as high as 14.2-17.4% were obtained.

The "Series-Parallel" kinetic mechanism was found to better predict the photocatalytic degradation of malic acid. It was found that the sensory attributes of apple juice were preserved with irradiation times being limit to 1 hour of exposure time. This time was proved by some authors to be sufficient to promote the 5-log CFU/ml microbial reduction, required by the FDA (21CFR120.24, 2012).

Keywords

photocatalysis, TiO_2-film, back-face irradiation, malic acid, malonic acid, kinetic modeling, Langmuir-Hinshelwood, quantum yield, apple juice, sensory attributes.

Acknowledgments

I would like to first thank Dr. Hugo de Lasa for his encouragement and support. His expertise and coaching were an essential part of my success as a Master's student.

I wish to thank the University of Western Ontario along with Dr. Hugo de Lasa for the financial support granted to me during my entire Graduate Program.

I would also like to thank the entire Chemical Reaction Engineering Centre (CREC) that in many ways were very helpful and made my work more enjoyable: Yira Aponte, Angel Lanza, Patricio Valades, Gabriela Navarro, Juan Manuel Garcia, Salvador Escobedo, Cristina Lugo, Jose Munoz and Pastor Solano. I also want to thank Dr. Domenico Santoro for his support as my Co-Advisor.

I am grateful to Jesus Moreira for his invaluable contributions in the development of my research project.

I am grateful to Kara Mallot, Kristen Hunt, Joanna Bloom and April Finkenhoefer, the Graduate Affairs Coordinators, for their cooperation in administrative matters during my Master Program.

Lastly my gratitude to all my family that always encouraged me and believed in my academic potential. I want to specially thank my parents Regina Celia Silveira Rodgher and Antonio Sergio Rodgher, as well as my brother and sister, Renan Silveira Rodgher and Daniela Silveira Rodgher who have always been an integral part of my personal and professional life. Finally, I would like to express my deepest gratitude to my lovely husband, David Rayo, who supported me during my entire Program and without whom all this would not have been possible.

Table of Contents

CERTIFICATE OF EXAMINATION ii

Abstract iii

Acknowledgments iv

Table of Contents v

List of Tables viii

List of Figures ix

List of Appendices xii

Nomenclature xiii

Chapter 1 1

1 Introduction 1

Chapter 2 6

2 Scope of the Research 6

Chapter 3 7

3 Literature Review 7

3.1 Current Methods for Opaque Fluid Disinfection 7

3.1.1 Studies Using HTST, PEF and UV Methods for Opaque Fluids Disinfection 9

3.2 Photocatalytic Oxidation Process 13

3.2.1 Application of Photocatalysis for Opaque Fluid Decontamination 16

3.3 Conclusions 32

Chapter 4 35

4 Experimental Methods 35

4.1 Introduction 35

4.2 Reactor Setup for the Preliminaries Experiments with Apple Juice 36

4.3 TiO_2-film 1.5 wt% Preparation 37

4.3.1 Important information about the prepared TiO_2-film 39

4.3.2 TiO_2-film Characterization 39

4.4 Reactants 40

4.5 Reactor Cell Setup of this Study 41

4.6 Photocatalytic Degradation Experiments 43

4.7 Detection and Quantification of Malic and Malonic Acid 43

4.8 Radiation Measurements Box Setup 44

4.9 Conclusions 45

Chapter 5 46

5 Results and Discussion Part I: TiO_2-film Catalyst Preparation, Characterization and Degradation Studies with Malic and Malonic Acid in Water 46

5.1 TiO_2-film catalyst preparation and characterization 46

5.1.1 Absorption Spectra of Water vs. Opaque Fluids 46

5.1.2 TiO_2 Film Preparation and Characterization 48

5.2 Photolysis and Photocatalytic Degradation of Malic Acid Using TiO_2 Films and TiO_2 in Suspension 51

5.2.1 Concentration Profile during the Photodegradation of Malic and Malonic Acid under TiO_2 Film 51

5.2.2 Photolysis of Malic Acid 57

5.2.3 Concentration Profile during the Photodegradation of Malic and Malonic Acid under TiO_2 in Suspension 60

5.3 Conclusions 62

Chapter 6 64

6 Results and Discussion Part II: Reactor Irradiation Studies and Kinetic Modeling of Malic Acid Photocatalytic Degradation 64

6.1 Irradiation Measurements of TiO_2 Thin Coated Film 1.5 wt% 64

6.1.1 Calculation of P_a, P_l, P_{bs} and P_t 67

6.2 Kinetic Modelling for malic acid and its intermediate degradation under TiO_2-film 1.5 wt% 72

6.2.1 Photolysis of Malic and Malonic Acid 73

6.2.2 Kinetic Modeling of Malic Acid Photodegradation 74

6.3 Calculation of the Quantum Yield (φ) 87

6.3.1 Quantum Yield (φ) for the Reaction Mechanism One – "Series".....87

6.3.2 Quantum Yield (φ) for the Reaction Mechanism Two – "Series-Parallel" 89

6.4 Conclusions 91

Chapter 7.....93

7 Conclusions and Recommendations 93

7.1 Conclusions 93

7.2 Recommendations for Future Work.....94

References.....96

Appendices.....106

Curriculum Vitae 112

List of Tables

Table 3.1: Comparison of Volatile Compound Losses Applying both Methods, PEF and HTST (Aguilar-Rosas et al., 2007)..... 10

Table 3.2: Rate Constant for Aliphatic Carboxylic Acids (Chen et al., 2009) 24

Table 4.1: Characteristics of the Photo-CREC Water-II Reactor Setup (Slurry Reactor and UV-Lamp Source) 37

Table 4.2: Chemical Compounds Used for the Photocatalytic Degradation Studies 40

Table 4.3: Characteristics of the Reactor Cell Setup of this study (Batch Reactor, Outer Box, Cooler Tank and UV-Lamp Source) 42

Table 6.1: P_l (t), P_{bs} (t), P_t (t) and P_a (t) Calculated for the TiO_2-Film 72

Table 6.2: Kinetic Constants for the Photolysis of Malic and Malonic Acid 73

Table 6.3: Kinetic Parameters for the Photoconversion of Malic and Malonic Acid for the Simultaneous Optimization of 10, 20, 30 and 40 ppm for the Reaction Mechanism One 78

Table 6.4: Cross-Correlation Coefficients of the Kinetic Parameters Obtained for the Photoconversion of Malic and Malonic Acid for the Simultaneous Optimization of 10, 20, 30 and 40 ppm for the Reaction Mechanism One 79

Table 6.5: Kinetic Parameters for the Photoconversion of Malic and Malonic Acid for the Simultaneous Optimization of 10, 20, 30 and 40 ppm for the Reaction Mechanism Two 82

Table 6.6: Cross-Correlation Coefficients of the Kinetic Parameters Obtained for the Photoconversion of Malic and Malonic Acid for the Simultaneous Optimization of 10, 20, 30 and 40 ppm for the Reaction Mechanism Two 83

Table 6.7: Comparison between Kinetic Model One “Series” and Kinetic Model Two “Series-Parallel” 84

List of Figures

Figure 3.1: Log-Reduction of Pathogens in Apple Juice after it is submitted to Different Pasteurization Treatments (Noci et al., 2008) 12

Figure 3.2: Mechanism for the Photocatalytic Degradation of Malic Acid in the Presence of TiO_2 in Suspension at pH of 3 (Irawaty et al., 2011) 22

Figure 3.3: The Routes for the Photocatalytic Degradation of Malic Acid in the Presence of Fe(III) under UV-Light Source (Franch et al., 2004) 25

Figure 3.4: Main Reaction Pathway for Malic Acid Degradation under TiO_2 at 290 nm (Herrmann et al., 1999) 28

Figure 4.1: Photo-CREC Water-II Reactor Setup Employed in the Light Transmission Experiments with Apple Juice 36

Figure 4.2: Batch Rector of this Study Coated with the TiO_2-film 1.5 wt% 39

Figure 4.3: Batch Reactor Setup Employed for the Photocatalytic Degradation of Malic and Malonic Acid 41

Figure 4.4: Schematic Representation of the Radiation Measurements of the TiO_2-film 44

Figure 4.5: Measurements Scheme Contemplating the 49 Measurement Positions to Access the Non-Symmetrical Radiation Profile 45

Figure 5.1: Transmission Spectra for Commercial Allens Apple Juice at Position 4 (Brix: 11.90±0.1, pH: 3.10±0.05, Conc. of malic acid: 3.00±0.1 g/L) 47

Figure 5.2: Apple Juice Transmission Spectra vs. Water Transmission Spectra 47

Figure 5.3: Irradiation Paths Showing Formation of holes (h^+) Using TiO_2 (a) in a Suspension with TiO_2 Directly Irradiated and (b) in a Thin Film with Back Face Irradiation Only 49

Figure 5.4: SEM of TiO_2 Film (500x): Region 1 – Surface with no Catalyst Coverage; Region 2 – Catalyst Covered Area 50

Figure 5.5: EDX Analysis of TiO_2 Film – Regions 1 and 2 from Figure 5.4 51

Figure 5.6: a) Chromatograms of Malic Acid with 20ppm in Water (Peak 1) and b) Chromatograms of Malic Acid after 2 hours of Photocatalytic Reaction Time using a TiO_2 Film with Malonic Acid Formation (Peak 2)..... 53

Figure 5.7: Malic Acid Photodegradation and Malonic Acid Formation Using a TiO_2 Film and Near UV-Light..... 54

Figure 5.8: Malic Acid Photodegradation Profile for Different Initial Concentrations: 10, 20, 30 and 40ppm..... 55

Figure 5.9: Malonic Acid Photodegradation Profile for Different Initial Concentrations of: 10, 20, 30 and 40ppm 55

Figure 5.10: A 40ppm Malic Acid Concentration Photodegradation Experiment Using a TiO_2 Film at Two Different Mixing Speeds: 125 rpm and 250 rpm 57

Figure 5.11: Profile for the Photolysis and Photocatalysis Using a TiO_2 Film for Malic Acid 20ppm Under near UV-Light..... 59

Figure 5.12: Profile for the Photolysis and Photocatalysis Using a TiO_2 Film for Malic Acid 20ppm Under Near UV-Light Recalculated Using the Kinetic Photolysis and the Irradiation Profile for the Light Transmitted Through the Film (Table 6.1) 59

Figure 5.13: A 20ppm malic acid photodegradation profile for different TiO_2 concentrations in suspension: 0.01, 0.05, 0.10, 0.15, 0.20 and 0.30 gL^{-1} 61

Figure 5.14: Rate Equation for malic acid degradation ($r_{malic\ acid}$) for different TiO_2 concentrations in suspension (0.01 to 0.5 gL^{-1}). Initial concentration of malic acid: 20ppm. 62

Figure 6.1: Radiation Profile of BL Lamps a, b and c..... 66

Figure 6.2: Emission Spectrum for Lamp b (Wavelength Range of 320-420 nm) 66

Figure 6.3: Measurements Scheme to Assess the Non-Symmetrical Radiation Profile..... 69

Figure 6.4: P_l (t) Spectrum Along the 49 Positions 70

Figure 6.5: P_{bs} (t) Spectrum Along the 49 Positions 70

Figure 6.6: P_t (t) Spectrum Along the 49 Positions 71

Figure 6.7: Reaction Mechanism One – "Series" Mechanism Proposed for the Photocatalytic Degradation of Malic Acid in TiO_2-Film 1.5 wt%..... 74

Figure 6.8: Reaction Mechanism Two – "Series-Parallel" Mechanism Proposed for the Photocatalytic Degradation of Malic Acid in TiO_2-Film 1.5 wt%..... 74

Figure 6.9: Experimental and Model One Concentration Profiles for Malic Acid and Malonic Acid Photocatalytic Conversion at 10, 20, 30 and 40 ppm..... 78

Figure 6.10: Reconciliation Plot of the Predicted Concentration versus Experimental Concentration for the 4 Parameters Estimated Using the Reaction Mechanism One 80

Figure 6.11: Experimental and Model Two Concentration Profiles for Malic Acid and Malonic Acid Photocatalytic Conversion at 10, 20, 30 and 40 ppm..... 81

Figure 6.12: Reconciliation Plot of the Predicted Concentration versus Experimental Concentration for the 5 Parameters Estimated Using the Mechanism Two 84

Figure 6.13: CO_2 and TOC Profile for the Photocatalytic Degradation of Malic Acid at Initial Concentration of 40 ppm (13.6 ppm of Carbon) 86

Figure 6.14: Quantum Yield (φ) Profile for Malic Acid Photocatalytic Degradation at 10, 20, 30 and 40 ppm Applying the Kinetic Model One "Series"..... 89

Figure 6.15: Quantum Yield (φ) Profile for Malic Acid Photocatalytic Degradation at 10, 20, 30 and 40 ppm Applying the Kinetic Model Two "Series-parallel" 90

List of Appendices

Appendix A: Calculation of k_i and k_m 106

Appendix B: Calculation of P_a (t), P_l (t), P_{bs} (t) and P_t (t) using Macroscopic Radiation Balance.....109

Nomenclature

k_i	Kinetic constant for "i specie" photocatalytic degradation, m/s
k_1	Apparent photocatalytic kinetic constant, min^{-1}
$k_{overall}$	Overall photocatalytic kinetic constant, m/s
k_m	Mass Transfer coefficient, m/s
$k_{photolysis}$	Kinetic constant for photolysis, min^{-1}
wt%	Weight-weight percentage
$q_{z,\lambda,t}$	Radiative flux or Irradiation Intensity, $\mu W/cm^{2\alpha}$
P_a	Rate of radiation absorbed, Photons/s
P_l	Rate of radiation emitted, Photons/s
P_{bs}	Rate of radiation back scattered, Photons/s
P_t	Rate of radiation transmitted, Photons/s
h	Planck's constant, J.s
c	Speed of light, m/s
K^A_i	Adsorption constant for i "species", $ppm^{-1}L$
N_i	Number of mols for I "species", mol
W_{irrad}	Amount of TiO_2 catalyst irradiated, g
V	Reactor volume, L
C_i	"Species" concentration, ppm
t	Reaction time, s

Acronyms

US	Ultrasound
PEF	Radio Frequency Electric Field

HILP	High Intensity Light Pulses
FDA	Food and Drug Administration U.S.
Re	Reynolds number
CFR	Code of Federal Regulations
UV	Ultraviolet
SEM	Scanning Electron Microscope
EDX	Energy Dispersive X-Ray Spectroscopy
OMF	Oscillating Magnetic Field
CFU	Colony-forming unit
UVA	Ultraviolet A
SCV's	Small colony variants
CB	Conduction band
MDA	Malondialdehyde
ROS	Reactive oxygen species
SODIS	Solar water disinfection
AIJN	Association of the Industry of Juices and Nectars
FTIR	Fourier Transform Infrared Spectroscopy
HPLC	High-Performance Liquid Chromatograph
LH	Langmuir-Hinshelwood
TOC	Total Organic Carbon
XPS	X-Ray Photoelectron Spectroscopy
ATR-IR	Attenuated Total Reflectance Infrared Spectroscopy
POM's	Microporous Polyoxometalates
CREC	Chemical Reaction Engineering Centre

BL	Black-light
RPM	Revolutions per minute
Sh	Sherwood number, dimensionless
MB	Macroscopic Balance
LVRPA	Local volumetric rate of photon adsorption, W/m^3
MaAc	Malic Acid
MAc	Malonic Acid
ODE	Ordinary Differential Equations
CI	Confidence Interval
STD	Standard Deviation
R^2	Correlation Coefficient
CCC	Cross-correlation Factor
RP	Reconciliation Plot

Greek letters

φ_1	Number of molecules of OH radical consumed/s, molecules/s
φ	Quantum Yield, %
λ	Wavelength, nm
α	Percentage of light accounted for Photolysis

Chapter 1

1 Introduction

Opaque fluids or “non translucent” fluids, covers the broad area of fluids where there is limited transmission of light or/and irradiation. A possible definition of an opaque fluid is a fluid impenetrable by light; neither transparent nor translucent.

Decontamination of “opaque fluids” poses an important challenge to decontamination processes. The bulk of these fluids cannot be effectively irradiated and as result new approaches such as thin TiO_2 films are needed for the application of photocatalysis.

More specifically, concerns about the environment and about new regulations related to food, such as the ones from U. S. Food and Drug Administration (FDA), have driven researchers to test different methods for the conversion of organic contaminants in opaque fluids such as is the case of the ones contained in fruit juices and waste water.

Although there are many organic molecules in common between fruit juice media and wastewater, differing techniques have been used for their decontamination. Energy conservation needs have challenged researchers to look for new energy-efficient and cost-effective techniques. Opaque fluids such as fruit juice are mainly composed of organic acids. Carboxylic acids are defined as organic acids with at least one carboxyl group (RCOOH). This group is formed by malic acid, maleic acid, malonic acid, fumaric acid, oxalic acid, citric acid and acetic acid, among others. Small carboxylic acids are soluble in water and their solubility decreases with the increase of the carbon chain. These chemical species are classified as weak acids and are frequently formed as intermediates from the incomplete organic species degradation (Franch et al., 2004). Although, organic acids do not appear as hazardous compounds, their study is extremely important to understand how the degradation methods influence the main chemical composition of opaque fluids media such as apple juice.

Despite all the existent methods for the decontamination of opaque fluids, they can be classified in two groups: i) Thermal Methods and ii) Non-thermal Methods. Thermal

techniques, such as pasteurization, are the most common methods applied in food processing and are well-established given that they achieve the 5-log CFU/ml microorganism reduction recommended by the FDA.

However, non-thermal techniques have currently gained special interest due to consumer demand for the preservation of sensory qualities of the juice (Caminiti et al., 2011). Many researchers have investigated the viability of non-thermal methods and compared them with thermal Pasteurization. Non-thermal techniques include: (a) UV-light Treatment, (b) High Intensity Ultrasound (US), (c) Radio Frequency Electric Field (PEF), and (d) High Intensity Light Pulses (HILP), among others. These methods have been studied for the inactivation of pathogenic microorganisms such as Escherichia coli K-12 and Salmonella. Their results appear to be very promising, showing that new alternatives can be successfully applied for opaque fluid decontamination without changing the sensorial characteristics.

According to the FDA Regulations (21 CFR 179.39), the UV treatment approved since 2000 can be used as a pathogen reducer in juice. The specific conditions of application include: (a) turbulent flow (Re>2200), (b) low pressure of mercury lamps (90% of the emissions) and (c) a wavelength of 253.7 nanometers.

Unlike opaque fluids, wastewater involves a three step process for decontamination. The primary water treatment step consists of the removal of heavy solid material from the fluid. The secondary step aims to remove biological material. And the tertiary step, normally involving a physical or chemical process, has the objective of removing organic or inorganic compounds. These chemical species can be classified as contaminants and are hazardous chemicals in drinking water.

Separation techniques, such as: (a) Activation carbon adsorption, (c) Ion exchange on adsorbent surfaces, and (c) Ozonisation, among others, are widespread techniques applied in the tertiary step. However, these techniques have the disadvantage of generating undesirable species or transferring hazardous species from one phase to another during water treatment. They may also present high costs.

Recently, among the techniques for water treatment, the photocatalytic degradation process has been gaining importance in wastewater decontamination due to its: (a) low cost, (b) moderate temperature, (c) pressure requirements, (d) complete mineralization and (e) residue-free reaction (Bhatkhande et al., 2001).

Photocatalysis, using TiO_2 as a catalyst, is a well-known process for the degradation of pollutants in water treatment. A catalyst reaction (Herrmann et al., 1999) starts when the semiconductor catalyst is irradiated by a light source with a wavelength range smaller than 400nm (optimum 365 nm) and with a higher energy than the energy of the band gap. The light is absorbed by the catalyst creating electron-hole pairs. The holes react with water, producing OH radical and the electrons react with the dissolved O_2 producing oxidant species. Both holes and electrons react by degrading the organic molecules present in the solution into CO_2 and H_2O.

Photocatalyst reactions can be performed with the catalyst in suspension or immobilized on a thin film or a mesh. Although a photocatalyst in suspension is the most general form employed for the photocatalyst process, it appears to have important problems. The most significant one is the filtration requirement to remove the catalyst at the end of the reaction. On the other hand, the use of photocatalyst films has the benefit of not requiring the water effluent to be filtered, introducing significant cost and time savings in industrial scale processes.

Different methods for the preparation of photocatalyst films have been developed on surfaces like glass, quartz, stainless steel (Fernandez et al., 1995) and optical fibers (Danion et al., 2007). Their preparation includes different processes such as the immersion of a support in titanium mixtures, drying, and calcination, among others (Sumin et al., 2011; Danion et al., 2007; Choi et al., 2006; Song et al., 2001; Herrmann et al., 1999; Herrmann et al., 1997). These methods are time consuming and costly in terms of material and equipment. Thus, new techniques for photocatalyst immobilization at a low cost may be of great importance for the photodegradation of organic acids in water and subsequent application in opaque fluids.

Regarding the present investigation, a first approach was the study of the photocatalytic

degradation of organic compounds in apple juice using a very efficient Photo-CREC-Water II slurry reactor. Since the experiments showed that opaque fluids absorb a great amount of light competing with the photocatalyst, it was necessary to develop an alternative approach to immobilize the photocatalyst, placing it under good near UV-light source irradiation.

Thus, a photocatalyst layer was prepared using an UV-transparent/waterproof glue and a TiO_2 1.5 wt% solution in water, coated in a quartz slide. The apparatus was set placing the near UV-Light source strategically outside the photoreactor cell system to guarantee modest direct irradiation of the water solution containing the organic species and a high degree of absorbed photons on the TiO_2 layer. It was envisioned that in this way, only the mobile charges on the TiO_2 layer (solution side) would be able to contribute to photoconversion.

The photocatalyst film was analyzed using a Scanning Electron Microscope (SEM) and it showed the presence of TiO_2 on the surface of the film through an Energy-Dispersive X-Ray Spectroscopy (EDX) analysis.

The chemical species chosen for the degradation tests were malic acid and malonic acid dissolved in water. Malic acid is the main organic acid found in apple juice, and malonic acid is the main intermediate of malic acid photodegradation.

Regarding the results obtained in the present research project, they establish a first approach to describe malic acid and malonic acid degradation using a TiO_2 thin film under near UV-light. One should mention that the immobilized TiO_2 is not directly irradiated and only the mobile sites on the semiconductor non-irradiated surfaces are able to contribute to the photoconversion. It is our belief that this data are extremely important, not only to describe photodegradation of organic acids in opaque fluids media, but also to better understand the mechanism of photocatalysis.

Furthermore, the proposed research allows one to establish and “irradiation window” for microbial decontamination, which is the time allowed for microbial decontamination without affecting the key chemical species in order to provide a fruit juice whose special

sensorial properties are essentially intact.

Chapter 2

2 Scope of the Research

The main objective of the present MESc thesis is to prepare a cost-effective thin film of TiO_2 and to demonstrate its performance using the photodegradation of malic and malonic acid in water under near UV-Light.

It is also the goal of the present study to be able to elucidate the photodegradation mechanism using an "indirect" thin film irradiation. To achieve these goals, the following methods are proposed:

a. SEM and EDX analysis to characterize the prepared TiO_2 films.

b. Photocatalysis reactivity tests using TiO_2 suspensions and TiO_2 films.

c. Photodegradation of malic acid and malonic acid in water solutions under near UV-irradiation.

d. Radiation measurements to establish macroscopic balances calculating the rate of photons absorption on TiO_2 films.

e. Calculation of quantum efficiencies on "indirectly" irradiated TiO_2 thin films to gain knowledge on the potential mobility of the "h^+" sites.

f. Establishment of the limits for photocatalytic irradiation time (irradiation window) allowing microbial inactivation with the preservation of fruit juice sensory properties. This irradiation time limit is going to be assessed under conditions leading to minimum photoconversion of malic acid (AIJN 6.3 Reference Guide Apple – Revision May 2011).

Chapter 3

3 Literature Review

The objective of this chapter is to review the current methods for degradation of organic compounds in opaque fluids and wastewater media.

Regarding opaque fluids decontamination, the available methods can be divided into thermal and non-thermal techniques, with decontamination being mainly addressed to pathogens such as E. coli and Salmonella.

For water treatment, among all methods available, TiO_2 photocatalysis appears as a most promising one. In this respect, TiO_2 have been tested in different systems including TiO_2 in suspension, TiO_2 loaded with various additives in suspension and TiO_2 in thin films. The advantages, disadvantages and relevant conclusions for the applicability of these methods in the context of opaque fluids such as fruit juices, are discussed in the upcoming sections.

3.1 Current Methods for Opaque Fluid Disinfection

In order to meet the demand for “fresh” foods, a significant body of research has led to the establishment of mildly treated food processes using non-thermal methods (Butz et al., 2002). These new methods allow for the preservation of flavours, integral nutrients and vitamins with few or no changes to their make-up. It is expected that non-thermal treatment deactivate unwanted enzymes and micro-organisms while keeping the integrity of the food’s nutritional and sensory attributes, which are often lost with the application of thermal treatment. The following sections in this chapter will be devoted to the discussion of ground-breaking methods in food preservation, such as Thermal Pasteurization, UV-Light/Pulsed Light, Pulsed Electric Field (PEF) and Oscillating Magnetic Field (OMF).

The most common way of inactivation of micro-organisms in apple juice is by submitting the juice with HTST (High Temperature Short Time) Pasteurization. Using this method,

the juice is circulated through a plate heat exchanger with the temperature being in 76.6 and 87.7^{o}C range and retention times between 25 and 30s (Moyer and Aitken, 1980). One should note that although the 5-log CFU/ml microorganism's reduction recommended by the Food and Drug Administration (Code of Federal Regulations, 21CFR120.24, 2012) is achieved applying Thermal Pasteurization, the use of heat causes a change in the taste, flavour and degradation of some key chemical compounds such as phenolic compounds (Aguilar-Rosas et al., 2007) and vitamins (Qin et al., 1995) in fruit juices such as apple juice.

UV-Light treatment is a well-known technique employed for the disinfection of fruit juice due to its capacity to accomplish the 5-log CFU/ml microorganism reduction without promoting significant change in the sensorial and physical-chemical characteristics of the juice (Hanes et al., 2002). According to Hanes et al., 2002, semitransparent juice such as apple juice absorbs UV-light at 253.7 nm and only a small amount of the light emitted reaches both organic molecules and microorganisms (Bolton and Linden, 2003).

Due to the low penetration of light in these fluids, UV systems are usually designed with the fluid injected as a thin film (Duffy et al., 2000; Hanes et al., 2000; Basaran et al., 2004). Duffy et al., 2000, proved the effectiveness of the 5-log CFU/ml reduction of E. coli using a thin film system with 10-UV lamps and laminar flow. Another important factor for the use of the UV-Light as a preservation treatment for juice, according to the FDA U.S., is that the flow rate of the fluid plays an important role in the microorganism reduction and consequently a turbulent flow is needed for effective use of UV-Light for fruit juice disinfection (21CFR120.24, 2012).

Food can also be non-thermally treated applying a Pulsed Electric Field (PEF). Preliminary studies with PEF were performed by Fetteman et al. in 1928, as reported by Butz et al., 2002. PEF consists on subjecting a fluid to pulses of high voltage (20-80 kV/cm) in diverse forms such as: (a) an exponentially decaying wave, (b) a square wave, (c) a bipolar wave, among others, between two electrodes, for a period of time less than 1 second at room temperature or slightly above room temperature. The high voltage applied

promotes an electric field which is responsible for the microbial reduction. Barbosa-Canovas et al., 1998 and Evrendilek et al., 2000 showed that PEF employed in apple juice promoted a 5-log CFU/ml microorganism reduction without significantly changes in its physical-chemical characteristics such as sensory properties, pH and vitamin C content. Butz et al., 2002, mention that there are some important factors while using PEF such as: (a) pulse width, (b) wave shape, (c) pulse intensity, (d) microorganism concentration and (e) pH, among others. These factors can affect the microbiological reduction and should be taken in account when choosing a method for microbiological reduction in juices.

Furthermore, according to Butz et al., 2002, although there are two industrial-scale PEF setups operating presently, differences between the lab and industrial scales make kinetic of the microorganisms reduction quite unreliable.

Oscillating magnetic fields (OMF) and Ultrasound (US) are also non-thermal methods used for the preservation of fruit juice. The OMF method consists of placing the fluid inside of a plastic bag, and treating it with 1-100 pulses for 25-100 ms at a temperature range of 0-50 ºC (Pothakamury et al., 1993). However, there is still controversy about the actual efficiency of OMF, for decreasing microorganism levels in foods (Tsuchiya et al., 1996).

Ultrasound (US) is a cyclic sound of approximately 20,000 Hz. Its application promotes juice preservation. This is caused by intracellular cavitation in the juice accompanied by temperature and pressure increase (Rahman et al., 1999). According to Raso et al., 1998, and Butz et al., 2002, the US method does not promote enough microbiological reduction for meeting food and safety requirements. Its use is thus, preferred as a complement to another preservation method.

3.1.1 Studies Using HTST, PEF and UV Methods for Opaque Fluids Disinfection

Aguilar-Rosas et al., 2007, have reported the difference between HTST and PEF methods through the comparison of the pH effects and the amount of E. coli remaining in apple

juice samples after filtration. The Pasteurization was tested with temperatures of 73, 80 and 83ºC and a holding time of 27s. For PEF, a Bench Scale OSU 4-H Pulsed Electric Field Processor Model was used, with electric fields of 12, 24 and 36 kV cm^{-1} and replication rates of 400, 600 and 800 pps, respectively. It was observed that the pH varied between 3.8 and 3.9 for both methods only. In terms of total phenol compounds, the reduction was greater when applying HTST (32.2%) than when using PEF (14.49%). This data agrees with the observations made by Gardner et al., 2000. However, the volatile compounds resulting from both methods affect the sensorial properties of the apple juice (Aguilar-Rosas et al., 2007). In particular, a considerable change of these properties using the HTST treatment method (see Table 3.1) can be observed.

Table 3.1: Comparison of Volatile Compound Losses Applying both Methods, PEF and HTST (Aguilar-Rosas et al., 2007)

	Loss Percentage	
Compound	**Pulsed Electric Field (PEF)**	**High temperature-short time (HTST)**
Acetic Acid	39.792 ± 20.84	100
Hexanal	7.042 ± 9.32	62.348 ± 5.35
Butyl Hexanoate	18.108 ± 7.72	36.273 ± 24.86
Ethyl acetate	77.458 ± 29.23	67.126 ± 39.33
Ethyl butyrate	60.190 ± 17.80	88.398 ± 12.46
Methyl butyrate	30.081 ± 31.37	51.200 ± 19.56
Hexyl acetate	8.408 ± 16.12	22.910 ± 21.99
1-Hexanal	14.101 ± 7.65	69.307 ± 5.62

The effects of HSTS and PEF treatment on the pH, colour and inactivation of Escherichia coli in apple juice were also investigated by Charles-Rodriguez et al., 2007. According to this author, when the Pasteurization (HSTS) is applied, the value of pH varies from 3.75 (at 25°C) to 4.0 (85°C). This is different from the results obtained by Aguilar-Rosas et al., 2007. In later case, the increasing pH value can be explained as the result of organic acids evaporation, reducing the acidity on the juice. This pH increase could also have a

negative effect on the apple juice life, due to the fact that higher pH media increases enzyme activity and yeasts growth. Regarding colour changes, after Thermal Pasteurization, there were not any which were significant.

On the other hand, neither pH nor colour varied during the PEF treatment, using electrical field strength equal to 36 kV cm^{-1}. In regards to microbial inactivation, PEF treatment was also efficient, showing a 6-log CFU/ml reduction using optimum electrical field strength of 36 kV cm^{-1} and maximum pulse frequency of 800 pps.

Noci et al., 2008, studied the difference between: (a) Thermal Treatment (HTST), (b) Ultraviolet Irradiation (UV), (c) Pulsed Electric Field (PEF) and (d) their combinations (UV+PEF and PEF+UV) in order to preserve the organoleptic properties and to reduce the microbiological contamination in fresh apple juice. While using the two Thermal Treatments, the temperature was set at 72ºC (T_1) and 94ºC (T_2), and the holding time was 26 seconds. For the UV method, the juice was exposed to a UV-Light output power of 30 W for 30 min under laminar flow. For the PEF treatment, monopolar square-wave pulses of 1 μs width and 15 Hz frequency, flow rate of 15.75 ml/min and a residence time of 6.67 s were used. The results obtained for the pH, the Brix and the enzyme activity did not show significant changes. These results agree with the ones found by Aguillar-Rosas et al., 2007. In their studies, a microbial change in the apple juice with a greater than 5-log CFU/ml pathogen reduction was observed with Thermal treatment (T_1 and T_2), UV, PEF, PEF+UV and UV+PEF.

Figure 3.1 reports a fresh apple juice with an initial microbial flora of 10^9 CFU/ml (48 hours incubated) displaying the greatest reduction (7.1 log CFU/ml) under Ultraviolet Light treatment combined with Pulsed Electric Field (UV+PEF).

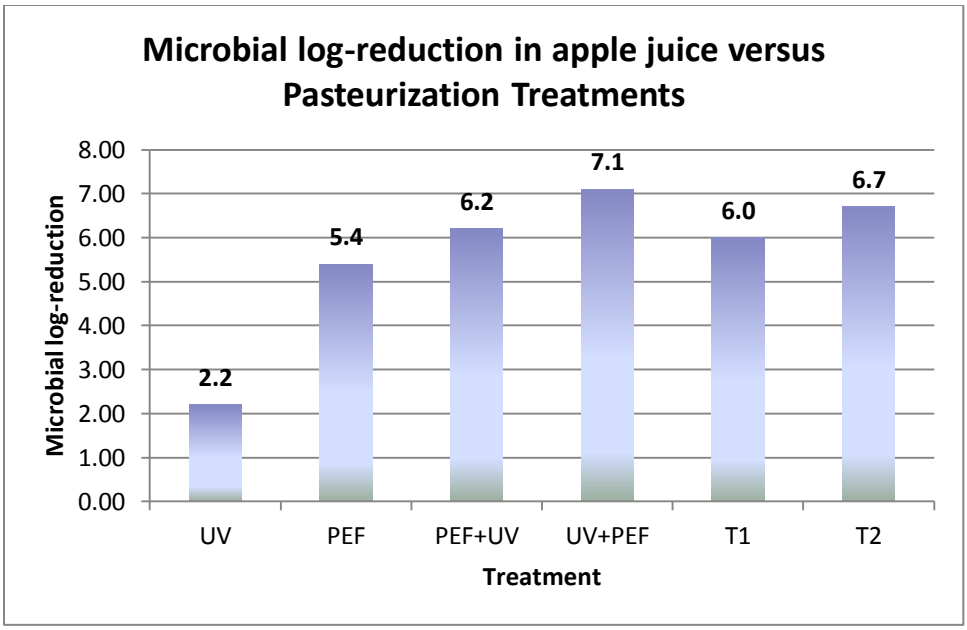

Figure 3.1: Log-Reduction of Pathogens in Apple Juice after it is submitted to Different Pasteurization Treatments (Noci et al., 2008)

Caminiti et al., 2011, studied the effect of combining Ultrasound (US) and UV-Light (UV) with High Intensity Light Pulses (HILP). Sensory properties such as juice appearance, odour, flavour, sweetness, acidity and overall acceptability of a blend of cranberry and apple juice were analyzed. The HIPL system was composed by a Xenon flash lamp with a total energy dosage of 3.3 J/cm^2 positioned at 1.9 cm from two quartz tubes where the juice was pumped with a 20.8 ml/min flow rate. Obtained results showed no significant change in pH, Brix and colour for the juice treated with the UV and HILP combined. However, when these two methods were combined with US, a noticeable change in flavour and odour was observed. The change in the fluid colour using sonication treatment (US) had been proved by Cheng et al., 2007 and Tiwari et al., 2008, using orange juice. Regarding the evaluation of overall juice acceptability (Caminiti et al., 2011), UV+PEF combined appeared to provide a method (score 5.8) yielding better results than Thermal Pasteurization.

Koutchma et al., 2004, investigated the efficacy of UV-Light for 5-log CFU/ml reduction of E. coli K-12 using laminar and turbulent flow. The effects of absorbance and turbidity were studied in a locally purchased pasteurized apple juice and compared to different

solutions of caramel in malate buffer. The laminar flow experiment used reactor volume of 0.217 L, flow rates of 56.8, 110.3 and 165.7 ml/s, mean residence times of 3.82, 1.97 and 1.31 s and a UV lamp output power of 312 W (8 x 39W). The turbulent flow was generated in a reactor volume of 14.72 L, with a flow rate of 250-1300 ml/s, a mean residence time of 60s and a UV lamp output power of 504 W (12 x 42W). These studies showed that the inactivation of E. coli in turbulent flows follow a linear first order kinetics and a 5-log CFU/ml reduction of E. coli in apple juice when passing the fluid seven times through the reactor. On the other hand, laminar flows present a non-linear kinetic for microorganisms inactivation making the reduction calculation insufficient to accomplish the safety requirements.

Thus, given the above described technical literature, one can notice the limitations of the various methods discussed such as: i) the HST treatment alters volatile compounds responsible for the sensorial characteristics of the juice, ii) the PEF offers challenges in the scale up, iii) the PEF has to be combined with US to achieve the 5-log CFU/ml microbial reduction, iv) the application of UV-Light involves complex degradation kinetics when the juice is treated in units with laminar flows.

As a result, one can see the need of new methods for degradation of microorganisms in fruit juice. In this respect, one can notice that advanced oxidation methods, have been successful for the degradation of organic pollutants in water and appear to be a very good alternative for organic acids degradation in opaque fluids.

3.2 Photocatalytic Oxidation Process

Advanced oxidation methods such as Photocatalysis (Sobczynski et al., 2001) were originally developed for the hydrogen production from water. However, photocatalysts display a high capacity to degrade organic compounds. This is the case when they are exposed to a source of near UV-Light. These properties are important for the photodegradation of organic pollutants in water.

Semiconductor photocatalysts (Ahmed et al., 2010 and Al-Rasheed et al., 2005), along with a light source and an oxidizing agent such as oxygen or air, destroy organic

pollutants during the process of photocatalytic oxidation. The precursor of this oxidation reaction is the excitation of valance band electrons by photons with energies higher than the band-gap energy. Once this happens, a positive hole in the valence band, along with an electron in the conduction band are produced. This initial phase is followed by a number of steps involving OH radicals. Furthermore, the oxygen available is reduced with the formed electrons in the conduction band.

According to Cho et al., 2004, the major photocatalytic reaction steps are as follows:

(I) $TiO_2 \xrightarrow{h\vartheta} TiO_2(h^+_{vb} + e^-_{cb})$

(II) $O_2 + e^-_{cb} \rightarrow O_2^- \bullet$

(III) $O_2^- \bullet + e^-_{cb} + 2H^+ \rightarrow H_2O_2$

(IV) $O_2^- \bullet + H_2O_2 \rightarrow \bullet OH + OH^- + O_2$

(V) $e^-_{cb} + H_2O_2 \rightarrow \bullet OH + OH^-$

(VI) $h^+_{vb} + OH^- \rightarrow \bullet OH$

(VII) $h^+_{vb} + H_2O \rightarrow H^+ + \bullet OH$

(VIII) $2 \bullet OH \rightarrow H_2O_2$

Hydroxyl radicals (OH·) and reactive oxygen species (ROS) such as $O_2^{\cdot}$ and H_2O_2 play an important role in the photoconversion of organic compounds using TiO_2 catalysts (Cho et al., 2004). Hydroxyl radicals are the primary oxidants, with oxygen acting as an electron scavenger, preventing hole pairs to re-combinate. In addition, if electrons accumulate in the conduction band (CB), an increase in the recombination of e^- and h^+ occurs. For this reason, the accumulation of electrons in photocatalytic oxidation should be prevented.

An important factor to be considered regarding the photocatalyst surface is that an ideal photocatalyst should be stable and should be chemically and biologically inert. It should

be widely available at a low cost, and it should be capable of absorbing reactants under efficient photonic activation (Sobczynski et al., 2001).

Titanium dioxide (TiO_2) is the measuring stick against which emerging materials are measured. There are two types of TiO_2 catalysts available: anatase and rutile. Degussa P25 has been extensively used for photocatalytic reactions and is composed of a mixture of anatase and rutile. This catalyst presents band gap energy of 3.2 eV. Thus, any photon with a wavelength smaller than 388 nm is capable of exciting the TiO_2 catalyst promoting photocatalytic degradation (de Lasa et al., 2005).

Additionally, other important issues to be considered before performing a photocatalytic reaction is the choice of the design characteristics of the PhotoReactor such as: i) the catalyst state, and ii) the type/position of light source (de Lasa et al., 2005). Regarding the catalyst state, it can be either in suspension or immobilized. The suspended photocatalyst presents degradation rates three times greater than the second (Mattews and McEvoy, 1992). However, in the case of the suspended photocatalyst, there is a need of particle separation at the end of the photoconversion process. Thus, immobilized TiO_2 is considered more economically viable.

Regarding the type of light source, there are two categories of sources: i) near UV lamps and ii) solar light. In this respect, the light source in the Reactor can be disposed in three different configurations: i) internal, ii) external and iii) distributed with an optical device that brings irradiation from an external source and distributes it inside the reactor. According to Friedmann et al., 2010, when choosing the light source, not only should one consider the increase of degradation efficiency but also the commercial availability related to the cost of the light source and the power consumption. This makes solar light sources a good alternative for photocatalysis.

The mechanism of degradation of organic compounds in presence of TiO_2 aims to achieve the complete photoconversion of the organic molecules in water and carbon dioxide. However, the presence of intermediates on the catalyst surface affects the kinetics of the photoconversion of the model organic compounds. For this reason intermediates need to be taken into account (Friedmann et al., 2010). The number of

intermediates and rate of decomposition depend on the chemical properties of the organic molecule to be degraded. In the case of carboxylic acids, they are known for their high adsorption on TiO_2 surfaces mainly at a low pH (Franch et al., 2004 and Tran et al., 2006). According to Irawaty et al., 2011, the reaction rate for the photoconversion of malic acid under TiO_2 in suspension, is influenced by intermediates formed during the reaction. This shows the importance of studying intermediates species in order to be able to establish the overall rate of the key organic species degradation.

3.2.1 Application of Photocatalysis for Opaque Fluid Decontamination

The photocatalytic degradation of microbial microorganisms such as E. coli in water media using TiO_2, both in suspension and immobilized, has been reported by diverse authors (Maness et al., 1999; Bhatkhande et al., 2001, Balasubramanian et al., 2004; Gelover et al., 2006; among others). These studies show good promise for photocatalysis applications with a 5-log CFU/ml pathogen reduction reached in water media. Moreover, the use of photocatalysis for organic acid photodegradation in water using TiO_2 suspended and immobilized has been also reported more recently (de Lasa et al., 2005; Fuleki et al., 1995; Chen et al., 2009; Irawaty et al., 2011; among others). In the case of opaque fluids, catalyst films appear as an alternative to overcome the high absorption of irradiation in these fluids. In this respect, one can envision immobilized TiO_2 on various substrates such as thin films in order to combine good microbial microorganisms' inactivation and very limited photodegradation of malic acid and its intermediates, in order to preserve the sensorial properties of opaque fluids.

3.2.1.1 TiO_2 Photocatalysis for the Degradation of Organic Contaminants in Water

3.2.1.1.1 Photocatalysis with TiO_2 in Suspension for Microbial Reduction

Photocatalysts are solid particles that promote reactions when irradiated with light, without being consumed during the reaction (Bhatkhande et al., 2001). Many studies

have been performed in this area, showing good promise of photocatalysis for water treatment.

Robertson et al., 2005, investigated the effectiveness of photocatalysis using TiO_2 in suspension in a batch reactor for water treatment. A sample of water inoculated with three bacterial pathogens (Escherichia coli, Salmonella enteric and Pseudomonas aeruginosa), was exposed to three types of treatment steps: 1) Adsorption on TiO_2 without irradiation; 2) Adsorption on TiO_2 combined with UVA-Light (spectral output 330-450 nm, light intensity of 3.42 x 10^{-5} Einstein s^{-1}, time of irradiation 2h) and 3) UVA-Light irradiation alone. Experiments were performed with values of pH between 5 and 8, and temperature varying from 21 to 29 ºC. Results showed a higher rate of reduction for the method using UVA-Light irradiation of the TiO_2 photocatalyst for E. coli and Salmonella inactivation, reaching a 5-log CFU/ml reduction. For the P. aeruginosa reduction, the method applying UVA-Light alone showed a higher rate of microbial reduction. However, in the experiments performed with UVA-Light only, the existence of small colony variants (SCV's) was observed. These were described as a colony phenotypes formed from the bacterial survivors. According to Proctor et al., 1995 and Haubler et al., 1999, SCV's can promote the reactivation of the microorganisms. For all these reasons, the method applying UVA-Light with TiO_2 was considered more efficient overall. Results of these studies are similar to those obtained by Rincon et al., 2003 and 2004.

Maness et al., 1999, also investigated the effect of TiO_2 on the photodegradation of E. coli. The experiments were developed using Degussa P25 in suspension from 0.1 to 1 mg ml^{-1}, 1.2 x 10^8 CFU/ml of E. coli K-12, two 40 W BL-lamps with Intensity 8 W m^{-2} and 356 nm maximum wavelength. Results showed that E. coli degradation increases with TiO_2 concentration reaching a maximum value for 1 mg/ml of TiO_2. By measuring the formation of malondialdehyde (MDA) and the lipid peroxidation product, it was proven that irradiated TiO_2 can promote the inactivation of E. coli. It is assumed that this may be due to E. coli cell membrane extra stresses causing the cell death. In their research, Maness et al., 1999, proposed that photocatalytic degradation of E. coli is promoted by reactive oxygen species (ROS) such as O_2^-, H_2O_2 and $OH^\bullet$.

In order to understand the degradation mechanism for microbial reduction, Cho et al., 2004, investigated how OH radicals and reactive oxygen species (ROS) interact with E. coli on TiO_2 surfaces. Photocatalytic inactivation experiments were performed in a 60 ml Pyrex slurry reactor with TiO_2 in suspension. Parameters such as: (a) dissolved O_2, (b) TiO_2 concentration, (c) light intensity, (d) temperature and (e) pH, were varied during the experiments. The value of CT (disinfectant dosage multiplied by contact time with the contaminant) obtained for OH radicals was 0.8×10^{-5} mg min/L. This is more than a thousand higher than the value for well-known disinfectants such as chlorine, ozone and chlorine dioxide (1.3×10^{-1} mg min/L, 4.0×10^{-2} mg min/L and 8.0×10^{-2} mg min/L, respectively). Furthermore, the results showed a good linear fit between the OH radicals produced and the E. coli degradation under TiO_2 photocatalysis (R^2 equal to 0.97). This confirms that the OH radicals are the greatest responsible species for E. coli reduction.

3.2.1.1.2 TiO_2 Immobilized Photocatalysis for Microbial Reduction

As discussed before, immobilized TiO_2 has been used in photodegradation of various organic compounds in water due to its advantage of making filtration a redundant step after the photodegradation, saving both time and cost in the industrial process.

Choi et al., 2007, investigated the use of membranes and nanostructure TiO_2 films in the photodegradation of organic pollutants in waste water. TiO_2 film with specific surface area of 147 m^2/g, 62.2 $\mu g/cm^2$ of catalyst and a predominant mesoporous size distribution degraded E. coli completely after 3 hours with a 4-log CFU/ml reduction. A TiO_2/Al_2O_3 membrane degraded 30 μM of methylene blue in 14 hours, with the formation of creatinine as an intermediate responsible for the delay in the degradation. By analyzing the amount of TiO_2 used in both film and membrane respectively (0.0078% m/v and 0.0234% m/v), it was concluded that the catalyst film/membrane showed a high activity and could be used for the photocatalytic degradation of organic compounds in water.

The preparation and characterization of TiO_2 film on a stainless steel support was also studied by Balasubramanian et al**,** 2004. The results were compared with commercial TiO_2 and sol-gel TiO_2 catalyst. The experiments were performed in a quartz batch reactor with a volume of 2.5 L and a temperature 25ºC. The reactor was continuously aerated

with humid air and irradiated with UV-Light at a wavelength range of 300-400 nm. TiO_2 immobilized on stainless steel and in suspension were used. It was observed, through the rate constant measurements, that the catalyst photoactivity increases with the number of coating layers for both types of catalyst films, these being: (a) conventional alkoxide sol and (b) Degussa P25 enriched alkoxide sol. Comparing the activity of the two different catalyst coatings, it was observed that the Degussa P25 enriched sol photocatalyst presented higher photoactivity. This can be explained by the presence of rutile in the Degussa P25 catalyst. Brown et al., 1989 and Wang et al., 1997, have reported that adding rutile to the anatase catalyst increases photoactivity. Even though the rutile has a smaller activity by itself, the increase in photoactivity of the mixture (anatase and rutile) occurs as a result of rutile capturing the electrons formed on the anatase surface. This stabilizes the holes in the anatase by preventing recombination.

Furthermore, once the activity of 0.5 g/L of TiO_2 was considered using pure anatase and Degussa P25. Degussa P25 (surface area 53 m^2/g) showed the highest activity with the rate constant being three times greater than anatase (surface area 320 m^2/g).

The use of sol-gel TiO_2 films in water disinfection using sunlight was investigated by Gelover et al., 2006. Comparing the results of the solar water disinfection (SODIS) and solar degradation with TiO_2 films (87.5 mg of TiO_2 per liter), with water having fecal coliforms and E. coli, it was observed that water samples not exposed to the sunlight did not show any change in their contamination level with catalyst or without photocatalyst. However, when exposed to sunlight, the sample ($3x10^3$ MPN/100 ml) had a complete inactivation of total coliforms after 20 minutes in the presence of a TiO_2 film and after 60 minutes without TiO_2. For the fecal coliforms, the sample in presence of TiO_2 was completely inactivated after 30 min. In the absence of TiO_2, it provided photodegradation from $3x10^3$ MPN/100 ml to 100 MPN/100 ml after 80 minutes of sunlight exposure. In both cases the experiments showed that coliforms do not grow again after the photocatalytic disinfection, confirming the efficacy and reliability of this method for water disinfection.

The use of immobilized nanoparticle TiO_2 films to photoconvert E. coli was investigated by Dheaya et al., 2009. This study was performed with water samples containing different organic and inorganic compounds. Degradation rate of $2x10^3$ CFU/ml of E. coli, with TiO_2 Degussa P25 was obtained. The UV-Light (maximum at 370 nm) was placed at the bottom of the reactor and the TiO_2 layer was irradiated through the layer face not in direct contact with the fluid. The results showed a zero order kinetic for E. coli inactivation in water using an optimum catalyst loading of 0.5 mg/cm^2. The change in pH did not affect the E. coli degradation rate. However, the presence of organic and inorganic species in surface water made the microbial reaction rate slower than its reaction using distilled water.

3.2.1.2 Photocatalytic Degradation of Carboxylic Acids (Malic and Malonic Acid) in Water

3.2.1.2.1 Photocatalysis with TiO_2 in Suspension and TiO_2 Composites in Suspension

As reported before, photocatalysis appears to be a good alternative for the non-thermal treatment of apple juice aiming to reduce the microbial amount for food safety reasons. This is accomplished while keeping the key compounds that are responsible for the authenticity of the juice. In this way, and due to the fact that organic acids are present in a significant amount in fruit juice, their identification and rate of photoconversion are critical (Fuleki et al., 1995).

Malic acid is the main organic acid found in apple juice and its minimum concentration required for the market commercialization is 3.0 g/L (AIJN 6.3 Reference Guide Apple - Revision May 2011). Thus, the study of malic acid photoconversion under TiO_2 photocatalysis is extremely important when considering the use of this method for apple juice preservation.

The photocatalytic degradation of carboxylic acids using slurried TiO_2 is quite well-known. It features the advantage of a high surface area ($50m^2/g$) which confers a high photocatalytic activity. However, it presents some disadvantages (Gelover et al., 2006)

such as: (a) particle agglomeration when working with high photocatalyst concentrations, (b) difficulties with particle recovery once photoreaction is complete, (c) low efficiency of the process due to the light scattering afar from the lamp source.

The mechanism of the photocatalytic degradation of malic acid was investigated using TiO_2 in suspension (Irawaty et al., 2011). The experiments were performed at pH of 3±0.05. The characteristics of the intermediates and products in each step of the reaction were noted. The results obtained display complete mineralization after 38 minutes. Figure 3.2 reports the formation of intermediate 1, malonic acid and acetic acid, with this being the case since the very beginning of the reaction. For instance, the photodegradation of malic acid was observed after 8 minutes, intermediate 1 and malonic were consumed after 24 minutes. Acetic acid was removed after 36 minutes.

According to Irawaty et al., 2011, the kinetics of malic acid degradation fits the Langmuir-Hinshelwood Model. The formation of three intermediates: intermediate 1, malonic acid, and acetic acid, is observed. Malic acid is completely degraded after 8 minutes while malonic acid and intermediate 1 reach a maximum concentration after 4 and 9 minutes, respectively. Malonic acid starts degrading only after complete photoconversion of malic acid. This demonstrates that although there is a competition between these two species for catalyst surface sites, malic acid adsorption is very likely to occur. According to these authors, organic acids absorb strongly on the TiO_2 surface, mainly at low pHs. This can be explained as a result that in acid media, these organic acids are chemically dissociated with the photocatalyst surface being positively charged.

Furthermore, at a concentration of malic acid lower than $1x10^{-3}$ mol/L, its photocatalytic degradation follows a first order rate equation. In addition, it is suggested that malic and malonic acid degradation occurs through a photo-Kolbe mechanism (molecule decarboxylation) promoted by holes photogenerated on the catalyst surface. On the other hand, acetic acid is weakly adsorbed on TiO_2 surface and thus, its degradation is suggested to occur by OH radicals in the bulk solution.

FTIR (Fourier Transform Infrared Spectroscopy), Zeta Potential and Dark Adsorption analysis showed the affinity between the organic acids and the TiO_2 surfaces, as well as

the competitive adsorption between those acids. This can explain the pathways observed in the reaction of Figure 3.2.

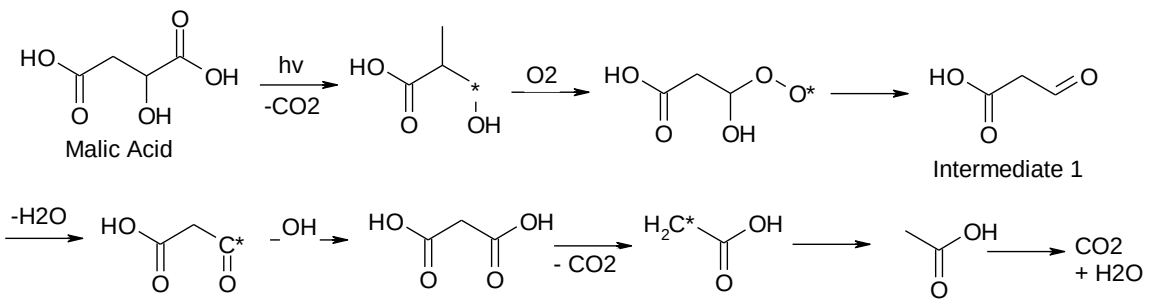

Figure 3.2: Mechanism for the Photocatalytic Degradation of Malic Acid in the Presence of TiO_2 in Suspension at pH of 3 (Irawaty et al., 2011)

Irawaty et al., 2011b, used a slurry spiral reactor for the photocatalytic degradation of succinic acid, malic acid and tartaric acid with 0.2 g/L of TiO_2 in suspension at a pH 3±0.05. Results were analyzed with a TOC and HPLC detectors and Zeta Potential Analyzer. Photolysis and photodegradation without irradiation (dark conditions) were not observed for any of the organic species. The complete mineralization of 210 μmol/L of malic acid was obtained after 38 minutes. The surface coverage was 0.41 molecules/nm^2, fitting the Langmuir-Hinshelwood mechanism as previously proposed by Chen et al., 2009.

The zeta potential for the malic acid degradation showed just a small change from 0 to 22 minutes. After this point, a significant increasing in the zeta potential occurred due to the removal of the intermediates and formation of ethanoic acid. Photodegradation experiments showed that the intermediate propaneodioic acid species was present. It was suggested that the intermediate A1 was 3-oxopropanoic acid. Thus, the degradation pathway study considers that carboxylation starts at the position adjacent to OH group.

Chen et al., 2009, investigated photocatalytic degradation of malic, maleic, propanoic, oxalic, succinic, propanoic and acetic acid was investigated by, using a slurry photoreactor. Degussa P25 powder and near UV-Light source, with a maximum wavelength in 365 nm were employed. The experimental results fit within the Langmuir-

Hinshelwood Model (see Equations 3.1 to 3.3), with k (apparent reaction rate constant) increasing with n (heterogeneity exponent) for species with the same number of carbon atoms. The effect of the initial concentration of carboxylic acids showed that k augments with the increase of the initial concentration of acetic, oxalic, malonic and propanoic acid, while k decreases with the increase of the initial concentration of malic, tartaric and succinic acid (Table 3.2).

Results can be explained due to malic, tartaric and propanoic acids produce more intermediates than acetic, oxalic, malonic and propanoic acid. Thus, the effect of competition for the active sites on the catalyst between intermediates and initial reactants reduce the photoreaction rate. It is interesting to note that the fastest photocatalytic degradation occurred with oxalic acid. This can be explained due to the fact that dicarboxylic acids display two hydroxyl groups bonded to a single Ti site. This is a stable configuration when compared to ones of the other organic acids.

The effect of catalyst dosage shows that k increases with the increase in the TiO_2 concentration until it reaches a stable value (around 2 g/L). Further increases in photocatalyst loading decrease k due to catalyst agglomeration with reduced irradiation of photocatalyst sample. In addition, increasing light intensity from 1.38 to 2.44 mW/cm^2 augments the value of k. Moreover, it is shown that k values increase at lower pHs. This shows that H^+ species have an important effect on the photocatalytic degradation of carboxylic acids, as is claimed by Chen et al., 2009. These authors found higher adsorption of carboxylic acids in TiO_2 at low pH values. Experiments performed using a slurry reactor in presence of TiO_2 Degussa P25 can be used in the study of the kinetic degradation of pollutants in water applying the Langmuir-Freundlich-Hinshelwood Model (Chen et al., 2009).

$$r = -\frac{dC}{dt} = k\theta \tag{3.1}$$

$$\theta = \frac{(KC)^n}{1+(KC)^n} \tag{3.2}$$

$$r = -\frac{dC}{dt} = \frac{k(KC)^n}{1+(KC)^n} \tag{3.3}$$

Where k is the apparent kinetic constant, θ is the surface coverage factor, C is the organic compound concentration, K is the adsorption constant and n is the heterogeneity exponent (catalyst adsorption capacity).

Table 3.2: Rate Constant for Aliphatic Carboxylic Acids (Chen et al., 2009)

Carboxylic Acids	Rate constant equation
Acetic acid	$k = 1.10 \times 10^{-3} + 1.13 \times 10^{-5} C_0$
Oxalic acid	$k = 1.17 \times 10^{-3} + 1.24 \times 10^{-5} C_0$
Propanoic acid	$k = 1.01 \times 10^{-4} + 5.83 \times 10^{-6} C_0$
Malonic acid	$k = 4.93 \times 10^{-3} + 4.12 \times 10^{-5} C_0$
Succinic acid	$k = 0.27 + 1.12 \times 10^{-2} C_0$
Malic acid	$k = 1.00 C_0^{-0.36}$
Tartaric acid	$k = 0.51 C_0^{-0.05}$

Another approach to improve the rate of photocatalytic degradation of organic acids in water is to use some chemical species such as Fe (III). These iron cation when in contact with TiO_2, form chemical complexes, increasing the photoactivity of the catalyst (Balzani et al., 1970). The photocatalytic degradation of malic acid and malonic acid in the presence of $Fe_2(SO_4)_3$ and $FeCl_3$ (Franch et al., 2004) was studied.

TOC measurements showed that the same intermediates are formed in the two different Fe(III) solutions. For the $Fe_2(SO_4)_3$, the main intermediate for the malic acid degradation was found to be malonic acid. It was formed as a result of the decarboxylation at the position α (first carbon adjacent to the C=O) and with the addition of oxygen to the carbon containing radicals. Traces of tartaric acid, glyoxylic acid, formic acid and acetic acid were also observed as intermediates.

In the presence of $FeCl_3$, glyoxylic acid appears in a higher concentration at the beginning of the reaction and this when compared with the photoreaction using $Fe_2(SO_4)_3$. After 120 minutes, glyoxylic acid disappears and the formation and consumption of malonic acid is slower than when using $Fe_2(SO_4)_3$. The proposed mechanism for malic acid degradation is explained in the Figure 3.3.

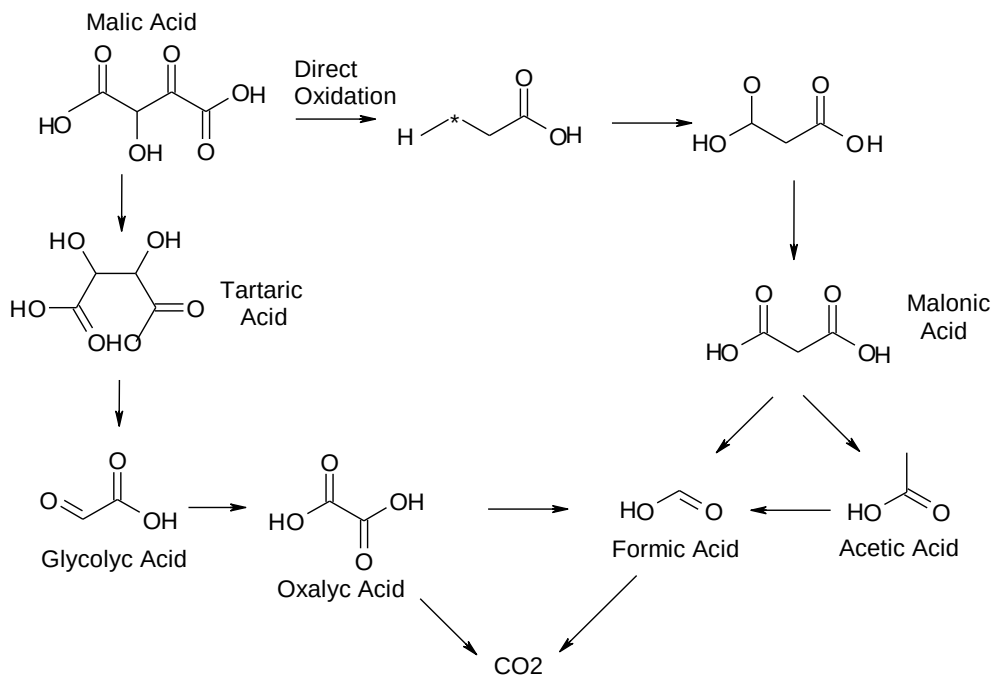

Figure 3.3: The Routes for the Photocatalytic Degradation of Malic Acid in the Presence of Fe(III) under UV-Light Source (Franch et al., 2004)

For the degradation of malonic acid (Franch et al., 2004), the two intermediates found were formic acid and acetic acid, with the latter being very stable and responsible for the low decline in the TOC values.

The proposed mechanism for malonic acid degradation is shown below:

$$Fe(III) - O_2CCH_2CO_2^- \rightarrow {}^-O_2C - CH_2^\bullet + CO_2 + Fe(III) \quad (3.4)$$

$${}^-O_2C - CH_2^\bullet + RH \rightarrow {}^-O_2C - CH_3 + R^\bullet \quad (3.5)$$

$${}^-O_2C - CH_2 + O_2 \rightarrow {}^-O_2C - CH_2O_2^\bullet \quad (3.6)$$

$${}^-O_2C - CH_2O_2^\bullet \rightarrow \rightarrow \rightarrow \ HCO_2H \quad (3.7)$$

Overall, since Fe(III) solutions are found in natural waters, understanding how these species affect the photocatalytic degradation of organic compounds is important. According to Franch et al., 2004, reactions followed a zero-order kinetics with the values of the rate constants being a function of the Fe(III) salt solution used. These finds provide

evidence that the organic acids can be very reactive with this being a function of the Fe(III) salt solutions used.

3.2.1.2.2 TiO_2 Immobilized Photocatalysis

As discussed before, the popularity of the use of immobilized photocatalysts and in particular photocatalyst thin films has increased recently for the degradation of organic compounds in water solutions. These applications appear to be important alternatives for industrial processes given that there is no filtration step required (Watanabe et al., 1999 and Zeman et al., 2003).

Thin film applications were demonstrated with the photoconversion of malic acid (50 mg/L) using a 220 ml volume reactor housing 57 optical fibers. Fibers were coated with five layers of TiO_2. A 340 nm cut-off filter was used to prevent the photochemical reaction of malic acid (Danion et al., 2007). The degradation of malic acid and the formation of intermediates were measured using HPLC with a UV detector as well as by utilizing Total Organic Carbon analysis. Results showed that the adsorption of malic acid on TiO_2 during the initial period without irradiation was reached in one hour and the amount adsorbed was 4%. Regarding the degradation kinetics under UV-light (wavelength of 340nm), it was observed to be of first order. Experiments showed that five intermediate species (tartaric acid, maleic acid, pyruvic acid, malonic acid and fumaric acid) were formed during photodegradation. Malonic acid appeared to be the main intermediate displaying a predominant photo-Kolbe mechanism. Overall, the photoreaction showed a 21% reduction of total organic carbon (TOC) with 3% representing various intermediate species. The photonic efficiency based on the photons irradiated from the source was assessed at 6.0%, with this being higher than the one of conventional slurry reactors (2.8%).

Herrmann et al., 1999, performed malic acid photodegradation experiments in two reactors: (a) a Batch Reactor Laboratory Scale irradiated by an external high pressure mercury lamp of 125 W and, (b) a Slurry Solar Reactor unit. Experiments were performed using powered TiO_2 and immobilized TiO_2 supported on quartz, glass and steel.

In the smaller batch laboratory reactor, a solution of 500 ppm of malic acid was treated under three different conditions: i) No loaded TiO_2 which resulted in a negligible malic acid concentration reduction, ii) TiO_2 loaded without irradiation (dark conditions) which resulted in a 10% malic acid concentration decrease, iii) TiO_2 and UV-light (λ = 290nm) which resulted in a complete malic acid degradation after 90 minutes. Photodegradation kinetics appears to follow a Langmuir-Hinshelwood rate. Among the 15 intermediates found during the experiments while having TiO_2 under irradiation, the main observed intermediate species was 3-oxopropanoic acid (malonaldehydic acid). It suggests a mechanism of photo-Kolbe reaction (abstraction of a molecule of CO_2) by an h^+ specie on the carboxylic group adjacent to C-OH (α position). Posterior H abstraction on the α position by an $OH^\bullet$ promotes the formation of the 3-oxopropanoic acid.

In the solar irradiated large reactor, the degradation of 500 ppm of malic acid happened after a residence time of 120 min and appeared to occur as a zero order reaction Langmuir-Hinshelwood mechanism. However, the TOC reduction required a longer time (270 min). This was the case when compared to the malic acid degradation due to the presence of intermediates in the solution. Regarding intermediates, they were the same type found in the small scale reactor but in smaller quantities. This demonstrates that faster reaction can be expected in a solar irradiated unit.

Regarding the supported photocatalyst, it was deposited on quartz displaying a higher degree of crystalline phase than those prepared on glass. Furthermore, a faster degradation of malic acid was found in 1 hour versus the 3 hours required for TiO_2/glass and TiO_2/steel.

The kinetic constants for the various supports were: 4.73×10^2 $g.h^{-1}$ for TiO_2/glass, 1.29×10^2 $g.h^{-1}$ for TiO_2/steel, 3.74×10^3 $g.h^{-1}$ for TiO_2/quartz and 2.43×10^3 $g.h^{-1}$ for TiO_2 Degussa P25 in suspension. This shows that the TiO_2/quartz layer can provide a kinetic constant of one order of magnitude higher than the other two types of immobilized catalyst. The Figure 3.4 reports the main pathway for the malic acid degradation.

Figure 3.4: Main Reaction Pathway for Malic Acid Degradation under TiO_2 at 290 nm (Herrmann et al., 1999)

Fernandez et al., 1995, tested dip coated TiO_2 on glass and quartz as well as electrophoretic deposition of TiO_2 on a metallic support in malic acid photocatalytic degradation. The XPS photoelectron graphs showed the presence of Na and Si (9 to 12 atom-%) in the layers prepared on glass due to the diffusion of these ions during the calcination at 673K. In addition, UV-visible absorption spectra showed that the samples are only partially transparent with some specular and diffuse reflectance. Regarding malic acid adsorption, it can be noted that a similar extent of adsorption for the three supports occurred with the complete photocatalytic degradation being faster using a quartz support (1 hour) than a steel (3 hours) support. Malic acid photolysis was considerably reduced using the photocatalyst layer, which acted as a radiation filter.

On the other hand, the photocatalytic degradation followed a Langmuir-Hinshelwood Mechanism. Due to the small concentration of malic acid studied (50 ppm), the reaction could be approximated using an apparent first order reaction as follows:

$$r = -k\theta = -\frac{kKC}{(1+KC)} \tag{3.8}$$

with k being the intrinsic rate constant and K the adsorption constant

Since the initial concentration is very small, KC can be neglected and the rate equation becomes:

$$r = -\frac{dC}{dt} = kKC = -kKC \tag{3.9}$$

Regarding the better activity of the catalyst on quartz, when compared to the other supports, it was explained that this was due to the interaction between TiO_2 with the supports during photocatalyst layer preparation. The heat treatment may cause migration of the Na^+ and Si^{4+} cations from the glass as shown with XPS analysis and the movement of Fe^{3+} and Cr^{3+} from stainless steel as proven with EDX. These phenomena caused inhibition of the TiO_2 activity on these two supports. Quartz, on the other hand is a very stable support under the influence of heat with the various side effects described above being circumvented.

A cylindrical photoreactor (Herrmann et al., 1997) open to the air and with quartz (Q) plates supporting the catalyst (TiO_2/Q and Ag-TiO_2/Q) in a vertical position from the light source was used to study the photodegradation of malic acid at 50 ppm concentrations. Results of the mineralization reaction (COOH-CHOH + $3O_2 \rightarrow 4CO_2 + 3H_2O$) were analyzed by HPLC and compared to the performance of a slurry reactor using TiO_2 in a powder form. The analysis of both catalysts showed that Ag-TiO_2/Q film is more transparent and smoother than TiO_2/Q, which appears partially opaque. Values of total surface area of the catalyst exposed in the TiO_2/Q and Ag-TiO_2/Q films were estimated. This was done by first calculating the ratio of moles adsorbed by TiO_2/Q and Ag-TiO_2/Q films and by multiplying this value by the total surface area of 5 mg of the TiO_2 in powder (0.25 m^2). Moreover, the photoconversion rates observed show that malic

acid is completely degraded in 30 to 60 min and that the kinetic constants values follow this order: Ag-TiO_2/Q ≤ TiO_2/Q < Ag-TiO_2/Q (hν) < TiO_2 (powder). The degradation of both catalysts follows a Langmuir-Hinshelwood model with an apparent first order rate equation. It appears that the presence of Ag ions prevent electron-hole recombination given that Ag^+ attracts electrons.

Sarantopoulos et al., 2009, investigated the preparation of catalyst films on flat glass and micro-fibber plates. The two films were characterized by X-ray Diffraction, Scanning Electron Microscopy (SEM), and BET method. Following this step, the two films were used to study the photodegradation of malic acid. The morphology of the layer was shown to depend on both, the preparation temperature and layer thickness. For a thickness smaller than 400 nm and temperature of 400ºC, the catalyst layer has a columnar morphology (crystals grow in the vertical direction upwards). Comparing the catalyst layer on flat glass and micro-fiber plates with a similar thickness, it was observed that the void fraction and the specific surface area was the highest for flat glass: 50% and 17 m^2/g.

Photocatalytic activity was shown to depend on plate geometry. For instance, it was observed that for a catalyst layer prepared at 400ºC, the malic acid degradation rate increases with the thickness of up to 750 nm at which point it stabilizes given this increase. A thicker layer causes the irradiation penetration to diminish.

Malonic acid degradation was investigated in a small flow-through cell with a TiO_2 film deposited in a Germanium Internal Reflection Element (IRE), presenting a high refractive index, and with an ATR-IR Spectroscopy detector attached to the system (Dolamic et al., 2006). The reactant was circulated through the catalyst layer at a flow rate of 0.2 ml/min. The Absorbance Spectrum versus wavelength shows that when the cell is irradiated, the malonic acid coverage on the TiO_2 layer decreases: the band at 1350 cm^{-1} is negative while the bands at 1690 cm^{-1} and 1708 cm^{-1} are positive. This allows speculating the formation of chemical species. Species formed at 1708 cm^{-1} do not contain hydrogen, showing the oxalate structure. On the other hand, two bands were observed in the 1700

cm^{-1} range and were assigned to two C=O groups indicating a symmetrical adsorption of the malonic acid regarding the C=O position on the TiO_2 surface.

According to Dolamic et al., 2006, the mechanism for the degradation of malonic acid starts with a photo-Kolbe reaction (abstraction of a CO_2 molecule by an electron hole). Following this, the species produced react with CO_2. It is expected that these species will help to form acetic acid. However, acetic acid is weakly adsorbed in the spectra. In addition, radical species can also react with O_2 forming oxalic acid, which is observed in the Attenuated Total Reflected Infrared (ATR-IR) spectra. Oxalic acid is observed in small amounts in the water phase with larger amount of oxalic acid remaining on the catalyst surface. Another possible pathway is the h^+ reacting with oxalate ($^-OOC\text{-}COO^-$) adsorbed on the TiO_2 surface producing CO_2 and $CO_2^{\bullet -}$.

Guo et al., 2002, investigated the photochemical behavior of different microporous polyoxometalates designated as POM's ($H_3PW_{12}O_{40}/SiO_2$, $H_4SiW_{12}O_{40}/SiO_2$, $Na_4W_{10}O_{32}/SiO_2$) for the degradation of hydroxyl butanedioic acid (malic acid). Experiments were performed in a cylindrical quartz photoreactor using a mercury lamp (125 W), a temperature of 20±2°C and optical path length of 2cm.

Adsorption Isotherms of the POM showed that these compounds have pores size of 0.60 nm (type I Isotherm), providing a large surface area and pore volume when combined with a SiO_2 matrix. Best photodegradation results were observed under near UV light. Malic acid was completely photodegraded after 180 minutes using $H_3PW_{12}O_{40}/SiO_2$, $H_4SiW_{12}O_{40}/SiO_2$ and 90 minutes using $Na_4W_{10}O_{32}/SiO_2$.

Malic acid degradation using POM/SiO_2 showed higher rates for $Na_4W_{10}O_{32}/SiO_2$ than for $H_3PW_{12}O_{40}/SiO_2$, $H_4SiW_{12}O_{40}/SiO_2$. For any of the three POM's used, the malic acid photodegradation displayed a Langmuir-Hinshelwood apparent first-order model. Comparing the intermediates from POM/SiO_2 and TiO_2 photodegradation it was found that they both follow a similar reaction mechanism except for the formation of heteropoly blue, HPB (electron species produced by the POM reduction) on the POM/SiO_2 surface. This suggests that both $OH^\bullet$ and POM/SiO_2 are responsible for the photocatalytic degradation of malic acid.

3.3 Conclusions

Regarding the current methods for opaque fluids decontamination one can conclude from the authors:

a. Thermal Pasteurization (HSTS) achieves the 5-log microbial reduction required for food safety regulations. This method has the disadvantage of causing significant changes in the flavour, taste and key chemical species such as phenolic compounds and vitamin C.

b. Pulse Electric Filed (PEF) showed a similar efficiency as HSTS reaching 5-log CFU/ml reduction. However, there is an intrinsic difficulty with the scale up of PEF to industrial applications.

c. Ultrasound (US) method cannot achieve a 5-log CFU/ml microbial reduction by itself and has to be combined to other preservation methods.

d. Ultraviolet (UV) microorganism inactivation with laminar flows leads to the formation of small colony variants (SCV's) limiting its use for juice disinfection.

e. Ultraviolet (UV) degradation in turbulent flows allows achieving a 5-log CFU/ml microbial reduction and can be used for juice preservation purposes according to U.S. FDA Regulation (21 CFR 179).

Furthermore, regarding photocatalytic oxidation of organic acids with TiO_2 in suspension and immobilized in films, one can consider the following:

a. UVA-Light irradiation on TiO_2 suspensions provided higher rate of E. coli and Salmonella reduction compared to UVA-Light alone, reaching 4-log CFU/ml microbial reduction.

b. O_2 atmospheres enhance degradation of organic compounds in TiO_2 suspensions, with this being the case when compared with air. There is no degradation under N_2 media.

c. Photodegradation rates of organic acids in TiO_2 suspension increase with light intensity, temperature and are more favourable in acid pH media.

d. TiO_2 films under UV-Light provided faster organic acid photodegradation. This is the case when compared to UV-Light alone. In TiO_2 films, catalyst photoactivity increases with the number of coating layers.

Concerning photocatalytic degradation methods for carboxylic acid photoconversion and microorganisms inactivation, the following can be concluded:

a. In TiO_2 suspension photocatalysis, the kinetics of malic acid degradation fit the Langmuir-Hinshelwood Model. At low reactant concentrations, the reaction rate follows a first order reaction with the malic and malonic acid photodegradation mechanism being of the Photo-Kolbe type. The optimum pH to obtain the highest adsorption is a low pH. This is due to the fact that organic acid species are in acid media lead to organic acid dissociation with TiO_2 film surface charged positively.

b. In TiO_2 films, with a multi-fiber reactor configuration, malic acid degradation is of first order type with malonic acid being the main intermediate specie with the reported photonic efficiency being 6.0%.

c. In TiO_2 films supported on quartz, glass and steel, both 3-oxopropanoic acid and malonic acid appear as a main intermediate of malic acid photoconversion. The quartz support was found to display one order of magnitude faster malic acid photodegradation than the other two supports.

d. In TiO_2 supported on different microporous polyoxometalates composites (POM) both OH radical and POM/SiO_2 composites shared malic acid photodegradation.

According to the technical literature, there are still some important issues that should be considered while applying photocatalysis for apple juice disinfection:

a. Photocatalysis using TiO_2 suspended is not recommended to be used for apple juice disinfection due to the need of microfiltration at the end of the pre-treatment process to remove the photocatalyst.

b. There is little technical information about TiO_2 films indirectly irradiated by a near UV-Light.

c. There are no quantum yield calculations demonstrating photocatalysis viability using indirectly irradiated TiO_2 films for organic acid photodegradation.

d. There is limited information about advisable photocatalytic time that allows using immobilized TiO_2 films for microorganism inactivation, preserving juice sensory attributes.

Chapter 4

4 Experimental Methods

4.1 Introduction

The first approach of this research was to study the photoconversion of organic compounds in opaque fluids such as apple juice using the Photo-CREC Water II Reactor with a TiO_2 photocatalyst in suspension.

As the preliminary tests showed, given the high absorption of irradiation in apple juice, a new PhotoReactor Cell was required to be developed. The new PhotoReactor Cell was designed at the Chemical Reactor Engineering Centre (CREC Laboratory) along with the University Machine Services at Western University Canada. The main goal for the new Photo Reactor Cell was to develop a setup with an immobilized TiO_2 catalyst on a support plate. In this new setup, an external UV-lamp was placed facing the interface support-TiO_2 film. In this way, the TiO_2 film receives irradiation before irradiation reaches the opaque fluid. In order for this reaction to proceed, generated electron-hole pairs have to migrate to the other face of the quartz slide, where the catalyst film is in direct contact with the fluid. As a result, the thin films implemented, combined with back-irradiation in the Reactor Cell provide a beneficial approach for the photocatalytic degradation of opaque fluids.

The reactor type chosen for these experiments was a batch reactor with the TiO_2-film supported on a quartz surface placed in the bottom of the PhotoReactor Box. Both the details about the PhotoReactor Cell setup as well as the preparation and characterization methods of the TiO_2-film will be discussed in the upcoming sections of this chapter. In addition, the various experimental details regarding: (a) the photocatalytic conversion of malic and malonic acid, (b) the preparation of the reactants water solution used, (c) the reactor setup and (d) the auxiliary equipment components employed for chemical species detection, are described in this chapter.

It is important to emphasize that the rate of photons absorbed by the TiO_2-film during the photocatalytic conversion of malic acid in water was established via a macroscopic energy balance described in Chapter 6.

4.2 Reactor Setup for the Preliminaries Experiments with Apple Juice

The first set of experiments to shed light into transmission irradiation was performed using the Photo-CREC Water-II Reactor (Figure 4.1). This slurry reactor setup consists of: (1) a stirred tank, (2) a centrifugal pump, (3) a near UV-lamp or BL-lamp, (4) a Pyrex glass with 3.58 cm diameter inner tube, (5) a replaceable Pyrex glass with a 5.6 cm diameter inner tube and (6) fused-silica windows, (7) a StellarNet EPP2000C-25 LT16 Spectrometer and (8) a SpectraWiz Software.

The dimensions of the Photo-CREC Water-II Reactor are described in the Table 4.1:

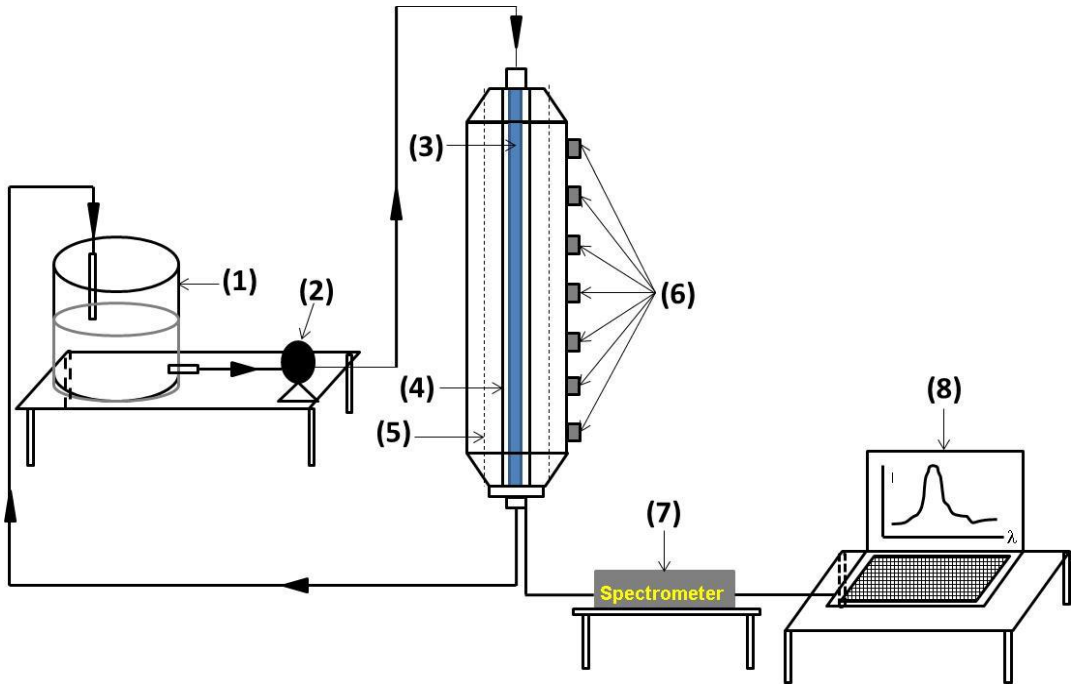

Figure 4.1: Photo-CREC Water-II Reactor Setup Employed in the Light Transmission Experiments with Apple Juice

Table 4.1: Characteristics of the Photo-CREC Water-II Reactor Setup (Slurry Reactor and UV-Lamp Source)

Component	Parameter	Measurement
Slurry Reactor	Internal radius	1.76 cm
	External radius	4.44 cm
	height	44.5 cm
	Internal Pyrex glass thickness	0.23 cm
	Illuminated reactor volume	2.5 L
UV-Lamp	length	41.3 cm
(UVP-XX-15BLB)	radius	1.33 cm
	Input power	15 W
	Output power	4 W
	Emission range	320 – 420 nm
	Emission rate	1.1910×10^{-5} Einstein.s^{-1}

In this setup, near UV irradiation of commercial apple juice (from concentrated) was studied and compared with the water spectrum. The significant extent of apple juice irradiation absorption in TiO_2 slurry reactor can be observed. It was the concluded that TiO_2 photocatalyst immobilization was required for effective use of photocatalysis in apple juice treatment.

4.3 TiO_2-film 1.5 wt% Preparation

In order to immobilize the TiO_2 catalyst, a thin layer containing a homogeneous coverage of TiO_2 catalyst was prepared. The support chosen for the TiO_2-film was quartz, which

appears to promote a better TiO_2 activity when compared to other supports (Herrmann et al., 1999; Fernandez et al., 1995).

In the initial step, the quartz surface of thickness 1.62 mm was washed with water, MICRO laboratory Cleaner (Cole-Parmer Instrument Company) and ethyl alcohol 95% (Commercial Alcohols Inc.). It was then dried before the coating. Since other more expensive methods have been proposed in the technical literature (Sumin et. al, 2011, Danion et al., 2007; Choi et. al, 2006; Song et al., 2001; Herrmann et al., 1999; Herrmann et al., 1997), a new method for TiO_2 film coating was developed.

The proposed method uses a UV-transparent/waterproof glue and a TiO_2 Degussa P25 1.5 wt% catalyst in water. This method has the advantage of being relatively simple, fast and low-cost when compared with other current methods. The glue employed on the quartz surface was the UV-transparent/waterproof glue LOCTITE® 3321™. The TiO_2 1.5wt% solution in water was prepared using TiO_2 Degussa P25 (Evonik Degussa Corporation Lot 4168012498).

The steps to prepare the TiO_2-film are as follows:

a. Spread Loctite Glue homogeneously over the quartz surface;

b. Let the glue dry partially for 24 hours;

c. Prepare a TiO_2 Degussa P25 1.5 wt% solution;

d. Spread the catalyst solution over the glue (repeat it three times);

e. Cure the layer for 1 hour with UV-visible light (radiation at 254 nm).

Figure 4.2 shows the batch PhotoReactor bottom surface coated with a TiO_2-film using the method developed in this study.

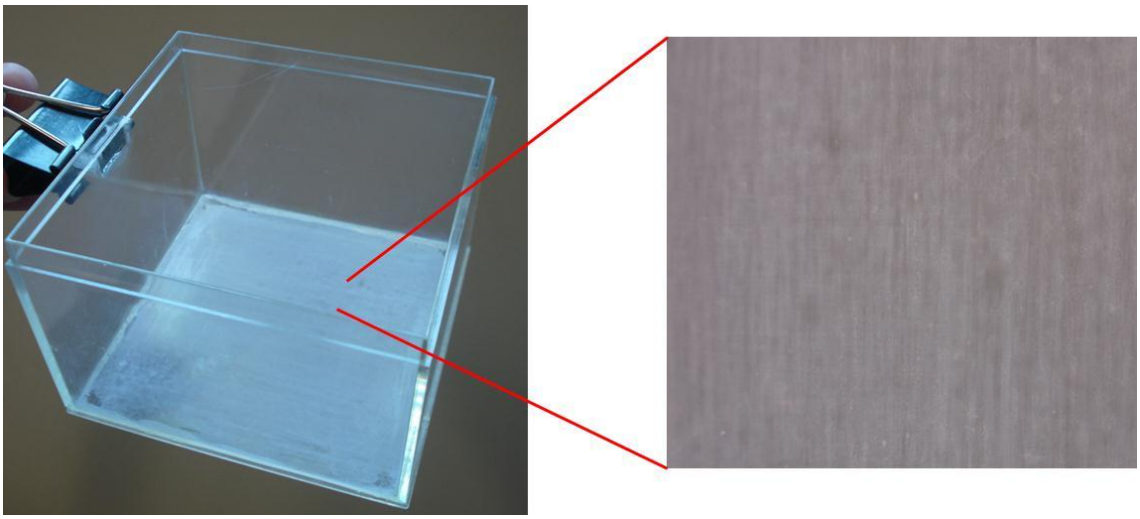

Figure 4.2: Batch Rector of this Study Coated with the TiO_2-film 1.5 wt%

4.3.1 Important information about the prepared TiO_2-film

The batch PhotoReactor Cell containing the bottom surface coated with TiO_2-film was kept in storage with minimum UV-visible light exposure. A cooler system composed of a cooling tank, an outer box and a pump, were the accessories that completed the PhotoReactor Cell setup. This allowed maintaining the cell temperature in the 10±5ºC range during the entire photodegradation experiment. The precautions were followed according to the Technical Data Sheet of the LOCTITE® 3321™, in order to keep the physical-chemical properties of the glue.

4.3.2 TiO_2-film Characterization

The TiO_2-film was characterized using a Hitachi S4500 field emission Scanning Electron Microscope (FE-SEM) equipped with a Quartz XOne energy dispersive X-ray (EDX) detector. The TiO_2-film coated on quartz surface was analyzed after the surface was cured with UV-visible light at 254 nm. The SEM and EDX system capabilities are: i) electron beam voltage of 10.0 kV for the SEM images, ii) magnification of image 500 times, iii) image scale bar of 60 microns.

4.4 Reactants

Regarding the study of the photoactivity of the TiO_2-film prepared in the present investigation, malic and malonic acids were chosen to perform the photocatalytic degradation studies. Table 4.2 reports information about these two organic acids as well as, the data about phosphoric acid, which is the mobile phase used for the HPLC analyses in this present study.

Table 4.2: Chemical Compounds Used for the Photocatalytic Degradation Studies

Name	Brand	Molar mass (g/mol)	Chemical Structure
Malic acid	Sigma-Aldrich Lot 058K0018V	134.09	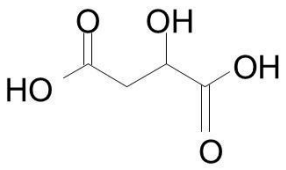
Malonic acid 99%	Sigma-Aldrich Batch 04008PC	104.06	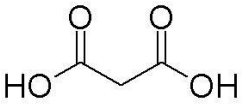
Phosphoric acid 85%	Fluka Analytical Lot BCBD9465	97.994	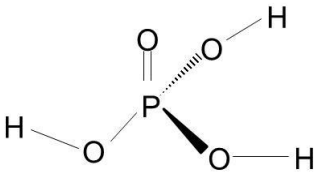

Samples of 10, 20, 30 and 40 ppm of malic acid and malonic acid were prepared in deionized water, to perform the photodegradation experiments. For the HPLC analysis, a phosphoric acid 0.1% (v/v) solution was prepared in deionized water and was used as the mobile phase.

4.5 Reactor Cell Setup of this Study

Figure 4.3 shows the PhotoReactor Cell setup employed for the photocatalytic degradation of malic and malonic acid. This PhotoReactor Cell consists of: (i) an external near UV-light lamp, (ii) an outer box to keep the temperature in the range of 10±5 ºC, (iii) a quartz window at the bottom of the outer box, (iv) a TiO_2-film 1.5 wt% coated on a quartz surface, (v) a Batch Photo Reactor, (vi) a Stirrer, (vii) a Cooler Tank and (viii) a Centrifugal Pump.

The PhotoReactor Cell setup as well as the properties of the near UV-lamp are described in Figure 4.3. The dimensions of the PhotoReactor cell are described in the Table 4.3:

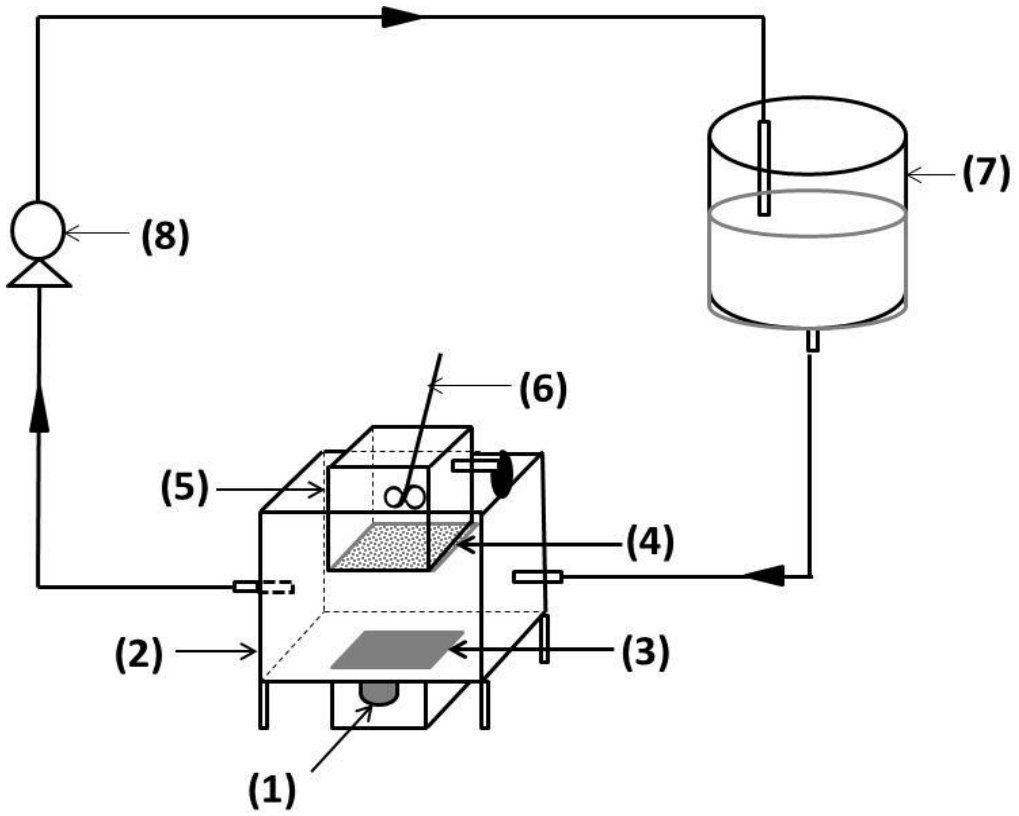

Figure 4.3: Batch Reactor Setup Employed for the Photocatalytic Degradation of Malic and Malonic Acid

Table 4.3: Characteristics of the Reactor Cell Setup of this study (Batch Reactor, Outer Box, Cooler Tank and UV-Lamp Source)

Component	Parameter	Measurement
Batch Reactor	length	9 cm
	width	9 cm
	height	9 cm
	volume	200 ml
	quartz thickness	0.16 cm
Outer Box	length	11.3 cm
	width	11.3 cm
	height	11.3 cm
Cooler Tank Stirrer	height legs	4.5 cm
	volume	5 L
	speed	250 RPM
UV-Lamp	length	41.3 cm
(UVP-XX-15BLB)	radius	1.33 cm
	Input power	15 W
	Output power	4 W
	Emission range	320 – 420 nm
	Emission rate	1.1910×10^{-5} Einstein.s^{-1}

4.6 Photocatalytic Degradation Experiments

Before each photodegradation experiment, the PhotoBatch Reactor was cleaned carefully with fresh water and rinsed with deionized water to eliminate any chemical species from previous runs.

Samples of malic and malonic acid at different concentrations (10, 20, 30 and 40 ppm) were both prepared from a 1000 ppm stock solution using deionized water. The mobile phase was prepared dissolving 85% phosphoric acid in deionized water to obtain a solution 0.1 % (v/v).

Before starting the experiments, a sample of each organic acid was taken and analyzed with the HPLC equipment. Following this, the reactor setup was run for 30 minutes in the dark and a second sample was taken. This procedure was performed to guarantee that a malic and malonic acid solution reached the adsorption equilibrium on the TiO_2 surface under “dark conditions” before starting the photocatalytic degradation.

Once the adsorption equilibrium was reached, the lamp was turned on and the photocatalytic degradation was initiated. At this point, samples were taking every 1 hour for 15 hours to analyze the change in malic and malonic acid concentrations during the photocatalytic conversion.

4.7 Detection and Quantification of Malic and Malonic Acid

The detection of malic and malonic acid were performed in a HPLC Shimadzu prominence LC 20AB, with a column oven CTO-0AC, an autosampler SIL-20AC.HT and a Diode Array Detector SPD-M20A. The column utilized for the organic acids measurements was an ion exchange Supelcogel C-610H column 30cm x 7.8mm ID (59320-U). The method used required the preparation of a calibration curve for malic and malonic acid and showed a good performance for organic acids detection. The mobile phase employed was phosphoric acid H_3PO_4 0.1% (v/v) at a flow rate of 0.5 ml/min. The temperature of the column oven was controlled to be in the range of 30±5 ºC, the UV detection wavelength was set to 210 nm and an injection volume of 50 μL for malic and

malonic acid solution was employed. All the samples analyzed in the HPLC were previously filtered using a PTFE Mandel 0.2 μm filter.

4.8 Radiation Measurements Box Setup

In order to determine the rate of photons absorbed by the TiO_2 film to perform the photocatalytic conversion of malic acid, radiation measurements of the catalyst layer were effected. A radiation box with the same dimensions of the PhotoReactor Cell was employed. The measurements were performed using a light detector probe which was connected to a Spectrometer and a Software called SpectraWiz. The Radiation measurements setup (Figure 4.4) is composed of: (1) a Radiation box, (2) a near UV-lamp, (3) a quartz window, (4) a light detector probe, (5) a Photo Batch Reactor, (6) a StellarNet EPP2000C-25 LT16 Spectrometer and (7) a SpectraWiz Software.

In this setup, the light was placed at the bottom of the radiation box. Its asymmetrical position is shown in Figure 4.5 which indicates the radiation profiles for the radiation emitted, back scattered, transmitted and reflected (Chapter 6).

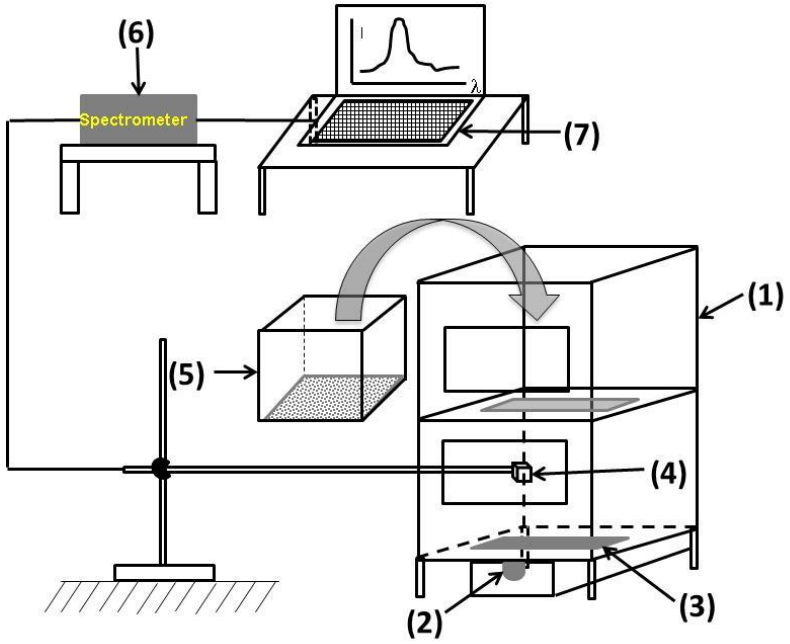

Figure 4.4: Schematic Representation of the Radiation Measurements of the TiO_2-film

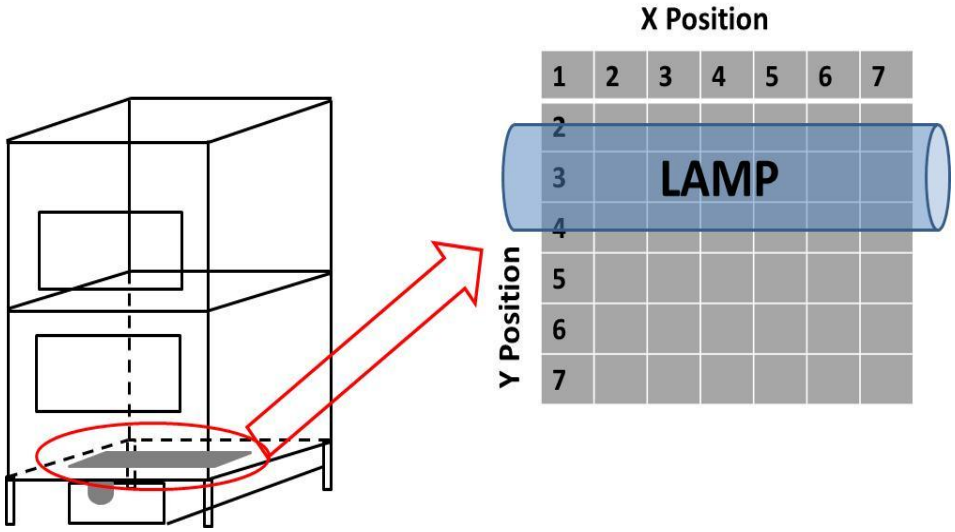

Figure 4.5: Measurements Scheme Contemplating the 49 Measurement Positions to Access the Non-Symmetrical Radiation Profile

4.9 Conclusions

This section reports the methods and equipment used in this present study. Initially, the methods for the TiO_2 preparation and characterization of the thin films are described. Following this, the PhotoReactor Cell setup using a TiO_2-film 1.5 wt% for the photocatalytic degradation experiments is reviewed together with the various malic and malonic acid water solutions used in the experiment. Finally, the results obtained with the Radiation Box setup developed to perform the radiation measurements of the TiO_2-film of the present study are reported.

Chapter 5

5 Results and Discussion Part I: TiO_2-film Catalyst Preparation, Characterization and Degradation Studies with Malic and Malonic Acid in Water

5.1 TiO_2-film catalyst preparation and characterization

The objective of this first section of the experimental study is to obtain enough information on photocatalytic reactor design in order to be able to perform photocatalytic degradation research of organic acids in opaque fluids. In this respect, a preliminary reactor set-up configuration was adopted for organic acid photoconversion in water media. Its results provided a good understanding of photocatalytic reactor parameters and were extremely helpful in the design of a photoreactor cell for opaque fluids.

5.1.1 Absorption Spectra of Water vs. Opaque Fluids

The first attempt to assess the photoconversion of organic acids in opaque fluids was performed using a commercial apple juice (Allens' concentrate). The apple juice was tested using the Photo-CREC Water-II. This reactor unit has been tested in depth and previously used for photodegradation of organic compounds in water treatment (Salaices-Arredondo, 2002; de Lasa et al., 2005; Serrano et al., 2009; Moreira, 2011; among others).

The Photo-CREC Water-II Reactor is cylindrical slurry reactor composed of seven windows distributed along the outer reactor surface. The spectra measurements for juice and water were performed along the positions 1 to 7, with the first and latest showing a very low value. Figure 5.1 and Figure 5.2 report the spectra at the axial position 4 for apple juice and water. Measurements were performed on a StellarNet EPP2000C-25 LT16 Spectrometer.

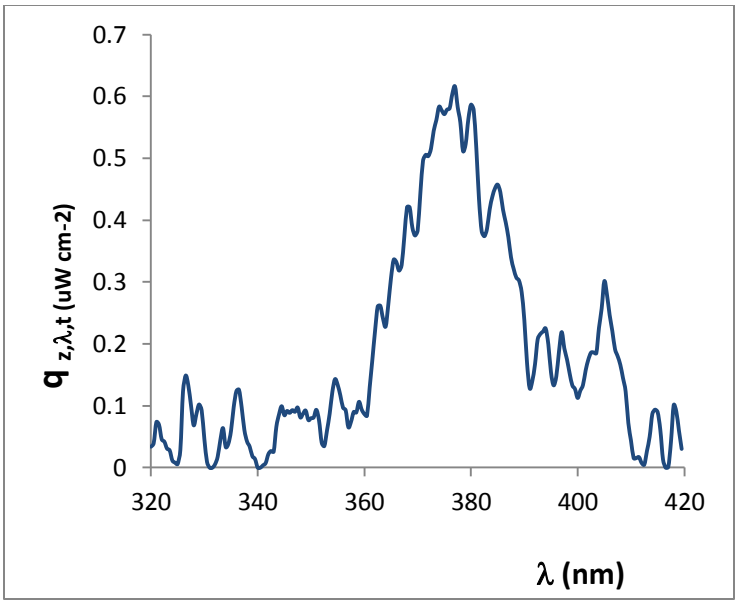

Figure 5.1: Transmission Spectra for Commercial Allens Apple Juice at Position 4 (Brix: 11.90±0.1, pH: 3.10±0.05, Conc. of malic acid: 3.00±0.1 g/L)

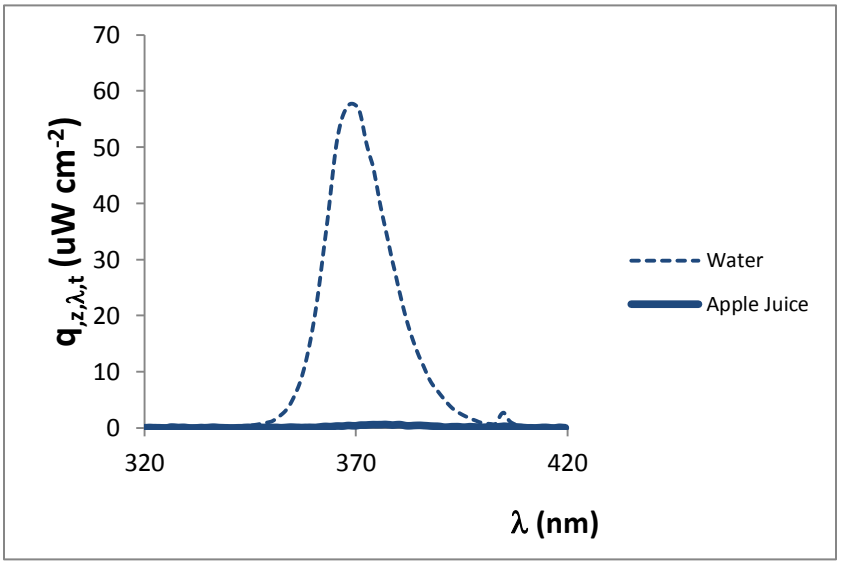

Figure 5.2: Apple Juice Transmission Spectra vs. Water Transmission Spectra

The apple juice transmission spectrum shows the light intensity distribution along the wavelength range of 320-420 nm. It can be observed that the maximum intensity is approximately 0.6 $\mu W/cm^2$ at 380nm. Comparing the apple juice spectrum with the one for water under the same experimental conditions (see Figure 5.2), one can observe that

the maximum intensity for the water spectra is 100 times greater (approximately 58 $\mu W/cm^2$ at 370nm) than the one for apple juice. This can be explained due to the fact that in opaque fluids, such as apple juice, there is a very significant irradiation absorption limiting transmittance in the near-wall region. Thus, in the case of apple juice, transmittance is significantly reduced and the amount of irradiation reaching the photocatalyst decreases considerably. This is the case when compared to the high transmitted values observed in water.

One can thus, conclude that the use of suspended TiO_2 in opaque fluids becomes impractical because the opacity of the fluid largely prevents light from reaching the photocatalyst. This reduces the formation of electron-hole pairs, which are the responsible components for the organic species photoconversion. Thus, to increase the chances of the photocatalyst receiving as much light as possible, it was necessary to develop a method to immobilize the photocatalyst in a thin film placed as close as possible to the UV-light source.

5.1.2 TiO_2 Film Preparation and Characterization

Given all of the above described facts, a catalyst layer, using UV-transparent/waterproof glue, was prepared aiming to increase the efficiency of the photocatalytic degradation of organic compounds in opaque fluids. The goal of this new setup is that the near UV-light first reaches the quartz side of the interface quartz-glue-TiO_2-film. The holes (h^+) formed on this side of the layer will then migrate to the side which is in contact with the solution (TiO_2-organic acid solution).

Figure 5.3 illustrates the two different mechanisms of electron hole formation using TiO_2 as a catalyst: a) Figure 5.3a shows TiO_2 directed irradiated as a photocatalyst in suspension and b) Figure 5.3b describes the TiO_2-film with the catalyst indirectly irradiated promoting the photoconversion.

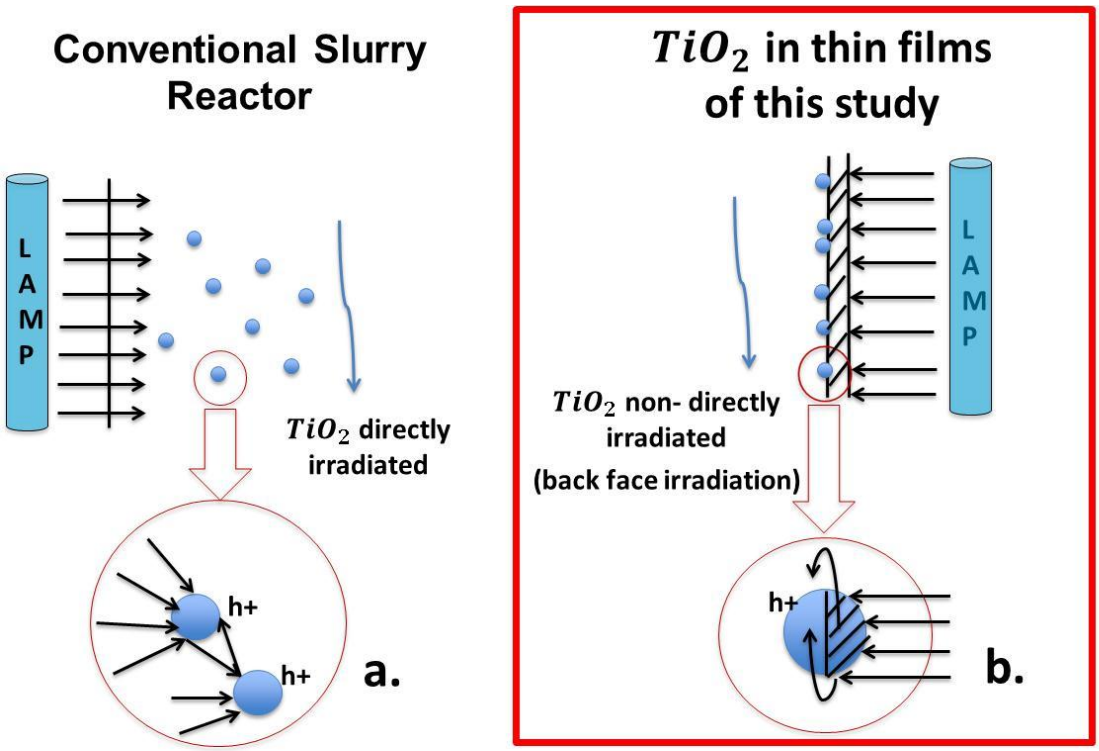

Figure 5.3: Irradiation Paths Showing Formation of holes (h^+) Using TiO_2 (a) in a Suspension with TiO_2 Directly Irradiated and (b) in a Thin Film with Back Face Irradiation Only

The TiO_2-thin film, prepared with UV-transparent-waterproof glue, was chosen to perform the photodegradation of malic acid in the present study. The film was prepared with a layer of TiO_2 (1.5 wt%), coated on a quartz slide. The TiO_2 film was cured under a middle UV-light (200 to 300 nm) and analyzed in a Scanning Electron Microscope, SEM (Figure 5.4).

The SEM coupled with Energy Dispersive X-ray (EDX) Spectroscopy is an analytical technique which consists in irradiating the surface with high energy electrons (primary), having an energy between 0.5 – 30 kV, and producing low energy electrons (secondary) which are detected. SEM gives information about the topography and morphology of the sample. These two combine techniques provide the means to acquire information on the chemical composition of the prepared film with immobilized TiO_2.

The SEM results showed that the film forms a wavy layer with both a thin and a thick region. Figure 5.5 reports EDX (Energy Dispersive X-Ray) analysis of TiO_2 films in specific regions of the film such as Regions 1 and 2. Region 2 (refer to Figure 5.4) showed the presence of TiO_2 on the film near the surface while region 1 did not show TiO_2.

This wavy thin film characteristic with two different levels of film thickness was assumed to be the result of glue properties and can be traced to the curing step, where the film was subjected to one hour of intense irradiation at wavelength 254 nm.

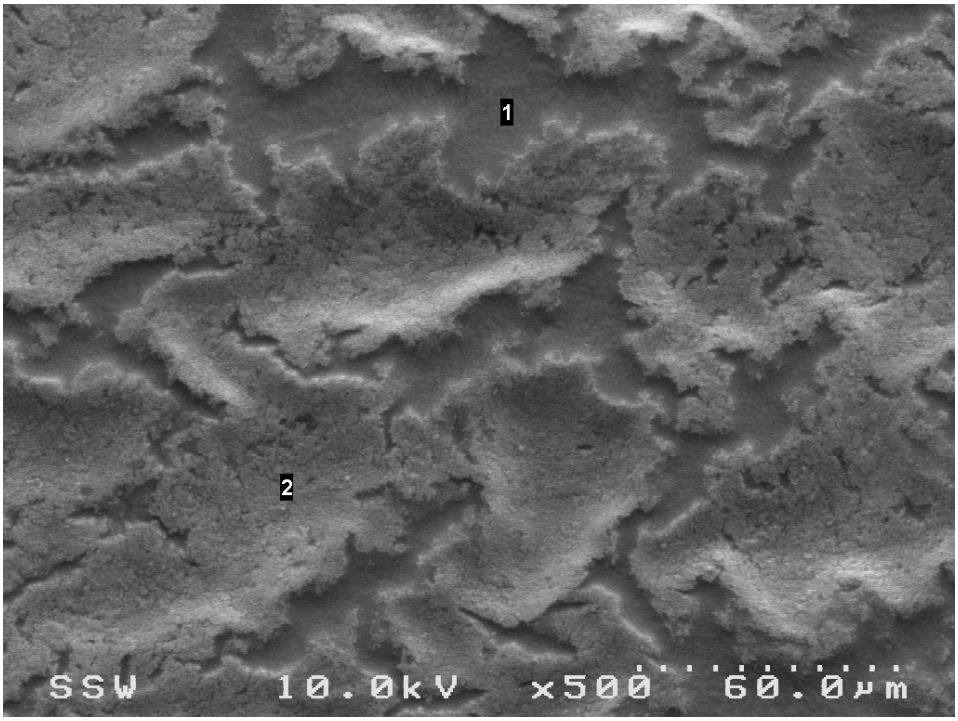

Figure 5.4: SEM of TiO_2 Film (500x): Region 1 – Surface with no Catalyst Coverage; Region 2 – Catalyst Covered Area

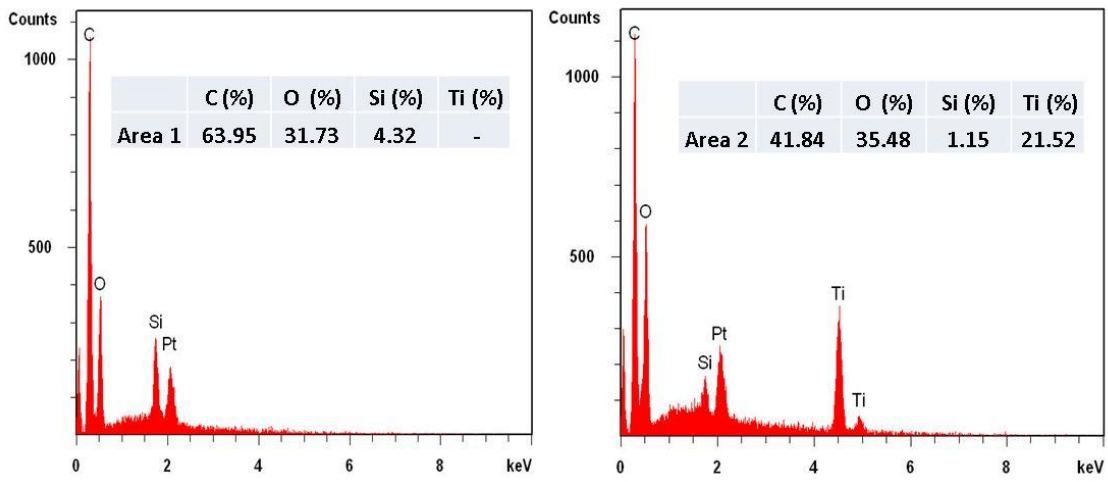

	C (%)	O (%)	Si (%)	Ti (%)
Area 1	63.95	31.73	4.32	-

	C (%)	O (%)	Si (%)	Ti (%)
Area 2	41.84	35.48	1.15	21.52

Figure 5.5: EDX Analysis of TiO_2 Film – Regions 1 and 2 from Figure 5.4

5.2 Photolysis and Photocatalytic Degradation of Malic Acid Using TiO_2 Films and TiO_2 in Suspension

According to the technical literature, there are several methods to identify and quantify organic acids in water and opaque fluids. One important technique used is HPLC coupled with an Ion Exchange Column (Chinnici et al., 2005; Mato et al., 2005; Herrmann et al., 1999; Calull et al., 1992). The photo conversion of malic acid with TiO_2 in suspension, as well as with TiO_2 films, has been extensively investigated by several researcher groups (Danion et al., 2007; Irawaty et al., 2011; Herrmann et al., 1999). Different malic acid reaction intermediates, such as tartaric acid, maleic acid, pyruvic acid, malonic acid, fumaric acid, ethanoic acid, 3-oxopropanoic acid, among others, have been observed. However, it has been found that the most common intermediate formed during the photodegradation of malic acid is malonic acid (Irawaty et al., 2011; Franch et al., 2004; Danion et al., 2007).

5.2.1 Concentration Profile during the Photodegradation of Malic and Malonic Acid under TiO_2 Film

In the present research study, the photo conversion of malic acid and formation of malonic acid in water are reported. The photocatalytic experiments were performed in a

batch reactor with the TiO_2 film coated on the bottom of the reactor and an external UV-light placed in the opposite side of the catalyst (quartz-catalyst interface). All the experiments were developed with constant operational parameters, such as: a) light intensity emission, b) catalyst loading, c) pH for initial concentration (4.0±0.1) and d) temperature (15±3 ºC).

Analyses of malic and malonic acids were effected on an HPLC by using: a) a Supelcogel C-610H ion exchange column 30cm x 7.8mm, b) phosphoric acid 0.1% as the mobile phase, c) a pH = 3±0.1, d) a flow rate of 0.5ml/min, e) a temperature of 35-40ºC and f) a UV-detection wavelength of 254nm. All the experimental runs were performed three times in order to ensure experimental reproducibility.

Figure 5.6 reports a HPLC chromatogram obtained during the photoconversion of malic acid. The first chromatogram represents a 20ppm malic acid sample (peak 1) taken before the photocatalyst reaction. Chromatogram 2 shows the formation of malonic acid (peak 2) after 2 hours of reaction on the TiO_2 film under near UV-light. Formation of other unknown intermediates can be observed in chromatogram 2. However, only the main intermediate, malonic acid, will be the object of discussion in this present study.

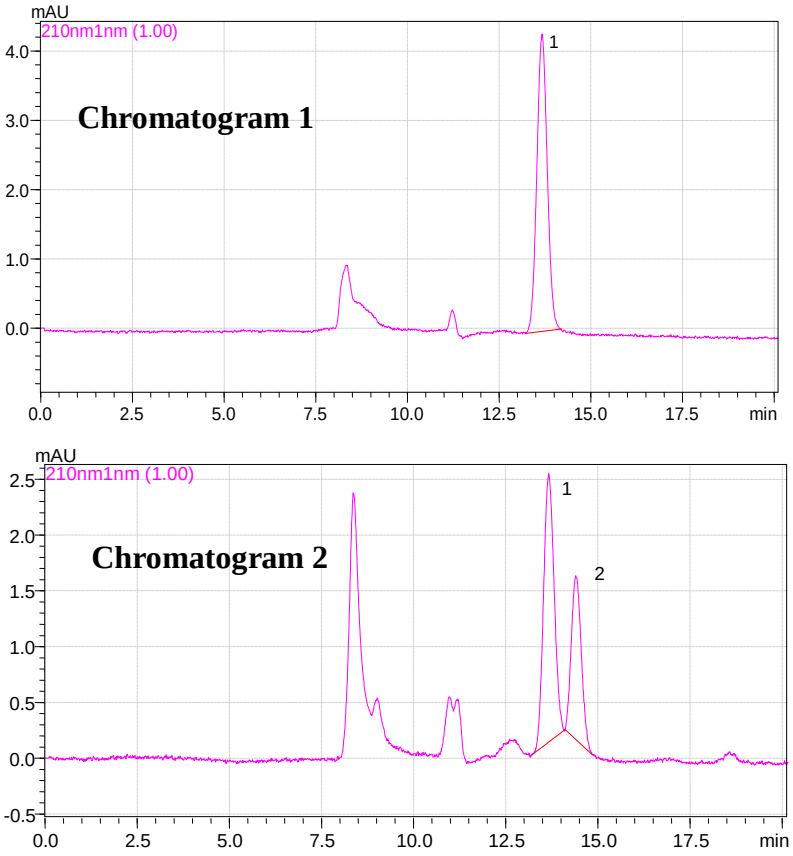

Figure 5.6: a) Chromatograms of Malic Acid with 20ppm in Water (Peak 1) and b) Chromatograms of Malic Acid after 2 hours of Photocatalytic Reaction Time using a TiO_2 Film with Malonic Acid Formation (Peak 2)

The concentration profile for malic acid degradation and malonic acid formation as a function of time is shown in Figure 5.7. It can be observed that the photo conversion of malic acid is achieved after 6 hours when the concentration of malonic acid appears to have a maximum value. The photocatalytic conversion of malonic acid is observed after 15 hours of reaction. The amount of malic acid remained in solution is negligible.

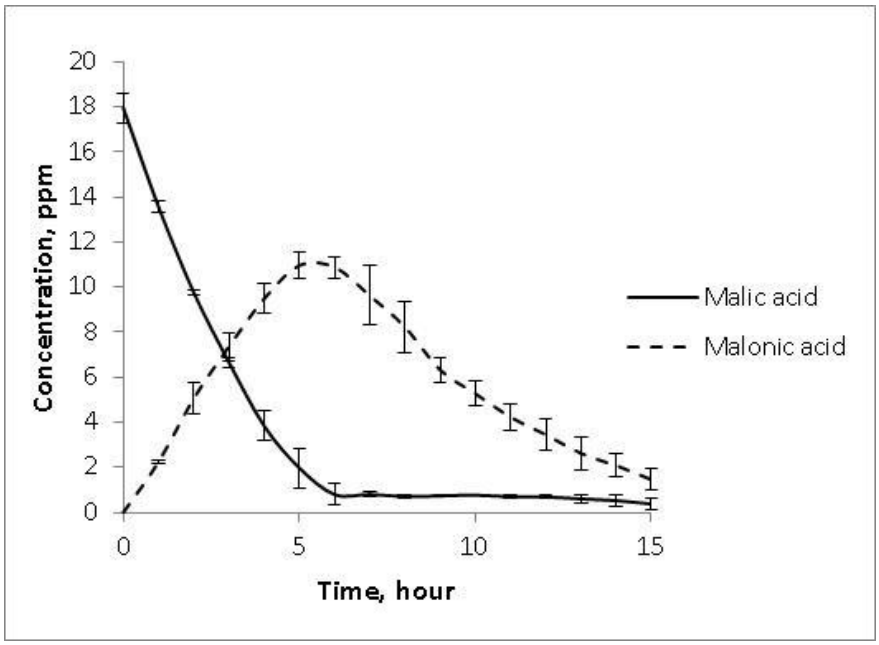

Figure 5.7: Malic Acid Photodegradation and Malonic Acid Formation Using a TiO_2 Film and Near UV-Light

The photoconversion of malic acid was performed during the present study at four different initial concentrations: 10, 20, 30 and 40 ppm. Consumption of malic acid and formation of malonic acid as a function of time are shown in Figure 5.8 and Figure 5.9. As observed in Figure 5.8, the complete photo conversion of malic acid occurs between 5 and 8 hours reaction time with a malic acid concentration range of 10 to 40 ppm.

Figure 5.9 also reports a displacement of the maximum concentration of malonic acid formed when the initial concentration of malic acid changes from 10 to 40ppm. The maximum concentration of malonic acid formed is reached after 5 hours (C_{Mac} = 5.50 ppm), 6 hours (C_{Mac} = 10.96 ppm), 7 hours (C_{Mac} = 16.51 ppm) and 8 hours (C_{Mac} = 22.95 ppm), for the malic acid initial concentrations of 10, 20, 30 and 40 ppm, respectively.

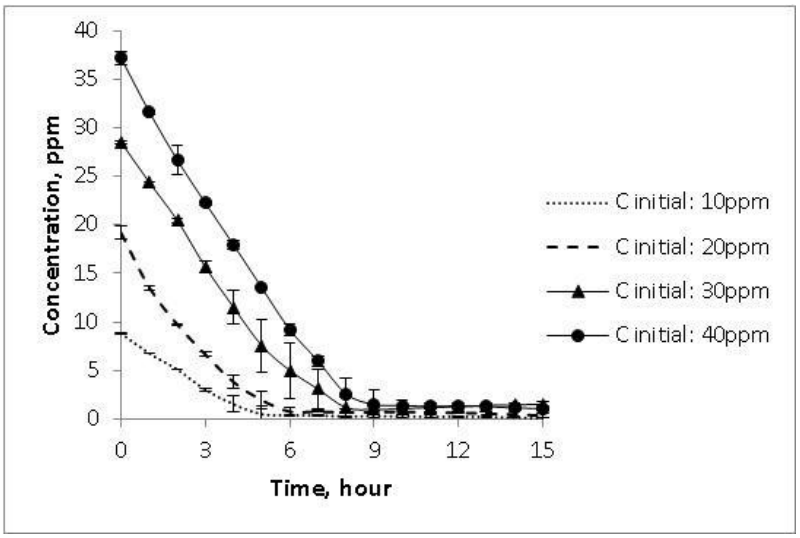

Figure 5.8: Malic Acid Photodegradation Profile for Different Initial Concentrations: 10, 20, 30 and 40ppm

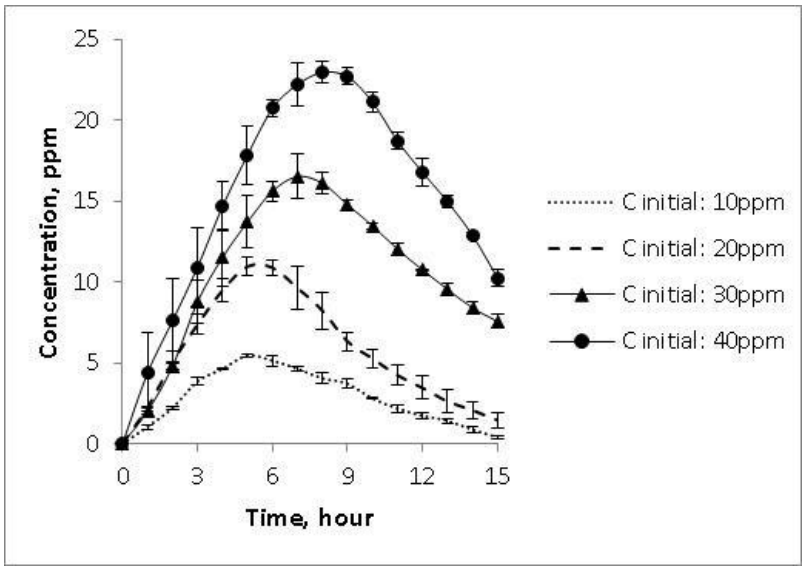

Figure 5.9: Malonic Acid Photodegradation Profile for Different Initial Concentrations of: 10, 20, 30 and 40ppm

According to the technical literature (Mukherjee et al., 1999, Chen et al., 2001), one of the main disadvantages of immobilized catalysts in photocatalytic degradation is their internal and external mass transfer limitations. These two effects are especially true in systems with thick photocatalyst films and with low fluid flow rates and internal film

mass transfer. According to Chen et al., 2001, the optimum thickness of TiO_2-film undirected irradiated (glass slide-catalyst) in order to prevent the mass transfer was approximately 5 μm.

In order to elucidate the effect of mass transfer in the photoconversion of malic acid using the TiO_2 film of this present experiment, the photodegradation of malic acid at 20 ppm was performed using two different mixing speeds, with three repetitions for each test. Figure 5.10 shows the photodegradation using 20 ppm of malic acid and a stirrer speed at 125 rpm and 250 rpm. According to these results, there is no considerable difference in the rate of photoconversion when the mixing speed is changed and it shows no mass transfer effects in the catalyst layer. This could be explained by the fact that the TiO_2 film is prepared with a very thin layer of glue and catalyst, facilitating the penetration of UV-light in the layer and that the relatively high fluid circulation in the cell is estimated at 24 and 47 cm/s, respectively for the two experimental mixing speeds**,** in the near film region. This prevents internal mass transfer. Regarding the external mass transfer effects, they are prevented by promoting in the near catalyst layer a vigorous mixing during all experiments.

Additionally, one can estimate the effect of mass transfer in the catalyst layer by making use of the Sherwood number (Sh) and by performing the mass balance between the catalyst film and bulk solution of malic acid. Thus, comparing the mass transfer coefficient (k_m) and kinetic constant (k_i), one can understand the effect of both parameters in the overall rate of malic acid photodegradation (see calculation in Appendix A). The results showed a k_m of 1.604 x 10^{-3} m/s and k_i of 4.45 x 10^{-6} m/s (Table 6.2). Since the rate equation for the malic acid photodegradation is proportional to $1/(1/k_m)$ and $1/(1/k_i)$, the greater magnitude of k_m (1000 times higher when compared to k_i) confirm that the mass transfer can be neglected for the malic acid photoconversion using the TiO_2 film developed in this research study.

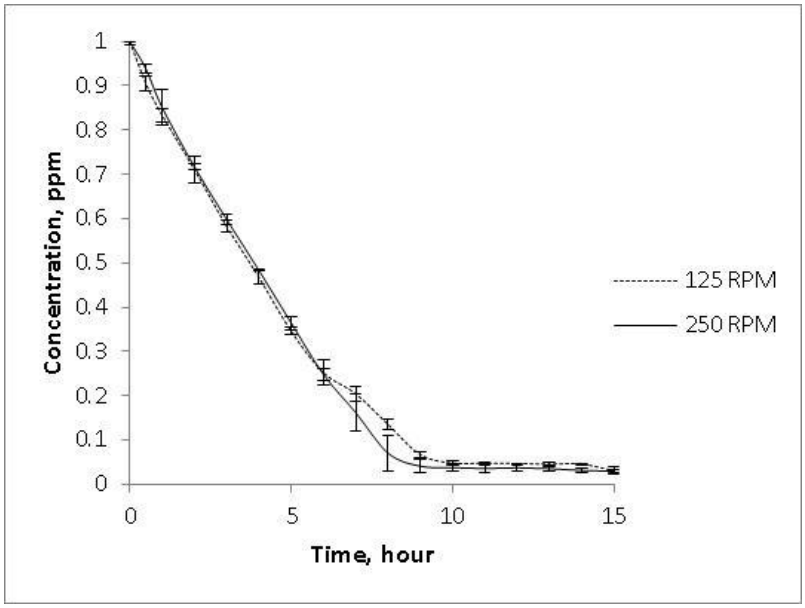

Figure 5.10: A 40ppm Malic Acid Concentration Photodegradation Experiment Using a TiO_2 Film at Two Different Mixing Speeds: 125 rpm and 250 rpm

5.2.2 Photolysis of Malic Acid

When organic compounds are irradiated by a light source, they could be degraded via photolysis. Researchers have been well aware of this phenomenon for quite a long time (Zepp et al., 1977; Kormann et al., 1991; Baxendale et al., 1956). Photolysis occurs with the absorption of light by the organic compound promoting subsequent chemical reactions.

The influence of photolysis in photodegradation of organic compounds has been studied in water as well as in opaque fluids. UV-light treatment has been used for opaque fluids disinfection such as for fruit juice. This has been the case despite the availability of conventional thermal-treatment methods as discussed before. UV-light treatment has a special feature given its ability to keep the taste and odor characteristics of fruit juices. UV-light treatment has also been approved since year 2000 by the American food organization as a pathogen reducer in juice (US FDA, 21CFR120).

Regarding non-thermal treatment methods for photoconversion of organic compounds, including UV-light treatment, photocatalysis applying UV-light+TiO_2 appears to provide

a most effective approach for the degradation of organic acids in wastewater. This is the case when compared to UV-light treatment alone. UV-light+TiO_2 use less energetic photons and as a result limit photolysis.

Despite of this, photolysis can affect the photoconversion. One needs to assess its influence for each reactor configuration and the TiO_2 film. For instance, in the case of malic acid one should compare the degradation profile with and without the TiO_2 film under the same experimental conditions. Using this data, one can accurately account for the role of photocatalytic malic acid photoconversion discounting the photolysis effect.

Figure 5.11 reports the change in of malic acid concentration when 20ppm of malic acid is exposed to near UV-light and when near UV-light is placed under the TiO_2-film. According to these results, the photocatalytic degradation of 20 ppm of malic acid is achieved after 6 hours, with only 0.8 ppm of malic acid remaining in the solution after the experiment. On the other hand, the concentration of malic acid during photolysis decreased by 24%, with 11.5 ppm of malic acid remaining in solution after 6 hours of experiment. This fact illustrates that using TiO_2 film plays an important role in the photodegradation of malic acid and photolysis may introduce a significant contribution.

However, in the case of the TiO_2 film and while assessing the role of, photolysis need to be carefully accounts all facts. This is the case given that experiments show that photolysis represents 30% of the total degradation of malic acid for the same irradiation period. In order to accomplish this, one has to establish a photolysis kinetic model with the data of Figure 5.11. The photolysis rate equation depends on the radiation intensity (I) reaching the malic acid solution as shown in the Equation 5.1. Once the photolysis kinetics is established (section 6.2) one can recalculate the expected concentration change in the malic acid solution, knowing that only 4% of the irradiation ($I^{'}$) is transmitted through the TiO_2-film (Table 6.1) and this represents the irradiation intensity involved in photolysis reaction. Figure 5.12 presents the concentration change in the malic acid solution considering only 4% of the irradiation emitted ($I^{'}$ = 0.04 x I) reaching the film.

$$r_{photolysis} = -k_{photolysis}C = -(k'_{photolysis}I)C = -(k'_{photolysis}0.04I')C \qquad (5.1)$$

The integration of eq. (5.1) shows revised photolysis results being much smaller than 30%, at about 1% only of the overall conversion. Thus, on this basis the approximate malic acid photolysis can be neglected from overall photoconversion analysis.

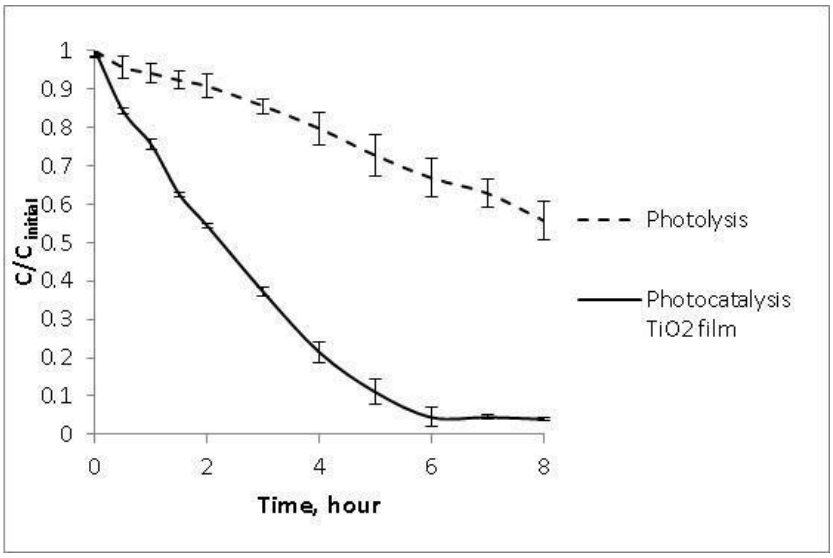

Figure 5.11: Profile for the Photolysis and Photocatalysis Using a TiO_2 Film for Malic Acid 20ppm Under near UV-Light

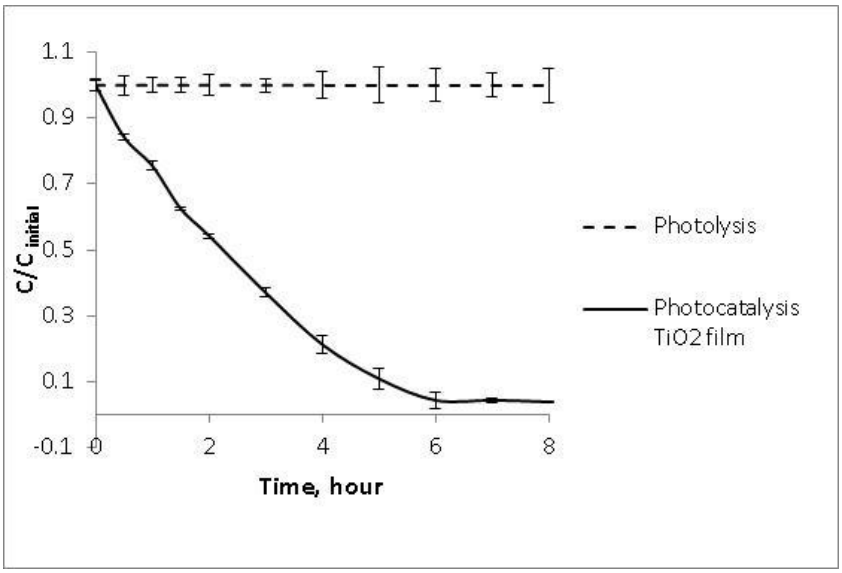

Figure 5.12: Profile for the Photolysis and Photocatalysis Using a TiO_2 Film for Malic Acid 20ppm Under Near UV-Light Recalculated Using the Kinetic Photolysis and the Irradiation Profile for the Light Transmitted Through the Film (Table 6.1)

5.2.3 Concentration Profile during the Photodegradation of Malic and Malonic Acid under TiO_2 in Suspension

As stated before, the use of TiO_2 in suspension to perform the photocatalytic degradation of organic compounds in water has been studied. Its high efficiency for the complete mineralization of organic compounds to CO_2 and H_2O has been demonstrated. This method has proven to be very successful for organic disinfection mainly for water treatment applications.

However, there are some disadvantages in using TiO_2 in suspension, the greater one being the need of a filtration step to remove almost entirely the photocatalyst at the end of the irradiation period. Contrary to photocatalysts in suspension, immobilized photocatalysts do not require filtration step, allowing reducing both cost and time, saving measure in an industrial scale process. This is particularly valuable if the treated fruit juice is going to be used for human consumption.

Thus, in order to compare the efficiency of malic acid photo conversion using TiO_2 1.5 wt% films with TiO_2 in suspension, some degradation experiments were performed with a malic acid 20 ppm solution in water. Different concentrations of TiO_2 in suspension were used (0.01, 0.05, 0.10, 0.15, 0.20 and 0.30 gL^{-1}) to find the optimum catalyst concentration. Results obtained are reported in Figure 5.13.

It can be observed from this Figure that the photoconversion rate for malic acid degradation increases with the catalyst concentration until it reaches an optimum catalyst concentration. After that, any amount of extra photocatalyst added does not change the rate of photo conversion. In the present experiment, the optimum concentration of TiO_2 in suspension was found to be 0.2 gL^{-1} (Figure 5.14).

However, even though the malic acid photo degradation rate is higher using fine TiO_2 particles in suspension with particle size range of 20 to 60 nm for TiO_2 Degussa P25 (de Lasa et al., 2005), the cylindrical slurry photocatalytic reactor requires as stated above, a filtration step. Besides, the application of TiO_2 in suspension for photocatalytic conversion is limited to translucent fluid.

As well TiO_2 films are especially tailored for photocatalytic degradation of organic compounds in opaque fluids. These TiO_2 films, with the active surface being the dark side of the TiO_2 particles as described in Figure 5.3, may also offer effective approaches to clarify the photocatalytic mechanism and quantum yields due to the mobility of h^+ sites.

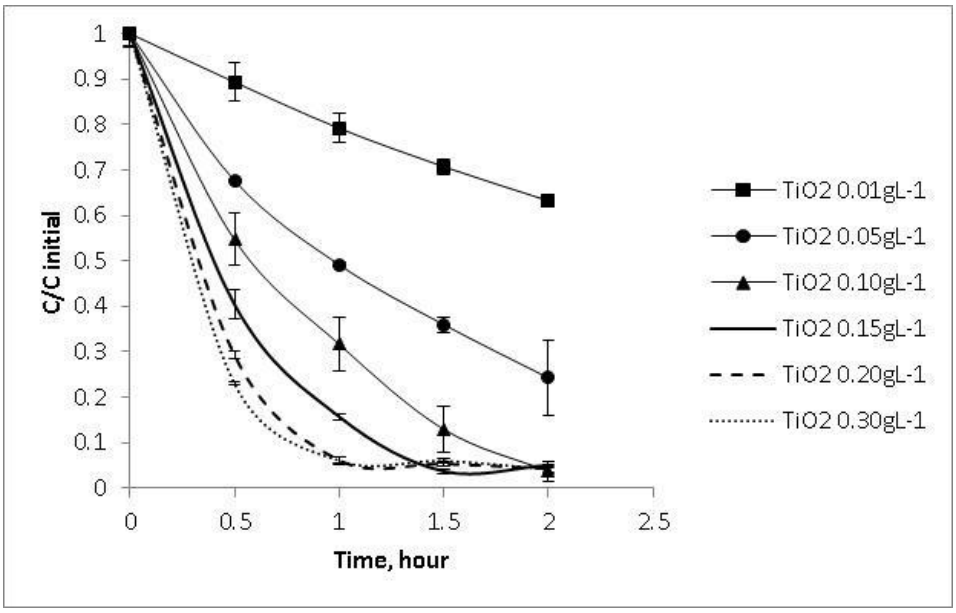

Figure 5.13: A 20ppm malic acid photodegradation profile for different TiO_2 concentrations in suspension: 0.01, 0.05, 0.10, 0.15, 0.20 and 0.30 gL^{-1}

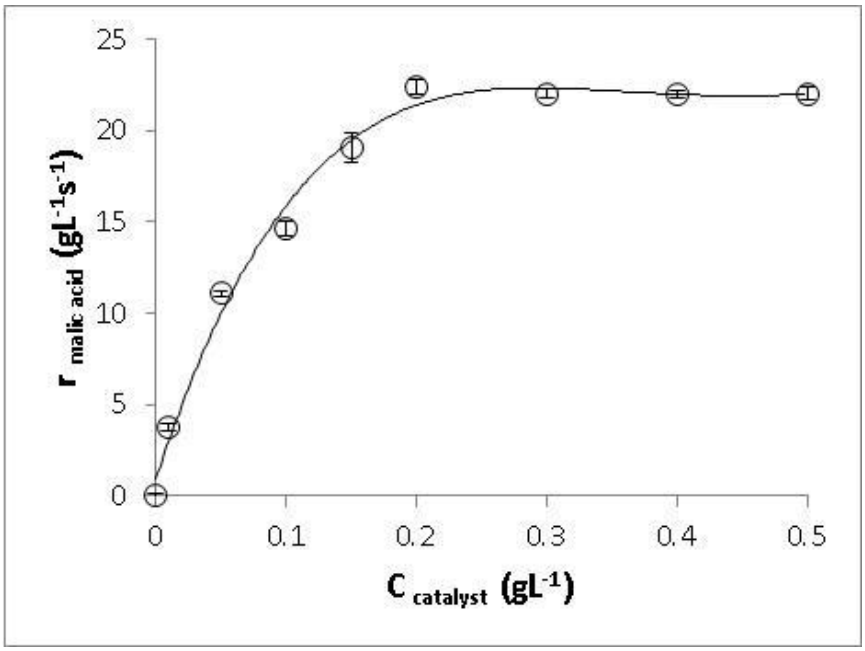

Figure 5.14: Rate Equation for malic acid degradation ($r_{malic\ acid}$) for different TiO_2 concentrations in suspension (0.01 to 0.5 gL^{-1}). Initial concentration of malic acid: 20ppm

5.3 Conclusions

a. SEM/EDX spectroscopy analysis of the thin TiO_2-films prepared in the present study showed a wavy layer with two characteristic regions identified: Region 1 free of TiO_2 particles, and Region 2 loaded with TiO_2 particles.

b. Photodegradation experiments using TiO_2-thin films confirm that photoconversion is a phenomenon involves mobile electrons holes on the semiconductor surfaces. This is concluded given that is spite that there is no opportunity for the organic species in water solution to reach the particle irradiated side, the photoconversion reaction takes place. Experiments performed at different mixing speeds showed that the overall photoconversion rate is not affected by mass transfer and that the influence of transport processes can be neglected on the TiO_2-films of this study.

c. Experimental results show that the photolysis of malic and malonic acid played a negligible role in the photocatalytic degradation of malic acid and as a consequence in the

resulting kinetic model. Photocatalytic experiments developed with malic acid prove as well that malonic acid is a key intermediate in malic acid photoconversion.

Chapter 6

6 Results and Discussion Part II: Reactor Irradiation Studies and Kinetic Modeling of Malic Acid Photocatalytic Degradation

The main goal of this chapter is to report radiation profiles inside a photoreactor cell and to establish malic and malonic acid photodegradation kinetics. One should notice that in the photocatalyst film of the present study, TiO_2 surfaces are "non-irradiated" (dark side) planes of the photocatalyst surface. As such, the proposed experiments provide very valuable insight into the mechanism of photocatalysis.

A number of researchers (Danion et al., 2007; Song et al., 2001; Sumin et al., 2001; Herrmann et al., 1999; Herrmann et al., 1997; among others) have considered photocatalyst films with irradiated surfaces contributing to the organic species photoconversion. We are not aware of studies allowing the non-irradiated surfaces of the photocatalyst to be the ones that can photoconvert organic species in water. In this respect, only moving "h^+" sites can justify the results of our experiments.

6.1 Irradiation Measurements of TiO_2 Thin Coated Film 1.5 wt%

Irradiation measurements are extremely important to predict the rate of photons absorbed by the photocatalyst. This variable is crucial for further studies on photocatalytic reactor designs and scale up. Irradiation analysis includes determining the following variables: (a) radiation being emitted by the lamp (P_l), (b) radiation reflected (back-scattered) by the catalyst film (P_{bs}), and (c) radiation transmitted through the film (P_t).

Salaices-Arredondo, 2002, used a macroscopic balance approach on an annular photo-reactor having the photocatalyst in suspension. A similar methodology can be used in the system of this study in order to determine radiation absorbed by the catalyst (P_a), with P_a being of the utmost importance for calculating reactor efficiencies in the photodegradation of organic compounds.

Titanium dioxide is extensively used as a photocatalyst because of its low-cost, thermal stability and its capacity of promoting complete mineralization of organic compounds leaving the degraded solution residue-free. Degussa P25 is a very well-known catalyst applied for the degradation of organic compounds in water. It is composed by approximately 70-80% of anatase and 20-30% of rutile. Its band gap energy is 3.2eV, which is equivalent to a wavelength of 388 nm (de Lasa et al., 2005). This large band gap value implies that all photocatalytic reactions under TiO_2 Degussa P25 will occur for wavelengths below 388 nm. Diverse authors have been discussing radiation measurements of photoreactors with TiO_2 in suspension. However, only a few researchers have studied the radiation profile in catalyst films. These catalyst films are usually prepared using thermal treatment methods and they are coated in diverse materials such as stainless steel, quartz, glass, optical fiber and polymer (Danion et al., 2007; Herrmann et al., 1999; Herrmann et al., 1997; Song et al., 2001; Choi et al., 2006).

In the present work, a new method for preparation of TiO_2 films applying a UV-transparent/waterproof glue was applied and the Reactor Cell uses an indirectly irradiated thin film.

Regarding the UV-light source, UV-black lamps (BL) are well-known to promote photocatalytic reactions. BL-lamps emit UV light for wavelength ranges below 388 nm and they can be used for photocatalytic reactions using TiO_2 Degussa P25. Different light measurements performed inside the Photo-CREC Water-II, employing three different UV BL-lamps, were performed. The radiation flux (q, mW/cm^2) for all BL lamps was measured along the axial direction (L, cm). Results from these measurements are presented in Figure 6.1. Lamp b was found to have the most symmetrical radiation distribution. Therefore, lamp b is chosen for all the photodegradation experiments in this study. It can also be observed from Figure 6.1b that radiation emissions in the axial position, between 10 and 30 cm in length, remain essentially constant. It is in this region where radiation measurements are more reliable.

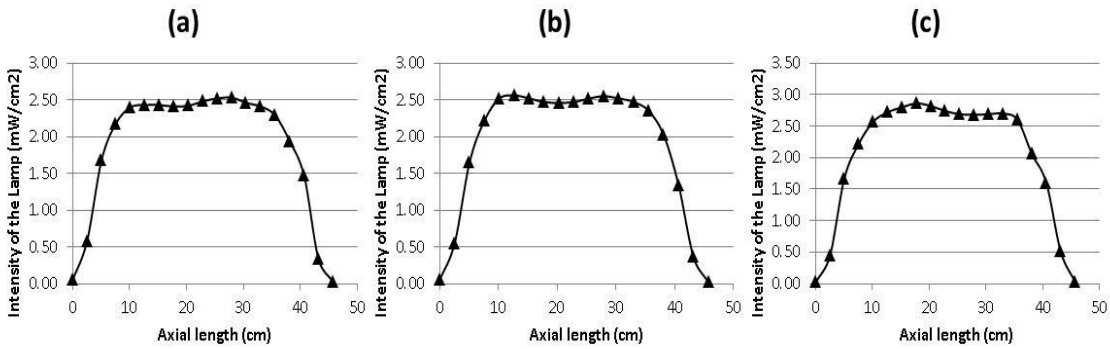

Figure 6.1: Radiation Profile of BL Lamps a, b and c

In our reactor set-up, the lamp is placed below the quartz box, by spacing of 18.5 cm and 27.5 cm below the box, well inside the lamp's constant radiation emission zone. This minimizes losses of light that occur at the edges of the lamp. Once lamp b was selected for the degradation experiments, its spectrum was measured and it is reported in Figure 6.2. This spectrum was measured at 4 cm from the center of the lamp and at 22 cm from its edge.

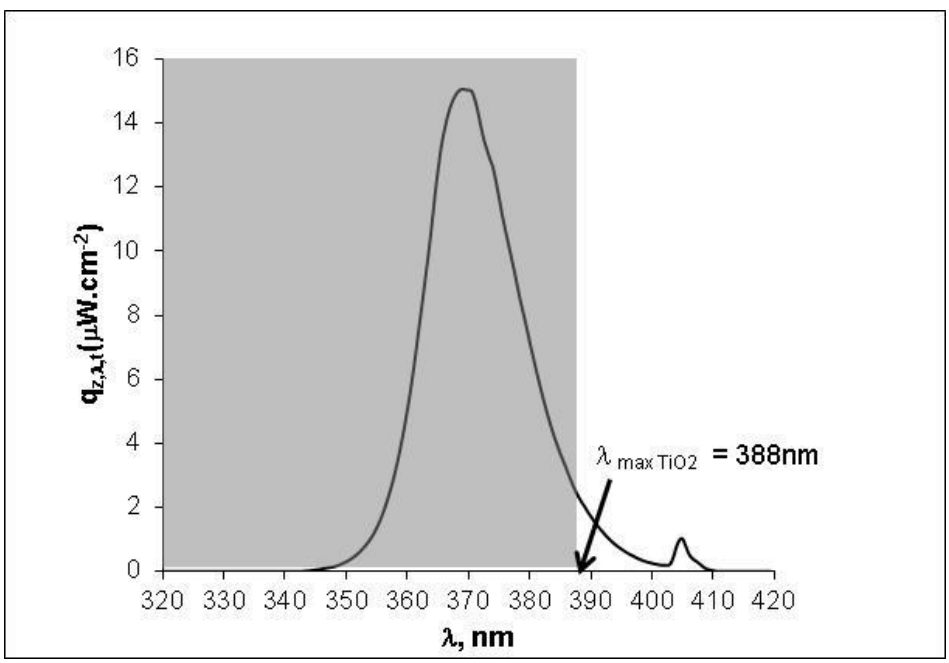

Figure 6.2: Emission Spectrum for Lamp b (Wavelength Range of 320-420 nm)

Another important variable when performing photocatalytic degradation is the lamp emission power decay after a certain time of usage. It is known that the reactor performance depends on the lamp operation conditions. It has been demonstrated by Salaices-Arredondo, 2002, that BL-lamps show asymmetric radiation emission behaviour after 1000 hours of use. This asymmetrical behaviour, compromises the calculation of rate of absorption of photos on the TiO_2 film. Given all the above, during all the photodegradation experiments performed in this study, the UV-lamp never transcended 1000 hours of operation; thus lamp emission decay is considered negligible.

6.1.1 Calculation of P_a, P_l, P_{bs} and P_t

This section shows irradiation measurements performed on the TiO_2-film 1.5 wt% indirectly irradiated with a near UV-light source. The analysis was performed in a batch reactor over a quartz slide coated with a thin film of TiO_2 using Macroscopic Radiation Balance (MB) (de Lasa et al., 2005).

In order to determine the rate of photons absorbed by the TiO_2 film (P_a) one needs to take in account: (a) the radiation emitted by the lamp source (P_l), (b) the radiation deflected by the catalyst film (P_{bs}, back scattered radiation) and (c) the radiation transmitted through the catalyst film (P_t).

A macroscopic radiation balance allows the calculation of the P_a, which is the rate of radiation absorbed by the TiO_2 film. This is done by using the results of: (a) the radiation emitted by the lamp, (b) the radiation reflected by the catalyst layer (backscattered) and (c) the radiation transmitted through the catalyst film with the expression shown in Equation 6.1 (de Lasa et al., 2005):

$$P_a(t) = P_l(t) - P_{bs}(t) - P_t(t) \tag{6.1}$$

where P_a (t) is the rate of absorption of photons, P_{bs} (t) is the rate of backscattered photons exiting the system, P_t (t) is the rate of transmission of photons, and P_l (t) is the rate of emission of photons by the lamp, all in Einstein.s^{-1} units.

P_l (Equation 6.2) was calculated by using the concept of the follow expression (de Lasa et al., 2005):

$$P_l(t) = \frac{\bar{\lambda}}{h.c}\int_{\lambda_1}^{\lambda_2}\int_0^{\infty}\int_0^{2\pi} q_{\theta,z,\lambda,t}.\, r.\, d\theta dz d\lambda \tag{6.2}$$

where h represents the Planck's constant (6.626 x 10^{-34} J.s), c denotes the speed of light (2.998 x 10^8 m/s), $q_{\theta,z,\lambda,t}$ stands for the radiative flux ($\mu W/cm^2$), r represents the radial coordinate (m), z denotes the axial coordinate (m) and $\bar{\lambda}$ stands the average emission wavelength (nm).

As mentioned before, in the setup of this study, an external near UV-lamp irradiates the batch through one radial side only. Thus, considering the symmetrical angular emission by the BL-lamp, the Equation 5.2 can be simplified as Equation 6.3.

$$P_l(t) = \frac{\bar{\lambda}}{h.c}\int_{\lambda_1}^{\lambda_2}\int_0^{L} q_{z,\lambda,t}.\, r.\, dz d\lambda \tag{6.3}$$

The average wavelength ($\bar{\lambda}$) was calculated by integrating the values of Intensity of the light at each wavelength with an interval of 320-388nm and applying the Weighted Mean method (see Equation 6.4).

$$\bar{\lambda}\,(\text{mean}) = \frac{\lambda_1 I_1 + \lambda_2 I_2 + \cdots + \lambda_n I_n}{I_1 + I_2 + \cdots + I_n} = \frac{\int_{\lambda_1}^{\lambda_2} \lambda.I(\lambda)d\lambda}{\int_{\lambda_1}^{\lambda_2} I(\lambda)d\lambda} \tag{6.4}$$

6.1.1.1 Irradiation Spectra for Near UV-Light Emitted, Reflected and Transmitted

The near UV lamp Intensity ($\mu W.cm^{-2}$) was measured between λ_1=320 nm and λ_2=420 nm along the 81 cm^2 area, which represents the quartz surface area covered by the TiO_2-film. Radiation measurements were performed using a StellarNet EPP2000C-25 LT16 spectrometer in 49 different positions, divided equally in 7 parts in each X and Y direction. In this way, it was possible to develop a precise radiation spectrum taking into consideration the asymmetrical position of the lamp in the photocatalytic reactor. One

should notice that in the experimental setup, the lamp was placed between the Y positions 2 and 4 along the X axis (see Figure 6.3).

Figure 6.4, Figure 6.5 and Figure 6.6 show the 3D spectra of lamp intensity emitted, backscattered and transmitted, respectively. These plots show an asymmetrical radiation profile, with higher values of intensity emitted (see Figure 6.4) in the Y position 3, between the X positions 3 and 5. For the reflected irradiation (see Figure 6.5), the radiation profile is considerably constant for the majority of the catalyst films, with a slightly higher values in the Y position at 5 along the X positions 3 to 5 which, is the area not directly covered by the lamp. Figure 6.6 also shows that transmitted irradiation increases at the same positions where the irradiation emitted display maximum values (Y position 3, between X positions 3 and 5).

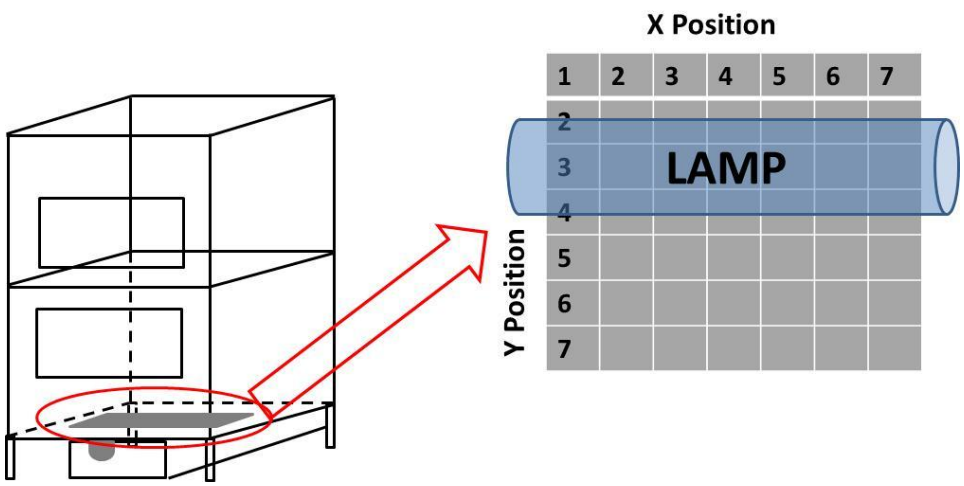

Figure 6.3: Measurements Scheme to Assess the Non-Symmetrical Radiation Profile

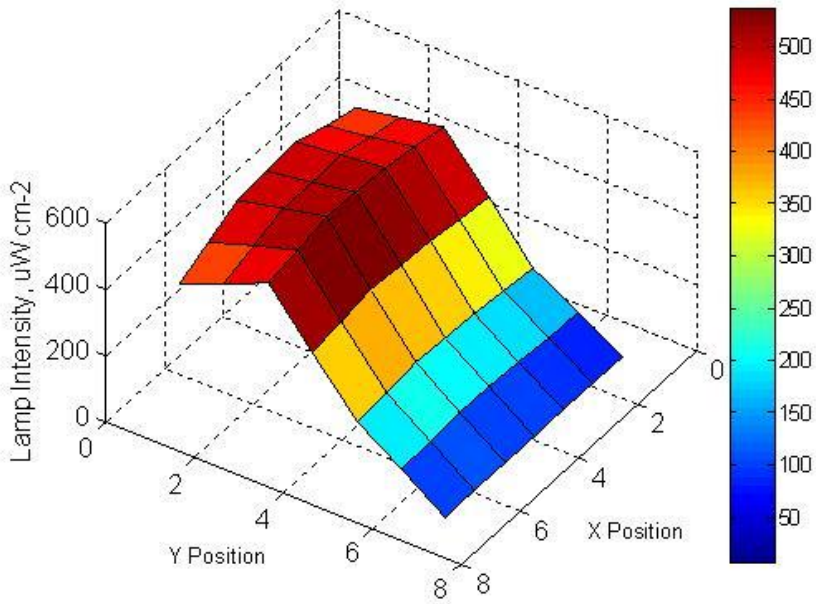

Figure 6.4: P_l (t) Spectrum Along the 49 Positions

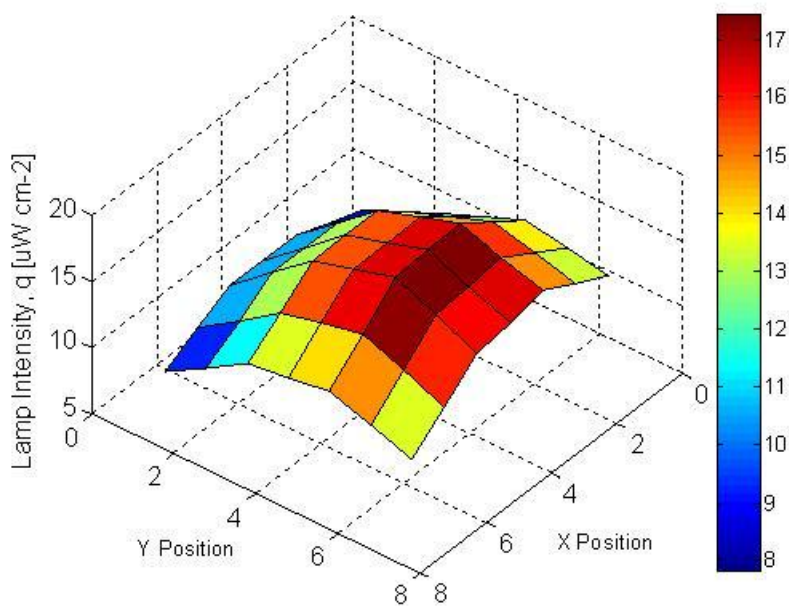

Figure 6.5: P_{bs} (t) Spectrum Along the 49 Positions

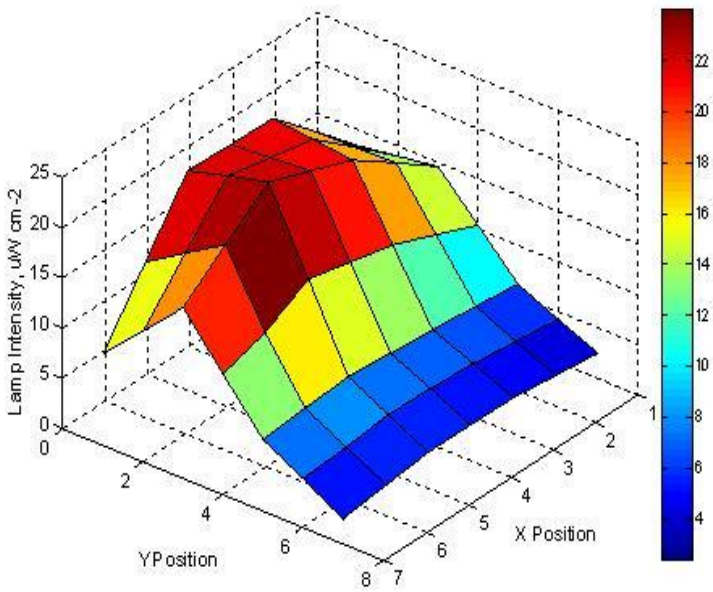

Figure 6.6: P_t (t) Spectrum Along the 49 Positions

Regarding the P_a, P_l, P_{bs} and P_t parameters involved in the radiation macroscopic balance, all of them were calculated by performing the integration of radiation measured in the 49 positions (Appendix B) and as it will be discussed in the next section.

6.1.1.1.1 Calculation of Lamp Emission (P_l)

An estimated P_l (t) value was established with 49 radiometric measurements**.** The result P_l (t) obtained was 4.04 x 10^{16} photons/s.

Calculation of P_a (t) was performed using Equation 6.1 and the P_{bs} (t) and P_t (t) data reported in Figure 6.5 and Figure 6.6 (see Table 6.1).

Table 6.1: P_l (t), P_{bs} (t), P_t (t) and P_a (t) Calculated for the TiO_2-Film

	Rate of Photon, Photons/s	Irradiation, %
Emitted, P_l (t)	4.41E+16	100
Back Scattered, P_{bs} (t)	1.95E+15	4
Transmitted, P_t (t)	1.75E+15	4
Absorbed, P_a (t)	4.04E+16	92

According to this Table 6.1, it can be concluded that a significant amount of the near UV radiation is absorbed by the TiO_2 film (92%). Comparing the obtained P_a (t) with data from the literature being $\Phi = 6.1 \times 10^{16}$ photons/s absorbed by the TiO_2 film (Danion et al., 2007), it can be observed that the results presented in this study appears to be very close in magnitude to the value reported for TiO_2-coated optical fibers.

6.2 Kinetic Modelling for malic acid and its intermediate degradation under TiO_2-film 1.5 wt%

According to several authors, (Irawaty et al., 2011; Chen et al., 2009; Herrmann et al., 1999; Herrmann et al., 1997; Fernandez et al., 1995) the kinetics of malic acid degradation with TiO_2 in suspension as well as with TiO_2 coated materials (quartz, glass and stainless steel) fits the Langmuir-Hinshelwood model.

The Langmuir-Hinshelwood approach is very well-known model to describe the catalytic conversion of chemical species involving adsorption at equilibrium. It has the advantage of considering not only the model compounds but also its intermediates formed during the photocatalytic conversion. According to different studies in the technical literature, in the malic acid photoconversion, more than one intermediate is observed. In the present study, only the main intermediate, malonic acid, was identified and as a result was the only one considered in the kinetic modeling.

6.2.1 Photolysis of Malic and Malonic Acid

Photolysis or homogeneous photoconversion of malic and malonic acid experiments were performed with a reaction cell having quartz window without TiO_2 coating. Photodegradation of malic and malonic acid were performed under these conditions at 10, 20, 30 and 40 ppm concentrations. Figure 5.12 showed that considering only 4% of total irradiation participating of the Photolysis, the change in concentration for malic acid at 20 ppm was only 1% despite the initial estimation of 30%.

Malic and malonic acid photolysis were accounted in our model considering the degradation of these compounds as following:

$$\frac{dC_i}{dt} = -k_{photolysis} C_i \tag{6.5}$$

where C_i represents the concentration at any the time during the photoconversion, t denotes the irradiation time and $k_{photolysis}$ stands for the reaction rate constant. Upon integration of Equation 6.5, one can obtain the following solution:

$$C_{final(i)} = C_{initial(i)} \exp(-k_{photolysis} t) \tag{6.6}$$

With this equation and the experimental data for the photolysis of 10, 20 and 30 ppm of malic and malonic acid, it is possible to obtain kinetic constants as reported in Table 6.2.

Table 6.2: Kinetic Constants for the Photolysis of Malic and Malonic Acid

Parameter	Compound	Value
$k_{photolysis}(min^{-1})$	Malic Acid	7.727×10^{-4}
$k_{photolysis}(min^{-1})$	Malonic Acid	3.984×10^{-4}

However, if one considers than in an actual photocatalytic experiment only 4% of the radiation is transmitted to the solution, photolysis can be assessed with Equation (6.7) and $\alpha = 0.04$:

$$C_{final(i)} = C_{initial(i)} \exp(-\propto k_{photolysis} t) \quad (6.7)$$

6.2.2 Kinetic Modeling of Malic Acid Photodegradation

Two reaction mechanisms are proposed for the kinetic modeling of malic photodegradation. Both models will consider malonic acid as an intermediate compound from malic acid photodegradation. These models are shown in Figure 6.7 and Figure 6.8. On one hand, Figure 6.7 shows reaction mechanism one, being a "series" reaction network. On the other hand, Figure 6.8 illustrates a "series-parallel" reaction network (reaction mechanism two).

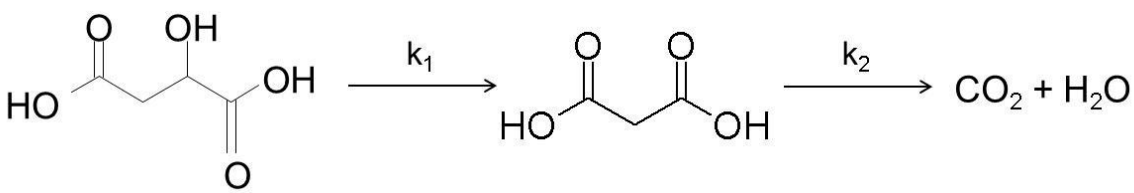

Figure 6.7: Reaction Mechanism One – "Series" Mechanism Proposed for the Photocatalytic Degradation of Malic Acid in TiO_2-Film 1.5 wt%

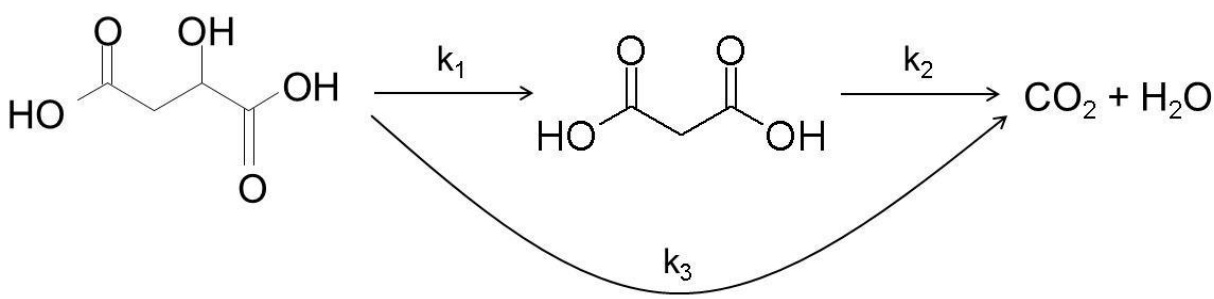

Figure 6.8: Reaction Mechanism Two – "Series-Parallel" Mechanism Proposed for the Photocatalytic Degradation of Malic Acid in TiO_2-Film 1.5 wt%

The proposed mechanisms refer to the concentration profile in Figure 5.8. This Figure 5.8 shows a decrease of malic acid concentration with the time of the reaction being close to the first order rate law for the first 5 to 9 hours of reaction (10 to 40ppm initial concentration of malic acid). One can notice that the final malic acid concentration

reaches almost zero with the formation of malonic acid being observed since the beginning of the photoconversion. The maximum value of malonic acid concentration is reached when malic acid concentration is near zero ppm. After that, malonic acid is converted progressively until its final concentration reaches again values close to zero.

The kinetic modelling for the two reaction mechanisms considers the following assumptions:

a. Malic and malonic acids adsorb on the TiO_2 film surface where the photocatalytic reactions take place.

b. The adsorption phenomenon is assumed to occur at equilibrium with the reaction rate on the catalytic surface controlling the overall reaction.

c. The final products CO_2 and H_2O products formed at the end of the reaction do not adsorb on the catalyst surface.

d. Photolysis of malic acid and its intermediates is considered in the modeling, being accounted for in the L-H kinetics.

6.2.2.1 Langmuir-Hinshelwood Reaction Rate

Following all these considerations, the Langmuir-Hinshelwood equation was applied for different authors to study the photodegradation of organic compounds under TiO_2 photocatalysis (Mehrvar et al., 2000; Salaices et al., 2004; Ortiz-Gomez et al., 2007; Laoufi et al., 2008; Montoya et al., 2009; Moreira et al., 2012). In the case of this study, given the asymmetrical radiation profile due to the position of the lamp in the setup, and the dark spots close to the edges of the reactor, the Langmuir-Hinshelwood equation has to consider a local volumetric rate of photon absorption (LVRPA) and the rate equation is given by equation 6.8 (Toepfer et al., 2006):

$$-r_i = k_{T,i}(\mathrm{LVRPA})^m \frac{K_i^A C_i}{1+\sum_{j=1}^{n} K_j^A C_j} = \frac{k_i^k K_i^A C_i}{1+\sum_{j=1}^{n} K_j^A C_j} \tag{6.8}$$

where i represents the main specie being degraded, “j” denotes each component that appears in the reaction, n is the number of species participating in the reaction, r_i is the reaction rate ($mol.g_{catalyst}^{-1}.hour^{-1}$), $k_{T,i}$ denotes the kinetic constant independent of photon

absorption, LVRPA stands for the local volumetric rate of photon absorption ($W.m^{-3}$), m represents the order of reaction related to VRPA ($0.5<m<1$), k^k_i denotes the reaction kinetic constant (mol g_{cat}^{-1} hour $^{-1}$), K^A_i stands for the adsorption constant (mol^{-1} l), and C_i represents the species' concentration ($mol.L^{-1}$). In this equation, the terms LVRPA and m were constant in all the experimental runs.

In a photocatalytic reactor operating in a batch mode, as the photoreactor used in this research, the rate equation for the photoconversion of the "i" specie can be expressed as Equation 6.9 (de Lasa et al., 2005):

$$-r_i = \frac{1}{W_{irrad}} \frac{dN_i}{dt} = \frac{V}{W_{irrad}} \frac{dC_i}{dt} \tag{6.9}$$

where W_{irrad} is the mass of TiO_2 in the catalyst film (g_{cat}), V is the reactor volume (L), N_i is the number of moles to be degraded (mol) and t is the reaction time (hour).

Combining the Equations 6.8 and 6.9, the reaction rate for each chemical compound can be written as:

$$\frac{dC_i}{dt} = \frac{\frac{V}{W_{irrad}} k_i^k K_i^A C_i}{1+\sum_{j=1}^{n} K_j^A C_j} \tag{6.10}$$

$$\frac{dC_i}{dt} = \frac{k_i C_i}{1+\sum_{j=1}^{n} K_j^A C_j} \tag{6.11}$$

where $k_i = \frac{W_{irrad}}{V} k_i^k K_i^A$

In developing the differential equations for the kinetic modeling presented in this paper, Equation 6.11 will be used to describe each component in the multi-component reaction model. An additional term will be added accounting for the effect that photolysis might have on the degradation of both, malic and malonic acids.

6.2.2.2 Reaction Mechanism One – "Series"

As discussed before (Figure 6.7), the mechanism one is represented as a series reaction and is shown below as:

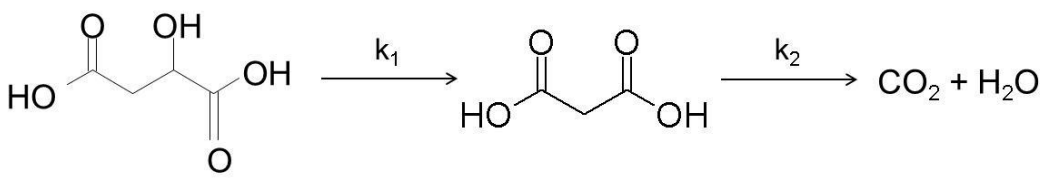

Based on the L-H equations, the photocatalytic degradation of malic acid (MaAc) and malonic acid (MAc) are given by the following equations:

$$\frac{dC_{MaAc}}{dt} = \frac{-k_1 C_{MaAc}}{1+K^A_{MaAc}C_{MaAc}+K^A_{MAc}C_{MAc}} - \alpha k_{photolysis\ MaAc} C_{MaAc} \quad (6.12)$$

$$\frac{dC_{MAc}}{dt} = \frac{k_1 C_{MaAc} - k_2 C_{MAc}}{1+K^A_{MaAc}C_{MaAc}+K^A_{MAc}C_{MAc}} - \alpha k_{photolysis\ MAc} C_{MAc} \quad (6.13)$$

where k_1 and k_2 are the reaction rate constants in min^{-1}, C is the concentration in ppm, MaAc and MAc represent malic and malonic acid respectively. K^A is the adsorption constant in ppm^{-1} L. The second term in the Equations 6.12 and 6.13 represent the degradation of malic and malonic acid due to photolysis. According to the radiation balance measurements, the amount of light transmitted through the TiO_2 film was 4% (Table 6.1). In this sense, both kinetic constants were multiplied by a factor "α" of 0.04.

Regarding the L-H model, malic and malonic acid photoconversion generates a system of two Ordinary Differential Equations (ODE) with two kinetic and two adsorption constants (k_1, k_2, K^A_{MaAc} and K^A_{Mac}, respectively).

The kinetic parameters were calculated with a MATLAB program, applying non-linear least square fit (lsqcurvefit). This method considers that the adjustment of parameters is obtained with a minimum value for the sum of the square residuals (difference between the value fit by the model and the value calculated/observed). Figure 6.9 shows malic and malonic acid photo conversion obtained experimentally for initial concentrations of 10, 20, 30 and 40 ppm and its correspondent fit model. From the Figure 6.9, it can be concluded that the model obtained with the mechanism one "series" fits the experimental data very well yielding a R^2 of 0.983.

Values of the kinetic and adsorption constants for Reaction Mechanism One are shown in Table 6.3. According to the relatively small values for 95% confidence interval (CI) and for the standard deviation (STD), it can be concluded that the model proposed predicts the data obtained very well from the photocatalytic degradation experiments.

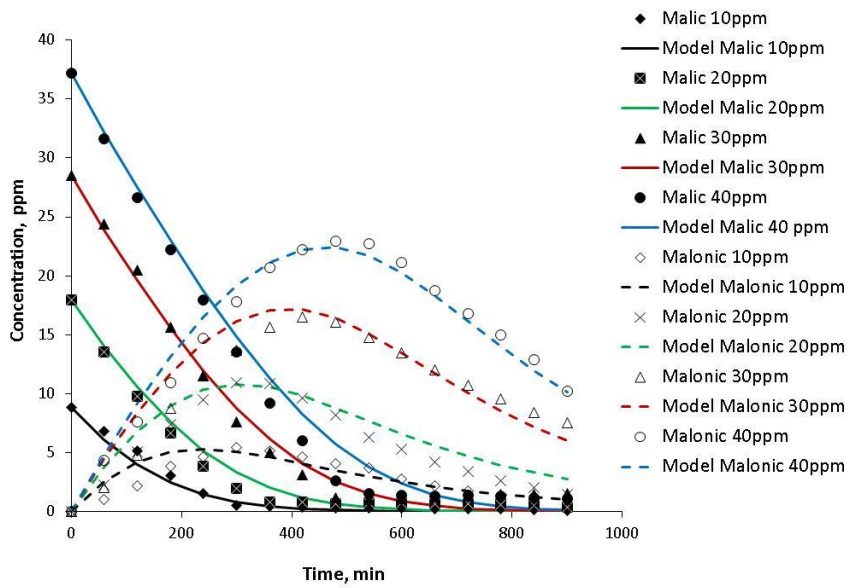

Figure 6.9: Experimental and Model One Concentration Profiles for Malic Acid and Malonic Acid Photocatalytic Conversion at 10, 20, 30 and 40 ppm

Table 6.3: Kinetic Parameters for the Photoconversion of Malic and Malonic Acid for the Simultaneous Optimization of 10, 20, 30 and 40 ppm for the Reaction Mechanism One

Parameter	Value	95% CI	STD
$k_1(min^{-1})$	$1.082x10^{-2}$	$1.680x10^{-3}$	$4.485x10^{-4}$
$k_2(min^{-1})$	$3.047x10^{-3}$	$4.442x10^{-4}$	$1.186x10^{-4}$
$K^A_{MaAc}\,(ppm^{-1})$	$1.043x10^{-1}$	$2.220x10^{-2}$	$5.927x10^{-3}$
$K^A_{MAc}\,(ppm^{-1})$	$2.859x10^{-3}$	$6.064x10^{-4}$	$2.841x10^{-3}$

Table 6.4 reports the cross-correlation coefficients for different parameters obtained in the modeling Mechanism One or the "In-series" Model, for the photoconversion of malic and malonic acid. Cross-correlation coefficients are a very useful instrument to predict the similarity between two independent variables. When cross-correlation coefficients are near to ±1, they suggest that the two variables have a high correlation and that multiple solutions for kinetic and absorption constants can be obtained. Considering the values reported in this Table 6.4, it is observed that only the parameters k_1 and K^A_{MaAc} exhibit cross-correlation coefficients close to 1 (e.g. 0.93).

Table 6.4: Cross-Correlation Coefficients of the Kinetic Parameters Obtained for the Photoconversion of Malic and Malonic Acid for the Simultaneous Optimization of 10, 20, 30 and 40 ppm for the Reaction Mechanism One

Parameter	k_1	k_2	K^A_{MaAc}	K^A_{MAc}
k_1	1			
k_2	0.78	1		
K^A_{MaAc}	0.93	0.62	1	
K^A_{MAc}	0.58	0.86	0.30	1

Figure 6.10 shows the reconciliation plot combining the experimental results and the results predicted by the kinetic model using the Mechanism One or "In-series". Reconciliation plots provide a good understanding of the reliability of the parameters obtained. It is known that plots presenting vertical bands show an over-parameterization of the kinetic model. The presence of horizontal bands in the reconciliation plots may indicate that the model is somewhat incomplete with at least one parameter missing in the kinetic model. As observed in Figure 6.10, the experimental and modeled points are randomly distributed. This confirms a good fit between the experimental and model values of concentration.

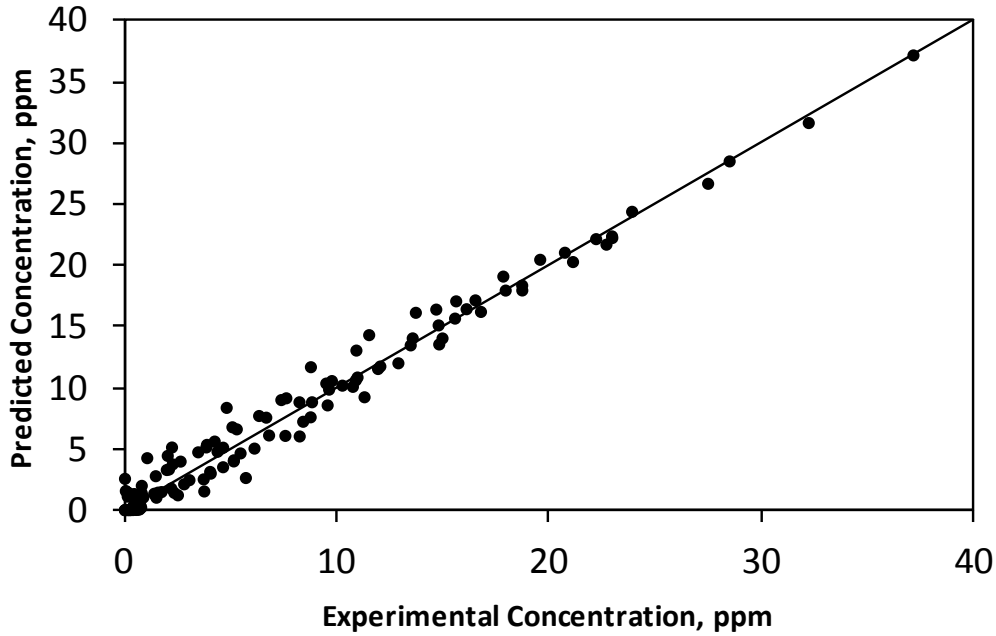

Figure 6.10: Reconciliation Plot of the Predicted Concentration versus Experimental Concentration for the 4 Parameters Estimated Using the Reaction Mechanism One

6.2.2.3 Reaction Mechanism Two – "Series-Parallel"

As discussed before (Figure 6.8), the Mechanism Two is represented as:

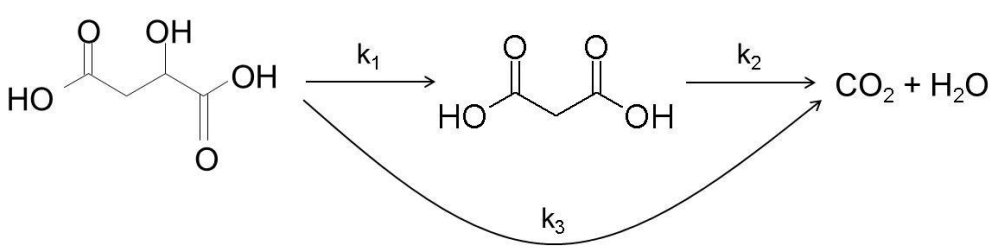

Based on the L-H equations, the photodegradation of malic acid (MaAc) and malonic acid (MAc) are given by the following equations:

$$\frac{dC_{MaAc}}{dt} = \frac{-(k_1+k_3)C_{MaAc}}{1+K^A_{MaAc}C_{MaAc}+K^A_{MAc}C_{MAc}} - \alpha k_{photolysis\ MaAc}C_{MaAc} \tag{6.14}$$

$$\frac{dC_{MAc}}{dt} = \frac{k_1C_{MaAc} - k_2C_{MAc}}{1+K^A_{MaAc}C_{MaAc}+K^A_{MAc}C_{MAc}} - \alpha k_{photolysis\ MAc}C_{MAc} \tag{6.15}$$

where k_1, k_2 and k_3 are the reaction rate constants in min^{-1}, C denotes the concentration in ppm, K^A represents the adsorption constant in ppm^{-1} L and "α" stands for the Photolysis factor related to the amount of irradiation reaching the malic and malonic acid solution, which was found to be equal to 0.04.

Figure 6.11 reports the experimental and estimated photocatalytic degradation profiles of malic and malonic acid using the Model Mechanism Two. Results are presented for initial concentration of malic acid, with these being 10, 20, 30 and 40 ppm. This model also show a very good fit between the experimental and model concentration profiles for malic and malonic acid photodegradation yielding a R^2 of 0.988.

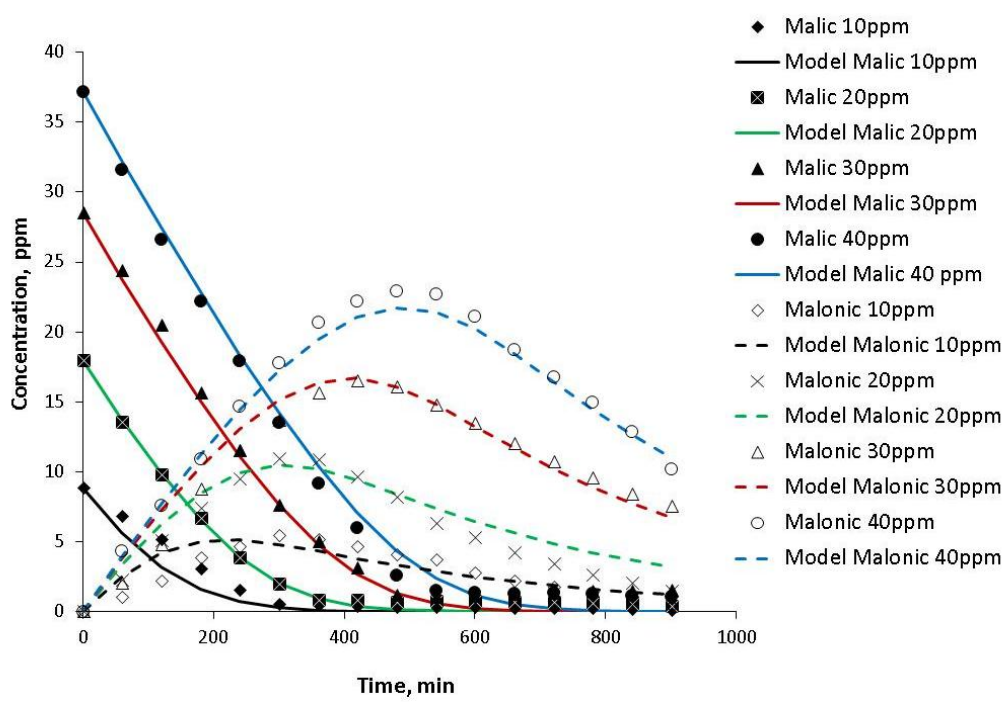

Figure 6.11: Experimental and Model Two Concentration Profiles for Malic Acid and Malonic Acid Photocatalytic Conversion at 10, 20, 30 and 40 ppm

Table 6.5 reports values for the kinetic and adsorption constants involved in Kinetic Model Two or in a "Series-parallel" model. This table also reports the 95% CI as well as the standard deviation values. This Model Two presents narrow spans for both, the CI and STD. Therefore, the proposed mechanism predicts the data obtained very well from the photocatalytic degradation experiments.

Table 6.5: Kinetic Parameters for the Photoconversion of Malic and Malonic Acid for the Simultaneous Optimization of 10, 20, 30 and 40 ppm for the Reaction Mechanism Two

Parameter	Value	95% CI	STD
$k_1(min^{-1})$	$1.365x10^{-2}$	$2.285x10^{-3}$	$6.083x10^{-4}$
$k_2(min^{-1})$	$2.429x10^{-3}$	$3.977x10^{-4}$	$1.059x10^{-6}$
$k_3(min^{-1})$	$2.942x10^{-3}$	$1.097x10^{-3}$	$2.920x10^{-4}$
K^A_{MaAc} $(ppm^{-1}L)$	$1.758x10^{-1}$	$4.375x10^{-2}$	$1.165x10^{-2}$
K^A_{MAc} $(ppm^{-1}L)$	$4.109x10^{-3}$	$6.203x10^{-4}$	$1.651x10^{-3}$

Table 6.6 presents the cross-correlation coefficients for different parameters obtained in the Modeling Mechanism Two "Series-parallel". With respect to the cross-correlation coefficient values, it is observed that the parameters k_1 and K^A_{MaAc} exhibit cross-correlation coefficient of 0.98 (near one) and the parameters k_3 and K^A_{MaAc} exhibited cross-correlation coefficients of 0.90. Lastly, it is also noticed that there is a relatively high cross-correlation between k_1 and k_3 kinetic constants. Therefore, it is concluded that this model could potentially present uncertainty for both kinetic and adsorption parameters.

Table 6.6: Cross-Correlation Coefficients of the Kinetic Parameters Obtained for the Photoconversion of Malic and Malonic Acid for the Simultaneous Optimization of 10, 20, 30 and 40 ppm for the Reaction Mechanism Two

Parameter	k_1	k_2	k_3	K^A_{MaAc}	K^A_{Mac}
k_1	1				
k_2	0.24	1			
k_3	0.88	0.18	1		
K^A_{MaAc}	0.98	0.22	0.90	1	
K^A_{MAc}	0.26	0.06	0.53	0.22	1

Figure 6.12 shows the reconciliation plot combining the experimental results and the results predicted by the kinetic model using the Mechanism Two “Series-parallel”. As observed in Figure 6.12, there are no vertical or horizontal bands in the reconciliation plot with the experimental and modeled points randomly distributed confirming a good fit between the experimental and model values of concentration.

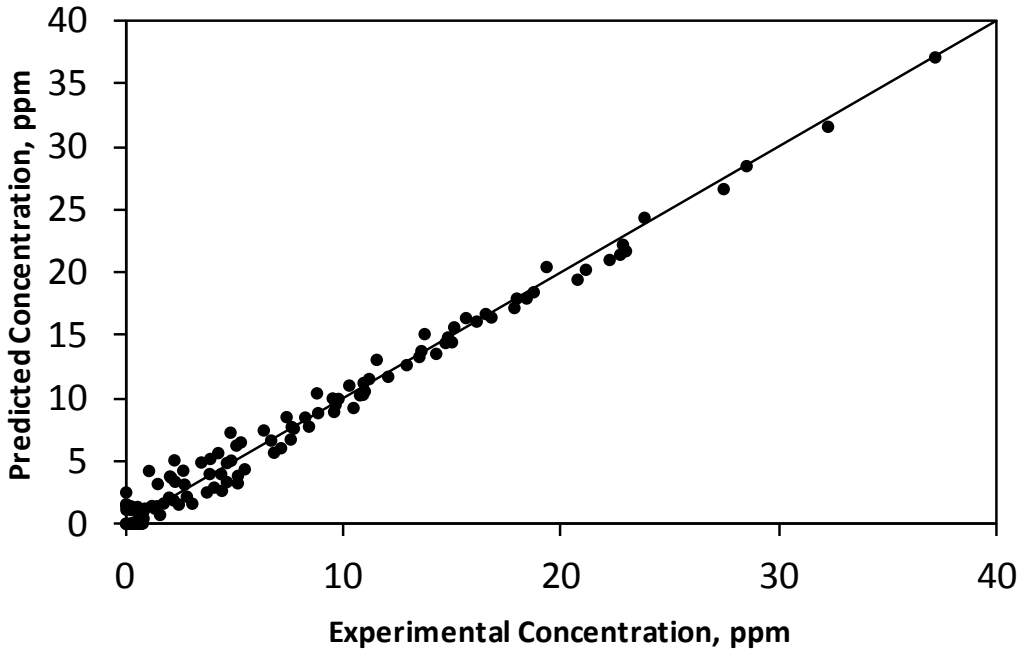

Figure 6.12: Reconciliation Plot of the Predicted Concentration versus Experimental Concentration for the 5 Parameters Estimated Using the Mechanism Two

6.2.2.4 Comparison between Kinetic Model One "Series" and Kinetic Model Two "Series-parallel"

In order to assess the best kinetic model for the photoconversion of malic and malonic acid under TiO_2-film 1.5 wt%, the following analysis comparing the experimental results with the predicted results obtained applying the Models One and Two were performed (Table 6.7):

a. Correlation Coefficient (R^2)

b. 95% Confidence Interval (CI) and % Difference CI

c. Standard Deviation (STD)

d. Overall Cross-correlation Factor (CCC)

e. Reconciliation Plot (RP)

Table 6.7: Comparison between Kinetic Model One "Series" and Kinetic Model Two "Series-Parallel"

	Model One "Series"	**Model Two "Series-Parallel"**	**Best Model Fit**
R^2	0.983	0.988	Model Two
95% CI **(% diff. CI)**	$4.442x10^{-4}$ – $2.220x10^{-2}$ (14 – 21%)	$3.977x10^{-6}$ – $1.097x10^{-3}$ (1 – 37%)	Model One
STD	$1.196x10^{-4}$ – $5.744x10^{-3}$	$9.881x10^{-5}$ – $1.131x10^{-2}$	Model One
CCC	0.93 0.86	0.98 0.90 0.88	Model One
RP	No Horizontal Bands No Vertical Bands	No Horizontal Bands No Vertical Bands	Both Models

Regarding the analysis performed in Table 6.7, both methods showed a very good fit of the Kinetic Model proposed when compared to the experimental results. As shown in Table 6.7, from the five analyses performed, three were more favorable when using Model One; meanwhile, only the correlation factor was found to have a better value when using Kinetic Model Two. However, more information is needed in order to predict the best model for the malic and malonic acid photocatalytic degradation.

In order to elucidate what model predicts better the photocatalytic conversion of malic and malonic acid in water better using the reactor setup of this study, it was necessary to calculate the concentration of CO_2 formed during the experiments. Figure 6.13 shows the concentration profile of Carbon in ppm, for the CO_2 and the Total Organic Carbon (TOC) calculated during the photocatalytic conversion of 40 ppm of malic acid. According to the Figure 6.13, the formation of CO_2 is observed in the very beginning of the photocatalytic

reaction. It shows that complete mineralization of malic acid into CO_2 and H_2O is observed already at the very early stages of the photocatalytic conversion.

However, one can also notice that the rate of CO_2 formation (in ppm of Carbon) is smaller than the rate of malic acid photoconversion (about 1 mole of CO_2/2 moles of Malic Acid ratio). It shows that Mechanism Two or in "Series-parallel" should better predict malic acid photocatalytic conversion. This higher reliability of the in "Series-parallel" overall mechanism was also observed in the photocatalytic degradation of phenol in water using a cylindrical slurry unit (Moreira, 2011). According to this author, the Series-parallel mechanism dominates due to a non-uniform OH radical density in the slurry reactor.

In the reactor setup of this study, however, both axial and radial radiation gradients were not observed. Hence it is expected that formation of hydroxyl radicals should in principal be more uniform than in annular photoreactors with suspended TiO_2. A uniform density of hydroxyl radicals promotes a higher probability of applicability of the "In series" model. However, one cannot fully guarantee such a homogeneous radiation profile along TiO_2 films, and thus the use of an in "Series-parallel" model appears still be required.

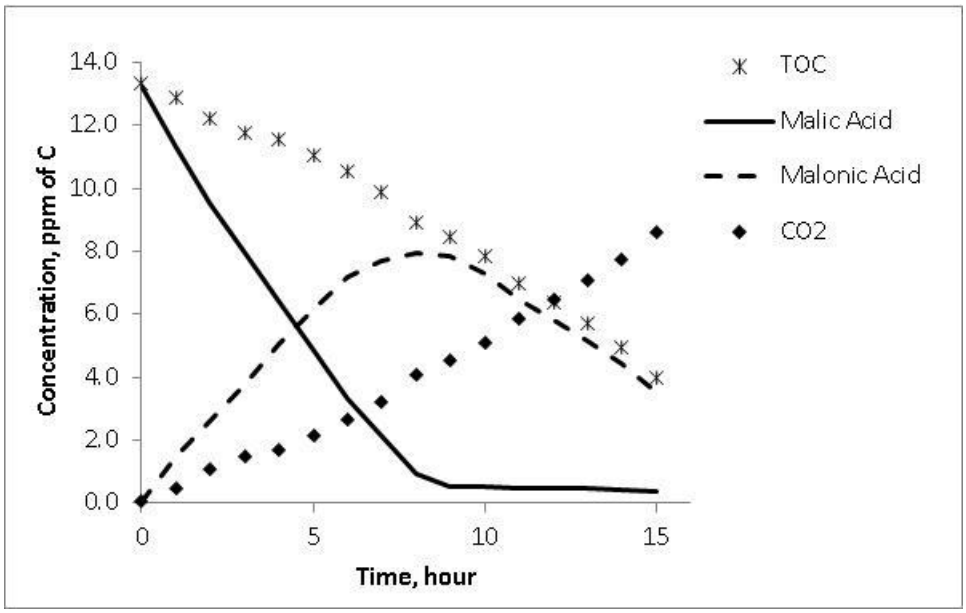

Figure 6.13: CO_2 and TOC Profile for the Photocatalytic Degradation of Malic Acid at Initial Concentration of 40 ppm (13.6 ppm of Carbon)

6.3 Calculation of the Quantum Yield (φ)

There are different definitions for quantum yields, such as: (a) primary quantum yield (Cassano et al., 1995 and Davydov et al., 1999), (b) overall quantum yield (Cassano et al., 1995), (c) apparent quantum yield (Fox and Dulay, 1993; Nimlos et al., 1996; Sczechowski et al., 1995 and Zhang et al., 1994), (d) minimum apparent quantum yield (Garcia-Hernandez, 2012) and (e) quantum yield (Peill and Hoffmann, 1995; Valladares and Bolton, 1993 and Yamazaki-Nishida et al., 1994). For heterogeneous systems, the calculation of the quantum yield is more complex than for homogeneous systems and backscattered phenomena needs to be taken in account. As part of the characterization of the catalyst layer activity, quantum yield calculation appears to be extremely important. In the present report, the value of quantum yield was determined applying the minimum apparent quantum yield concept (see Equation 6.16) which consists of the ratio of the number of molecules of OH radicals converted per second and the number of photons absorbed by the catalyst film per second.

$$\varphi = \frac{\text{Number of molecules of OH}^{\bullet}\text{ consumed/s}}{\text{Number of photons absorbed by the TiO}_2\text{ layer/s}} = \frac{\varphi_1}{P_a(t)} \tag{6.16}$$

The value of $P_a(t)$ was calculated using the irradiation profile measured (Figure 6.4, Figure 6.5 and Figure 6.6) for different concentrations of malic acid (10, 20, 30 and 40ppm). The number of molecules of OH radicals consumed/s (φ_1) was estimated through the malic acid degradation stoichiometry, considering the two possible mechanisms proposed: in “Series” and in “Series-parallel” reaction networks.

6.3.1 Quantum Yield (φ) for the Reaction Mechanism One – “Series”

Malic acid photodegradation Mechanism One “Series” occurs with the consumption of 4 molecules of OH radicals in the first step (Equation 6.17) and with the consumption of 8 molecules of OH radicals in the second step forming CO_2 and H_2O (Equation 6.18).

$$3\ C_4H_6O_5 + 4\ OH^{\bullet} \xrightarrow{k_1} 4\ C_3H_4O_4 + 3\ H_2O \tag{6.17}$$

$$1\ C_3H_4O_4 + 8\ OH^{\bullet} \xrightarrow{k_2} CO_2 + 6\ H_2O \tag{6.18}$$

Considering a hypothetical reaction $\nu_{abc}\ C_aH_bO_c + \nu_{OH^{\cdot}}\ OH^{\cdot} \rightarrow \nu_{xyz}\ C_xH_yO_z + \nu_{H2O}\ H_2O$, the number of total molecules of OH radicals consumed/s (φ_1) can be estimated according to Equation 6.19 (Serrano et al., 2009). The hydroxyl radical consumption (φ_1) can also be expressed in terms of concentration profile changes (Equation 6.20) and can be written as a function of kinetic constants and adsorption constants of the malic and malonic acid (Equation 6.21).

$$\varphi_1 = r_{OH^{\cdot}\ Total} = \sum \frac{\nu_{OH^{\cdot}}}{\nu_{C_aH_bO_c}} r_{C_aH_bO_c} \tag{6.19}$$

$$\varphi_1 = r_{OH^{\cdot}\ Total} = \frac{4}{3}\frac{dC_4H_6O_5}{dt} + 8\frac{dC_3H_4O_4}{dt} \tag{6.20}$$

$$\varphi_1 = r_{OH^{\cdot}\ Total} = \frac{\frac{4}{3}k_1C_{MaAc} + 8k_2C_{MAc}}{1+K^A_{MaAc}C_{MaAc}+K^A_{MAc}C_{MAc}} \tag{6.21}$$

The values of k_1, k_2, K^A_{MaAc} and K^A_{Mac} for the mechanism model one (Table 6.3) along with $P_a(t)$ equal $4.04x10^{16}$ photons/s (Table 6.1) were employed in the Equation 6.21. The values of quantum yield (φ) as a function of time for the photocatalytic conversion of malic acid at 10, 20, 30 and 40 ppm using the Model Mechanism One is shown in the Figure 6.14.

Figure 6.14 displays the values of φ increasing in the beginning of the malic acid degradation until it reaches a maximum value which coincides with the maximum concentration of the intermediate formed (malonic acid). According to Figure 6.14, the maximum quantum yield obtained is 17.4% after 8 hours of malic acid photocatalytic degradation at 40 ppm.

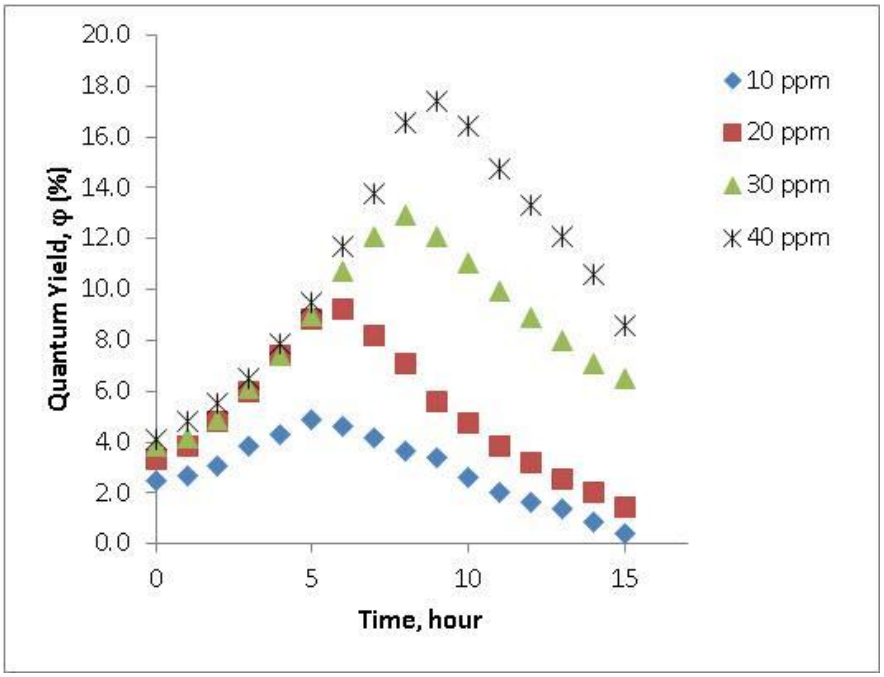

Figure 6.14: Quantum Yield (φ) Profile for Malic Acid Photocatalytic Degradation at 10, 20, 30 and 40 ppm Applying the Kinetic Model One "Series"

6.3.2 Quantum Yield (φ) for the Reaction Mechanism Two – "Series-Parallel"

For the in "Series-parallel" mechanism for malic acid photoconversion, malic acid is simultaneously converted into malonic acid (Equation 6.17) with subsequent conversion into CO_2 (Equation 6.18). Malic acid can also be directly converted into CO_2 (Equation 6.22), with water produced in the two pathways.

$$1\ C_4H_6O_5 + 12\ OH^{\bullet} \xrightarrow{k_3} 4\ CO_2 + 9\ H_2O \tag{6.22}$$

Applying the stoichiometry of Equations 6.17, 6.18 and 6.22, and the Langmuir-Hinshelwood Kinetic model for the Mechanism Two "Series-parallel", the reaction rate for the hydroxyl radical consumption (φ_1) can be written as a function of kinetic constants and adsorption constants of the malic and malonic acid (Equation 6.23).

$$\varphi_1 = r_{OH\cdot\,Total} = \frac{\left(\frac{4}{3}k_1+12k_3\right)C_{MaAc} + 8k_2C_{MAc}}{1+K^A_{MaAc}C_{MaAc}+K^A_{MAc}C_{MAc}} \tag{6.23}$$

The calculations were performed in the same manner as with Model One. The values of the quantum yield (φ) as a function of time for the photocatalytic conversion of malic acid at 10, 20, 30 and 40 ppm employing the Model Mechanism Two are shown in the Figure 6.15.

Figure 6.15 illustrates that, unlike the Model Mechanism One "Series", the value of φ for the Series-parallel Model decreases with time for an initial concentration of 10 and 20 ppm of malic acid, showing a maximum φ value in the very beginning of the reaction. For the other concentrations (30 and 40 ppm), φ increases in the beginning of the run until it reaches a maximum value coinciding with the maximum concentration of the intermediate formed (malonic acid), as observed when using Model Mechanism One. The maximum value of φ is 14.2%, obtained after 9 hours of photocatalytic conversion of malic acid at 40 ppm.

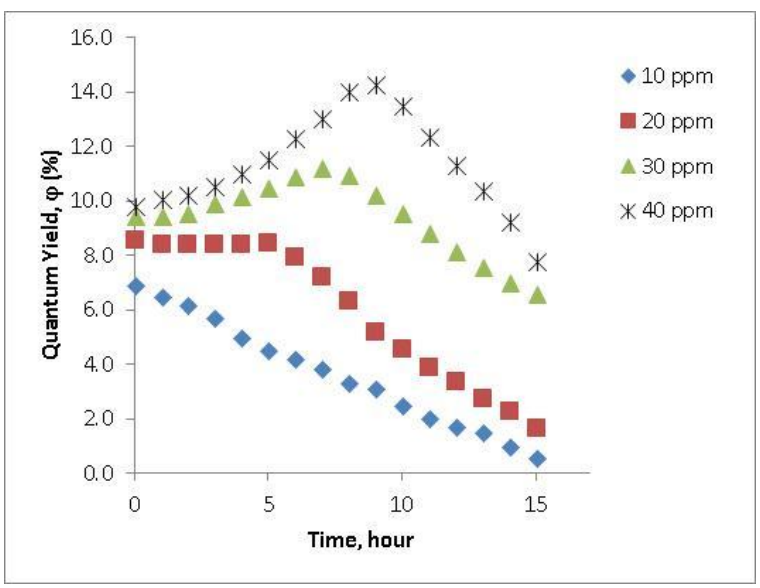

Figure 6.15: Quantum Yield (φ) Profile for Malic Acid Photocatalytic Degradation at 10, 20, 30 and 40 ppm Applying the Kinetic Model Two "Series-parallel"

Quantum yield values as high as 17.4 % (Mechanism One - “Series”) calculated using the StellarNet EPP2000C-25 LT16 Spectrometer demonstrate that indirect irradiation is able to promote the photocatalytic degradation of malic acid at various initial concentrations (10, 20, 30 and 40 ppm). To explain this phenomenon, one can consider that the holes (h^+) formed in the quartz-glue-TiO_2 surface (back face) are mobile holes that can migrate to the opposite side of the TiO_2 layer in contact with the malic acid solution. This h^+ site mobility and migration promotes the formation of OH radicals which degrade the malic acid molecules. When comparing the maximum value of quantum yield obtained for the photocatalytic conversion of malic acid 20 ppm (φ_{series} = 9.2 % and $\varphi_{series\text{-}parallel}$ = 8.6 %) with the best value reported in the literature, φ = 6% (Danion et al., 2007), it can be concluded that the setup of the present experiment shows excellent photoactivity even when compared with catalyst surfaces directly irradiated. These data also highlight the importance of results providing insight into the photoactivity of catalyst surfaces undirected irradiated. Furthermore, these findings prove that the mobility of electron-hole pairs on the photocatalyst surface can occur with this being a key for promoting the photocatalytic conversion of organic compounds using thin films.

6.4 Conclusions

a. Macroscopic Radiation Balance measurements showed that 92% of the light emitted is absorbed by the TiO_2-film of this study.

b. A kinetic model for the photocatalytic degradation of Malic and Malonic acid including the photolysis parameter was predicted using the Langmuir-Hinshelwood model equation.

c. Both, Kinetic Model One (in “Series”) and Kinetic Model Two (in “Series-Parallel”), showed a good fit with the experimental data, yielding R^2 of 0.983 and 0.988, respectively.

d. Comparing the Kinetic Model Mechanism One (in “Series”) and Kinetic Model Two (in “Series-Parallel”), it was observed from the concentration profile of CO_2 that the

Mechanism Two (in “Series-Parallel”) predicts better the photocatalytic conversion of Malic Acid in water.

e. Quantum yield (φ) as high as 17.4 and 14.2% for the reaction Mechanism One “Series” and reaction Mechanism Two “Series-Parallel” were obtained using a TiO_2-film for the photodegradation of 40 ppm of malic acid.

Chapter 7

7 Conclusions and Recommendations

This Chapter reports the conclusions regarding the results obtained in this Master study as well as the recommendations for the future work.

7.1 Conclusions

In order to overcome the high irradiation absorption of opaque fluids such as apple juice and develop a method for the photocatalytic conversion of organic species in these fluids, a catalyst film was prepared and a new PhotoReactor Cell was designed. The main contributions of the present study are found below:

a. A cost-effective thin catalyst film using a UV-transparent/waterproof glue and a TiO_2 1.5 wt% in water was prepared. The SEM/EDX analysis showed the presence of a photoactive region on the catalyst thin film, characterized by the presence of TiO_2 particles.

b. A new PhotoReactor Cell using the TiO_2–film of this study was designed. The near UV-lamp placed at the bottom of the Batch Reactor allowed the irradiation to reach the TiO_2 film before irradiation reached the opaque fluid. As a result, the thin films implemented, combined with back-irradiation and electron-hole pair mobility in the Reactor Cell, provide a beneficial approach for the photocatalytic degradation of opaque fluids.

c. Photodegradation experiments under near UV-light using the TiO_2 film, of malic and malonic acid in water at different concentrations (10, 20, 30 and 40 ppm) demonstrated that malic acid is completely degraded after 5 to 8 hours, depending on the initial concentration. The minimum concentration of malic acid is reached with maximum concentrations of malonic acid, showing that malonic acid is the key intermediate in malic acid photocatalytic degradation.

d. Experiments performed at different mixing speeds showed that the influence of external thin film transport processes as well as the photolysis of malic and malonic acid can be neglected while, modeling photocatalytic degradation with the TiO_2 films of the present study.

e. Macroscopic Radiation Balance measurements showed that 92% of the light emitted is absorbed by the TiO_2-film of this study. Quantum yield (φ) as high as 17.4 and 14.2% for the reaction Mechanism One "Series" and Mechanism Two "Series-Parallel" were obtained using a TiO_2-film for the photodegradation of 40 ppm of malic acid.

f. A kinetic model for the photocatalytic degradation of malic and malonic acid was predicted using the Langmuir-Hinshelwood model equation for both, Kinetic Model One "Series" and Two "Series-Parallel. This model showed a good fit with the experimental data. Statistical analyses in both cases yielded to R^2 close to one, small values for 95% CI and STD and CCC and, a Reconciliation Plot (RP) with experimental and modeled points which were randomly distributed.

g. Comparing the Kinetic Model Mechanism One "Series" and Two "Series-Parallel", it was observed from the concentration profile of CO_2 that the Mechanism Two "Series-Parallel" predicts better the photocatalytic conversion of malic acid in water.

f. Preservation of the sensory attributes of apple juice includes adequate concentration of malic acid in its composition. Thus, photocatalysis can be applied for the apple juice preservation with near UV irradiation times not surpassing 1 hour. This exposure time, (Rincon et al., 2003 and Ireland et al., 1993), are efficient to promote the 5-log CFU/ml reduction of E. coli.

7.2 Recommendations for Future Work

Based on the results obtained in this present study, the recommendations for the future work are as follows:

a. To perform the photocatalytic degradation of E. coli using the PhotoReactor Cell of this study and evaluate its concentration after 1 hour of reaction.

b. To test other types of UV-transparent/waterproof glues. It was found that the UV-transparent glue used in the present study is slightly soluble in water after diverse runs.

c. To further investigate and identify the unknown species likely linked to the UV-transparent glue as observed via HPLC.

d. To change the PhotoReactor Cell setup, placing the lamp symmetrically and repeat the photocatalytic degradations tests. This would be done to compare the results obtained with those of the present study with the lamp placed asymmetrically.

e. To perform experiments with apple juice and measure the photocatalytic degradation of malic acid and E. coli using the new PhotoReactor Cell and thus, evaluate its application to treat opaque fluids.

References

Aguillar-Rosas, S. F., Ballinas-Casarrubias, M. L., Nevarez-Moorilon, G. V., Martin-Belloso, O., Ortega-Rivas, E. **(2007)** Thermal and pulsed electric fields pasteurization of apple juice: Effects on physicochemical properties and flavours compounds. Journal of Food Engineering, 83, 41-46.

Ahmed, S., Rasul, M. G., Martens, W., N., Brown, R. and Hashib, M. A. **(2010)** Heterogeneous photocatalytic degradation of phenols in wastewater: A review on current status and developments. Desalination, 261, 3-18.

Al-Rasheed, R. A. **(2005)** Water treatment by heterogeneous photocatalysis an overview. Saline water desalination Research Institute.

Balasubramanian, G., Dionysiou, D., Suidan, M., Baudin, I., Laine, J.-M. **(2004)** Evaluating the activities of immobilized TiO_2 powder films for the photocatalytic degradation of organic contaminants in water. Applied Catalysis B: Environmental 47, 73-84.

Balzani, V. C., Carassiti, V. **(1970)** Photochemistry of Co-ordination Compounds.Academic Press, New York, 172–174.

Barbosa-Canovas, G. V., Pothakamury, U. R., Palou, E., & Swanson, B.G. **(1998)** Biological effects and applications of pulsed electric fields for the preservation of foods. In G. V. Barbosa-Canovas, U. R. Pothakamury, E. Palou & B. G. Swanson (Eds.), Nonthermal Preservation of Foods (pp. 73–112). New York: Marcel Dekker Inc.

Basaran, N., Quintero-Ramos A., Moake M. M., Churrey, J. J. and Worobo R. W. **(2004)** Influence of apple cultivars on inactivation of different strains of Escherichia coli O157:H7 in apple cider by UV irradiation. Applied and Environmental Microbiology, 70, 6061-6065.

Baxendale, J. H. and Wilson, J. A. **(1956)** The photolysis of hydrogen peroxide at high light intensities. Chemistry Dept., University of Manchester.

Bhatkhande, D. S., Pangarkar, V. G. and Beenackers, A. ACM B. **(2001)** Photocatalytic degradation for environmental applications – A review. Journal of Chemical Technology and Biotechnology, 77: 102-116.

Bolton, J. R. and Linden, K. G. **(2003)** Standardization of methods for fluence UV dose determination in bench-scale UV experiments. Journal of Environmental Engineering, 129, 209-215.

Brown, J.D., Williamson, D.L., Nozik, A.J., J. **(1989)** Phys. Chem. 89, 3076.

Butz, P., Tauscher, B. **(2002)** Emerging Technologies: chemical aspects. Food Research International, 35, 279–284.

Caminiti, I. M., Noci, F., Munoz, A., Whyte, P., Morgan, D. J., Cronin, D. A., Lyng, J. G. **(2011)** Impact of selected combinations of non-thermal processing technologies on the quality of an apple and cranberry juice blend. Food Chemistry, 124, 1387-1392.

Cassano, A.; Martín, C.; Brandi, R.; Alfano, O. **(1995)** Photoreactor Analysis and Design: Fundamentals and Applications. Industrial and Engineering Chemistry Research 34, 2155-2201.

Charles-Rodriguez, A. V., Nevarez-Moorilon, G. V. **(2007)** Comparison of thermal processing and pulsed electric fields treatment in pasteurization of apple juice. Doctoral Dissertation. Available from Trans IChemE, Part C.

Chen, D., Li, F., Ray, A.K. **(2001)** External and internal mass transfer effect on photocatalytic degradation. Catalysis Today 66, 475–485.

Chen, Q., Song, J. M., Pan, F., Xia, F. L., Yuan, J. Y. **(2009)** The kinetics of photocatalytic degradation of aliphatic carboxylic acids in an UV/TiO_2 suspension system. Environmental Technology: Vol. 30, No. 11, 1103-1109.

Cheng, L. H., Soh, C. Y., Liew, S. C., & Teh, F. F. **(2007)** Effects of sonication and carbonation on guava juice quality. Food Chemistry, 104(4), 1396–1401.

Chinnici, F., Spinabelli, U., Riponi, C., Amati, A. **(2005)** Optimization of the determination of organic acids and sugars in fruit juices by ion-exclusion liquid chromatography. Volume 18, Issues 2-3, 121-130.

Cho, M., Chung, H., Choi, W. and Yoon, J. **(2004)** Linear correlation between inactivation of E. coli and OH radical concentration in TiO2 photocatalytic disinfection. Water Research, 38, 1069-1077.

Choi, H., Stathatos, E., Dionysiou, D. **(2007)** Photocatalytic TiO2 films and membranes for the development of efficient wastewater treatment and reuse systems. Desalination 202, 199-206.

Choi, H., Stathatos, E., Dionysiou, D. D. **(2006)** Sol–gel preparation of mesoporous photocatalytic TiO2 films and TiO2/Al2O3 composite membranes for environmental applications. Applied Catalysis B: Environmental 63, 60–67.

Code of Federal Regulations (CFR), Title 21: Food and Drugs. **(2012)** Volume 2, Part 120.24(a), Food and Drug Administration, U.S.

Danion, A., Disdier, J., Guillard C., Jaffrezic-Renault. **(2007)** Malic acid photocatalytic degradation using a TiO_2-coated optical fiber reactor. Journal of Photochemistry and Photobiology A: Chemistry 190, 135-140.

Davydov, L.; Smirniotis, P. G.; Pratsinis, S. E. **(1999)** Novel Differential Reactor for the Measurement of Overall Quantum Yields. Industrial and Engineering Chemistry Research 38, 1376-1383.

de Lasa, H., Serrano, B., Salaices, M. **(2005)** Photocatalytic Reaction Engineering, Springer: New York.

Dolamic, I., Burgi, T. **(2006)** Photoassisted Decomposition of Malonic Acid on TiO_2 studied by in situ attenuated total reflection infrared spectroscopy. J. Phys. Chem. B, 110, 14898-14904.

Duffy, S., Churey, J., Worobo, R., & Schaffner, D. W. **(2000)** Analysis and modeling of the variability associated with UV inactivation of Escherichia coli in apple cider. Journal of Food Protection, 63, 1587 –1590.

Evrendilek, G. A., Jin, Z. T., Ruhlman, K. T., Qin, X., Zhang, Q. H., Richter, E. R. **(2000)** Microbial safety and shelf-life of apple juice and cider processed by bench ad pilot scale PEF systems. Inovative Food Science & Emerging Technologies 1, 77-86.

Fernandez, A., Lassaletta A., Jimenez V.M., Justo, A., Gonzalez-Elipe A.R., Herrmann, J-M., Tahiri, H., Ait-Ichou Y. **(1995)** Preparation and characterization of TiO2 photocatalysts supported on various rigid supports (glass, quartz and stainless steel). Comparative studies of photocatalytic activity in water purification. Applied Catalysis B: Environmental 7, 49-63.

Fetteman, J. C. **(1928)** The electrical conductivity method of processing milk. Agriculture and Engineering, 9, 107-108.

Fox M. A.; Dulay, M. T. **(1993)** Heterogeneous Photocatalysis. Chemical Reviews 93, 341-350.

Franch, M.I., Ayllon, J.A., Peral, J., Domenech, X. **(2004)** Fe(III) photocatalyzed degradation of low chain carboxylic acids implications of the iron salt. Applied Catalysis B: Environmental 50, 89-99.

Friedman, D., Mendive, C., Bahnemann, D. **(2010)** TiO_2 for water treatment: Parameters affecting the kinetics and mechanisms of Photocatalysis. Applied Catalysis B: Environmental 99, 398-406.

Garcia-Hernandez, M. **(2012)** Photocatalytic Reactors for Air Treatment: Energy Efficiencies and Kinetic Modeling PhD Thesis. The University of Western Ontario.

Gardner, P. T., White, T. A. C., McPhail, D. B., & Duthie, G. G. **(2000)** The relative contributions of vitamin C, carotenoids and phenolics to the antioxidant potencial of fruit juices. Food Chemistry, 68, 471-474.

Gelover, S., Gomez, L.A., Reyes, K., Leal, M.T. **(2006)** A practical demonstration of water disinfection using TiO2 fims and sunlight. Water research, 40, 3274-3280.

Guo, Y., Hu, Changwen, Jiang, S., Guo, C., Yang, Y., Wang. E. **(2002)** Heterogeneous photodegradation of aqueous hydroxyl butanedioic acid microporous polyoxometalates. Applied Catalysis B: Environmental, 36, 9-17.

Hanes, D. E., Orlandi, P. A., Burr, D. H., Miliotis, M. D., Robi,M. G., Bier, J. W., Jackson, G. J., Arrowood, M. J., Churey, J. J., & Worobo, R. W. **(2002)** Inactivation of Crytosporidium parvum oocysts in fresh apple cider using ultraviolet irradiation. Applied Environment Microbiology, 68, 4168 –4172.

Haubler, S., Rohde, M., Steinmetz, I. **(1999)** Med. Microbiol. Immunol. 188, 91–97.

Herrmann, J. **(1999)** Heterogeneous photocatalysis: fundamentals and applications to the removal of various types of aqueous pollutants. Catalysis Today 53, 115–129.

Herrmann, J-M., Tahiri, H., Ait-Ichou Y, Lassaletta, Gonzales-Elipe A.R, Fernandez A. **(1997)** Characterization and photocatalytic activity in aqueous medium of TiO2 and Ag- TiO2 coatings on quartz. Applied Catalysis B: Environmental 13, 219-228.

Irawaty, W., Friedmann D., Scott J., Amal, R. **(2011)** Relationship between mineralization kinetics and mechanistic pathway during malic acid photodegradation. Journal of Molecular Catalysis A: Chemical 335, 151-157.

Irawaty, W., Friedmann, D., Scott, J., Pichat, P., Amal, R. **(2011)** Photocatalysis and TiO_2 aqueous suspension: Effects of mono- or di-hydroxyl substitution of butanedioic acid on the disappearance and mineralisation rates. Catalysis Today: 178, 51-57.

Ireland, J. C., Klostermann, P., Rice, E. W., Clark, R. M. **(1993)** Inactivation of Escherichia coli by Titanium Dioxide Photocatalytic Oxidation. Applied and Environmental Microbiology, 59 (5), 1668-1670.

Kormann, C., Bahnemann, D. W. and Hoffmann, M. R. **(1991)** Photolysis of Chloroform and Other Organic Molecules in Aqueous TiO_2 Suspensions. Environ. Sci. Technol., 25, 494-500.

Koutchma, T., Keller, S., Chirtel, S., Parisi, B. **(2004)** Ultraviolet disinfection of juice products in laminar and turbulent flow reactors. Innovative Food Science & Emerging Technologies, 5, 179-189.

Laoufi, N. A., Tassalit, D., Bentahar, F. **(2008)** The degradation of phenol in water solution by TiO_2 photocatalysis in a helical reactor. Global NEST Journal, 10(3), 404-418.

Mattews, R. W., and McEvoy, S. R. **(1992)** Destruction of phenol in water with sun, sand, and photocatalysis. Solar Energy, 49(6): 507-513.

Mato, I., Suarez-Luque, S., Hidobro, J. F., **(2005)** A review of the analytical methods to determine organic acids in grape juices and wines, volume 38, Issue 10, 1175-1188.

Montoya, J. F., Velasquez, J. A., Salvador, P. **(2009)** The direct–indirect kinetic model in photocatalysis: A reanalysis of phenol and formic acid degradation rate dependence on photon flow and concentration in TiO2 aqueous dispersions. Applied Catalysis B: Environmental 88, 50–58

Moreira, J. **(2011)** Photocatalytic degradation of phenolic compounds in water: irradiation and kinetic modeling. PHD Thesis. University of Western Ontario.

Moreira, J., Serrano, B., Ortiz A., de Lasa, H. **(2012)** A unified kinetic model for phenol photocatalytic degradation over TiO_2 photocatalysts. Chemical Engineering Science 78, 186-203.

Moyer, J. C., & Aitken, H. C. **(1980)** Apple juice. In P. E. Nelson & D. K.Tressler (Eds.), Fruit and Vegetable Juice Processing Technology. Westport, CT, USA: AVI Publishing Co, 212-267.

Mukherjee, P.S., Ray, A.K., **(1999)** Major Challenges in the Design of a Large-Scale Photocatalytic Reactor for Water Treatment. Chemical Engineering and Technology 22, 253-260.

Nimlos, M. R.; Wolfrum, E. J.; Brewer, M. L.; Fennell, J. A.; Bintner, G. **(1996)** Gas-Phase Heterogeneous Oxidation of Ethanol: Pathways and Kinetic Modeling. Environmental Science & Technology 30, 3102-3110.

Noci, F., Riener, J., Walking-Ribeiro, M., Cronin, D. A., Morgan, D. J., Lyng, J. G. **(2008)** Ultraviolet irradiation and pulsed electric fields (PEF) in a hurdle strategy for the preservation of fresh apple juice. Journal of Food Engineering, 85, 141-146.

Peill, N. J.; Hoffmann, M. R. **(1995)** Development and optimization of a TiO2-coated fiber-optic cable reactor: photocatalytic degradation of 4-chlorophenol. Environmental Science & Technology 29, 2974-2981.

Pothakamury, U.R., Barbosa-Canovas, G.V., Swanson, B.G. **(1993)** Magnetic-field inactivation of microorganisms and generation of biological changes. Food Technol. 47, 85–93.

Proctor, R.A., van Langevelde, P., Kristjansson, M. **(1995)** J.N. Maslow, R.D. Arbeit, Clin. Infect. Dis. 20, 95–102.

Qin, B.-L., Chang, F.-J. Barbosa-Canovas, G. and Swanson B.V. (1995) Nonthermal Inactivation of Saccharomyces cerevisiae in Apple Juice Using Pulsed Electric Fields. Lebensm.-Wiss u.-TechnoL, 28, 564-56.

Rahman, M. S. **(1999)** Glass transition and other structural changes in foods. In M. S. Rahman, Handbook of food preservation (pp.75-93). New York: Marcel Dekker.

Raso, J., Pagan, R., Condon, S., & Sala, F. J. **(1998)** Influence of temperature and pressure on the lethality of ultrasound. Applied Environmental Microbiology, 64 (2), 465-471.

Rincon, A.G., Pulgarín, C. **(2003)** Photocatalytical inactivation of E. coli: effect of continuous-intermittent light intensity and of suspended-fixed TiO_2 concentration. Applied Catalysis B: Environmental 44(3), 263-284.

Rincon, A.G., Pulgarín, C. **(2004)** Effect of pH, inorganic ions, organic matter and H_2O_2 on E. coli K12 photocatalytic inactivation by TiO_2. Implications in solar water disinfection. Applied Catalysis B: Environmental, 51(4), 283-302.

Robertson, J. M. C., Robertson, P. K. J. and Lawton, L. A. **(2005)** A comparison of the effectiveness of TiO2 photocatalysis and UVA photolysis for the destruction of three pathogenic micro-organisms. Journal of Photochemistry and Photobiology A. Chemistry 175, 51-56.

Salaices, M., Serrano, B., de Lasa, H. I. **(2004)** Photocatalytic conversion of phenolic compounds in slurry reactors. Chemical Engineering Science 59, 3-15.

Salaices-Arredondo, M. **(2002)** Photocatalysis in slurry reactors radiation transmission and kinetic modeling. PHD Thesis. The University of Western Ontario.

Sarantopoulos, C., Puzenat, E., Guillard, C., Herrmann, J.-M., Gleizes, A., Maury, F. **(2009)** Microfibrous TiO_2 supported photocatalysts prepared by metal-organic chemical vapor infiltration for indoor air and waste water purification. Applied Catalysis B: Environmental, vol. 91 (n°1-2). 225-233.

Sczechowski, J. G., Koval, C. A., Noble, R. D. **(1995)** A Taylor Vortex Reactor for Heterogeneous Photocatalysis. Chemical Engineering Science 50, 3163-3173.

Serrano, B., Ortız, A., Moreira, J., de Lasa, H. **(2009)** Energy Efficiency in Photocatalytic Reactors for the Full Span of Reaction Times. Ind. Eng. Chem. Res., 48, 9864–9876.

Sobczynski, A. and Dosbosz, A., **(2001)** Water purification by photocatalysis on semiconductors. Polish Journal of Environmental Studies, Vol. 10, N. 4, 195-205.

Song, Y. K., Park, M. K., Kwon, Y. T., Lee, H. W., Chung, W. J., Lee, W. I. **(2001)** Preparation of Transparent Particulate MoO_3/TiO_2 and WO_3/TiO_2 Films and Their Photocatalytic Properties. Chem. Mater., 13, 2349-2355.

Sumin, Z., Zaifeng, S., Luyong, W. **(2011)** Characteristics of TiO_2 Film Immobilized on Glass and Stainless Steel Tube and Photodegradation of Phenol. 2011 International Conference on Computer Distributed Control and Intelligent Environmental Monitoring.

Tiwari, B. K., Muthukumarappan, K., O'Donnell, C. P., & Cullen, P. J. **(2008)** Colour degradation and quality parameters of sonicated orange juice using response surface methodology. LWT - Food Science and Technology, 41(10), 1876–1883.

Tran, H., Scott, J., Chiang, K., Amal, R. **(2006)** J. Photochem. Photobiol. A 183, 41-52.

Tsuchiya, K., Nakamura, K., Okuno, K., Ano, T., & Shoda, M. **(1996)** Effect of homogeneous and inhomogeneous high magnetic fields on the growth of Escherichia coli. Journal of Fermentation and Bioengineering, 81(4), 343–346.

Valladares, J. E.; Bolton, J. R. **(1993)** in: D.E. Ollis, H. Al-Ekabi (Eds.). Photocatalytic Purification and Treatment of Water and Air, Elsevier, New York.

Wang, R., Hashimoto, K., Fujishima, A., Chikuni, A., Kitamura, A., Shimohigoshi, M., Watanabe, T. **(1997)** Nature, 288, 431.

Watanabe T., Nakajima A., Wang R., Minabe M., Koizumi S., Fujishima A., Hashimoto K. **(1999)** Photocatalytic activity and photoinduced hydrophilicity of titanium dioxide coated glass. ThinSolid Films, 351: 260-263.

Yamazaki-Nishida, S.; Read, H. W.; Nagano, J. K.; Jarosch, T.; Eddy, C.; Cervera-March, S.; Anderson, M. A. **(1994)** Gas Phase Photocatalytic Degradation on TiO_2

Pellets of Volatile Chlorinated Organic Compounds from a Soil Vapor Extraction Well. Journal of Soil Contamination 3, 1-16.

Zeman P., Takabayashi S. **(2003)** Nano-scaled photocatalytic TiO_2 thin films prepared by magnetron sputtering. Thin Solid Films, 433: 57-62.

Zepp, R. G. and Cline, D. M. **(1977)** Rates of direct photolysis in aquatic environment. Environmental Science & Technology, volume 11, number 4.

Zhang, Y.; Crittenden, J. C.; Hand, D. W.; Perram, D. L. **(1994)** Fixed-bed photocatalysts for solar decontamination of water. Environmental Science and Technology 28, 435-442.

Appendices

Appendix A: Calculation of k_i and k_m

In order to evaluate the effect of the mass transfer in the photocatalytic degradation of malic acid using the TiO_2 film of this study, the following calculations were performed:

a) A mass balance between bulk solution of malic acid and TiO_2-fim interface requires the consideration of the following terms:

$$\begin{Bmatrix}\text{Axial}\\ \text{Mixing}\end{Bmatrix}+\begin{Bmatrix}\text{Convective}\\ \text{Term}\end{Bmatrix}+\begin{Bmatrix}\text{Radial}\\ \text{Mixing}\end{Bmatrix}+\begin{Bmatrix}\text{Chemical}\\ \text{Reaction}\end{Bmatrix}+\begin{Bmatrix}\text{Mass transfer}\\ \text{between}\\ \text{malic acid}\\ \text{solution}\\ \text{and } TiO_2\text{film}\end{Bmatrix}=\{\text{Accumulation}\} \qquad (A.1)$$

Considering that convection, and axial mixing or radial mixing, do not play a part in the photocatalytic conversion in the "batch" cell of this study, Eq. (A.1) can be simplified as follows:

$$\begin{Bmatrix}\text{Mass transfer between}\\ \text{malic acid solution}\\ \text{and } TiO_2\text{film}\end{Bmatrix}=\{\text{Accumulation}\}$$

$$k_m A_{irr}(C_b - C_i) = k_i C_i A_{irr} \qquad (A.2)$$

where the k_m is the mass transfer coefficient in $\frac{cm^3 fluid}{cm^2 s}$, A_{irr} is the area of the catalyst irradiated in cm^2, C_b is the concentration of malic acid in the bulk solution expressed as $\frac{mol}{cm^3 fluid}$, C_i is the concentration in the near catalyst interface in $\frac{mol}{cm^2}$, k_i is the kinetic constant for malic acid photoconversion in $\frac{cm^3 fluid}{cm^2 s}$.

Thus,

$$k_m C_b - k_m C_i = k_i C_i \qquad (A.3)$$

and

$$C_i(k_i + k_m) = k_m C_b \tag{A.4}$$

Futhermore,

$$C_i = \frac{k_m C_b}{k_i + k_m} \tag{A.5}$$

And finally,

$$r = -k_i C_i = -\frac{k_i k_m C_b}{k_i + k_m} = -\frac{C_b}{\frac{1}{k_m} + \frac{1}{k_i}} = -k_{overall} C_b \tag{A.6}$$

with $k_{overall}$ having the units $\frac{cm^3\,fluid}{cm^2\,s}$.

b) A mass balance can be performed in the photoconversion cell which operates as a batch reactor. Thus.

$$\{N_i|_t - N_i|_{t+\Delta t}\} = -rA_{irr}\Delta t \tag{A.7}$$

with r representing the rate of photoconversion in $\frac{mol}{cm^2\,s}$, A_{irr} standing for the irradiated surface in cm^2, and Δt denoting the incremental time in seconds.

Taking the limit of A.7 for the incremental time approaching zero, the following equation can be formulated:

$$\lim_{\Delta t \to 0} \frac{\{C_i|_t - C_i|_{t+\Delta t}\}}{\Delta t} = -r\frac{A_{irr}}{V} \tag{A.8}$$

Considering the definition of the photodegradation rate as in Eq. (A.6), it gives:

$$\frac{dC}{dt} = r\frac{A_{irr}}{V} = \left(-k_{overall}\frac{A_{irr}}{V}\right)C_b = -k_1 C_b \tag{A.9}$$

$$k_{overall} = \frac{k_1 V}{A_{irr}} \tag{A.10}$$

Given that in the case of our experiments: (a) the V volume of malic acid in the batch reactor is 200 cm^3, (b) the A_{irr} irradiated area of TiO_2 film is 81 cm^2 and (c) k_1 from Table 5.3 gives 1.082 x 10^{-2} min^{-1}, this results in:

$$k_{overall} = \frac{1.082x10^{-2}min^{-1}x\ 200cm^3}{81cm^2} x \frac{1min}{60s} x \frac{1m}{100cm} = 4.45x10^{-6}m/s$$

A k_m mass transfer coefficient can be calculated using the Sherwood Number.

c) The Sherwood number (Sh) can be used to determine the mass transfer coefficient (k_m). This allows establishing the potential influence of mass transfer in the malic acid degradation rate using the TiO_2 film.

The Sh number is a dimensionless ratio between the coefficient of convective mass transfer and diffusive mass transfer (Equations A.11 and A.12):

$$Sh = \frac{k_m D}{Diff} \quad (A.11)$$

$$k_m = \frac{Sh.Diff}{D} \quad (A.12)$$

where k_m is the mass transfer coefficient (m/s), Diff is the mass diffusivity coefficient of malic acid (m^2/s) to be degraded with D as a characteristic length (m).

Given that the conditions of the flow regime in the photocell are uncertain, a Sh number equal to 2 can be considered. This Sh of 2 will provide the lowest k_m value expected in the photocell. In addition, a characteristic D dimension for TiO_2 Degussa P25 agglomerates can be approximated as 1μm (de Lasa et al., 2005). The Diff for malic acid in water can be estimated as 8.06 x 10^{-6} cm^2/s (Teixeira et al., 1994). Thus, the mass transfer coefficient for malic acid in water can be approximated as 1.604 x 10^{-3} m/s.

As a result, when using Eq. (A.6), the effect of k_m on the overall rate of malic acid degradation can be expressed as $k_{overall}$ as a function of $1/(1/k_m) + 1/(1/k_i)$. One can thus see that with k_m = 1.604 x 10^{-3} m/s and $k_{overall}$ = 4.45 x 10^{-6} m/s, the magnitude of k_m is 1000 times higher than $k_{overall}$. Thus $1/k_{overall} >> 1/k_m$ and this shows that the mass transfer has a negligible effect on the malic acid photoconversion using the TiO_2 film developed in this research study.

Appendix B: Calculation of P_a (t), P_l (t), P_{bs} (t) and P_t (t) using Macroscopic Radiation Balance

The values of P_a (t), P_l (t), P_{bs} (t) and P_t (t) and can be determined performing the following two calculations:

$$P_a(t) = P_l(t) - P_{bs}(t) - P_t(t) \tag{B.1}$$

where P_a (t) represents the rate of absorption of photons, P_{bs} (t) the rate of back scattered photons exiting the system, P_t (t) the rate of transmission of photons, and P_l (t) the rate of emission of photons by the lamp, all in Photons/s.

$$P_{l,bs\ or\ t}(t) = \frac{\bar{\lambda}}{h.c}\int_{\lambda_1}^{\lambda_2}\int_0^L q_{z,\lambda,t}.\,r.\,dzd\lambda = \frac{\bar{\lambda}}{h.c} I_{Total} \tag{B.2}$$

where h represents the Planck's constant (6.626 x 10^{-34} J.s), c the speed of light (2.988 x 10^8 m/s), $\bar{\lambda}$ the average (mean) emission wavelength by the lamp (nm) and I_{Total} the total irradiation intensity emitted, back scattered or transmitted (μW/cm^2).

The values of $\bar{\lambda}$ (mean) and I_{Total} are calculated as below:

a) Calculation of mean wavelength ($\bar{\lambda}$):

$$\bar{\lambda}\,(\text{mean}) = \frac{\lambda_1 I_1 + \lambda_2 I_2 + \cdots + \lambda_n I_n}{I_1 + I_2 + \cdots + I_n} = \frac{\int_{\lambda_1}^{\lambda_2} \lambda.I(\lambda)d\lambda}{\int_{\lambda_1}^{\lambda_2} I(\lambda)d\lambda} \tag{B.3}$$

$$\bar{\lambda}\,(\text{mean}) = \frac{\int_{\lambda_{1=320\ nm}}^{\lambda_{2=388\ nm}} \lambda.\,I(\lambda)d\lambda}{\int_{\lambda_{1=320\ nm}}^{\lambda_{2=388\ nm}} I(\lambda)\,d\lambda} = \frac{1.58x10^5 nm\ \mu W/cm^2}{425.17\mu W/cm^2} = 372\ nm$$

b) Numerical Integration of Irradiation Intensity (Simpson's rule):

The values of $I_{Total/Area}$ were obtained performing the numerical integration of the irradiation intensity ($q_{\lambda,t,z}$) in 49 different measurement positions as a function of time between λ_1 = 320 nm and λ_2 = 388 nm (Figure B.1).

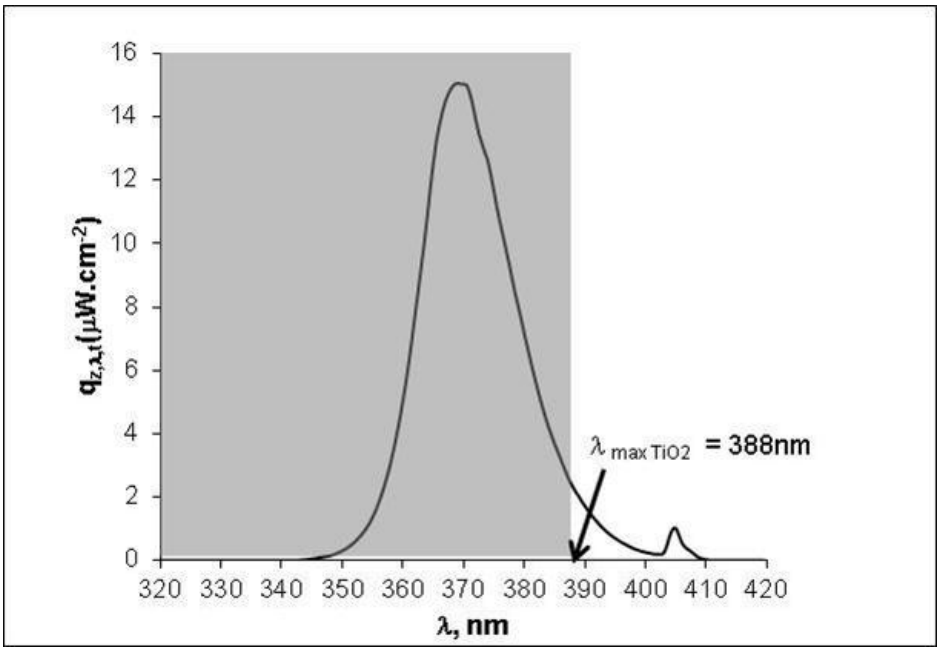

Figure B.1: Emission Spectrum for Lamp b (Wavelength Range of 320-420 nm)

Simpson's Rule (Eq. B.4) was applied in the calculation of the $I_{Total/Area}$ for the light emitted, back scattered and transmitted:

$$I_{\frac{Total}{Area}}(\mu W/cm^2) = \int_{\lambda_1}^{\lambda_2} I(t)dt = \frac{(\lambda_2-\lambda_1)}{3}\left[I(t_0) + 2\sum_{i=1}^{\frac{n}{2}-1} I(t_{2i}) + 4\sum_{i=1}^{\frac{n}{2}} I(t_{2i-1}) + I(t_n)\right] \quad (B.4)$$

The calculations were performed for the light emitted, back scattered and transmitted. The values obtained were multiplied by the quartz area covered by the TiO_2-film (81 cm^2) to achieve the $I_{Total\ Emitted}$, $I_{Total\ Back\ Scattered}$ and $I_{Total\ Transmitted}$:

$I_{Total\ Emitted} = 23{,}480.3\ \mu W$

$I_{Total\ Back\ Scattered} = 1{,}036.8\ \mu W$

$I_{Total\ Transmitted} = 933.9\ \mu W$

c) Calculation of P_l (t), P_{bs} (t) and P_t (t) and P_a (t):

$$P_l(t) = \frac{\bar{\lambda}}{h.c}\int_{\lambda_1}^{\lambda_2}\int_0^L q_{z,\lambda,t}.\,r.\,dzd\lambda = \frac{\bar{\lambda}}{h.c} I_{\text{Total Emitted}}$$

$$P_l(t) = \frac{372\text{x}10^{-9}\text{m}}{6.626\text{x}10^{-34}\text{J.s x } 2.988\text{x}10^{8}\text{m/s}} \text{ x } 23{,}480.3\ \mu\text{J/s} = 4.41 \text{ x } 10^{16} \text{ photons/s}$$

$$P_{bs}(t) = \frac{372\text{x}10^{-9}\text{m}}{6.626\text{x}10^{-34}\text{J.s x } 2.988\text{x}10^{8}\text{m/s}} \text{ x } 1{,}036.8\ \mu\text{J/s} = 1.95 \text{ x } 10^{15} \text{ photons/s}$$

$$P_t(t) = \frac{372\text{x}10^{-9}\text{m}}{6.626\text{x}10^{-34}\text{J.s x } 2.988\text{x}10^{8}\text{m/s}} \text{ x } 933.9\ \mu\text{J/s} = 1.75 \text{ x } 10^{15} \text{ photons/s}$$

$$P_a(t) = (44.1 - 1.95 - 1.75) \text{ x } 10^{15} = 4.04 \text{ x } 10^{16} \text{ photons/s}$$

Curriculum Vitae

Name:	Vanessa Rodgher
Post-secondary Education and Degrees:	Universidade Estadual Paulista Araraquara, Sao Paulo, Brazil 1999-2002 Bachelor of Chemistry The University of Western Ontario London, Ontario, Canada 2011-2012 MESc of Chemical Engineering
Honours and Awards:	Honour Roll student – Universidade Estadual Paulista 1999-2002
Related Work Experience	Teaching Assistant – Chemical Reaction Engineering Dept. The University of Western Ontario 2011-2012 Quality Assurance and Food Safety Coordinator Sucocitrico Cutrale Ltd., Sao Paulo, Brazil Coordinated and conducted internal Audits in compliance with the Food Safety Management Program (GMP, HACCP, QA ISO 9001, Allergens, Sanitization and Pest Control); assisted and collaborated in first, second and third party audits; controlled and followed up non-conformity products, corrective actions and preventive measures; conducted internal training and meetings to certify that all employees understood and worked in accordance to Food Safety Regulations. 2008-2010 Process Auditor Sucocitrico Cutrale Ltd., Sao Paulo, Brazil Inspected production procedures focusing on efficiency increase and continuous improvement of the process; attended new projects related to the Manufacturing Area. 2006-2008 Chemist Sucocitrico Cutrale Ltd., Sao Paulo, Brazil Performed physical-chemical and microbiological tests on final products; developed new methods of analysis for orange juice and by-products using HPLC and GC equipment, assured the conformity of final products to customers and regulatory agencies'

specification.
2003-2006

Publications:

Rodgher, V. S.; Okumura, L. L. ; Saczk, A. A.; Stradiotto, N. R. ; Zanoni, M. V. B. (2006). Electroanalysis and determination of acetaldehyde in fuel ethanol using the reaction with 2,4-dinitrophenylhydrazine. Journal of Analytical Chemistry (Moscow), v. 61, n. 9, 889-895.

Rodgher, V. S.; Stradiotto, N. R. ; Zanoni, M. V. B**.** (2006). Electroanalysis of acetaldehyde derived from hydrazine and determination in fuel ethanol by square wave voltammetry. Química Nova 29, 662-665.